

**Investigations of the Emissions and Fate of
Anthropogenic Air Pollutants from East Asia
Using Regional On-line and Off-line
Chemistry-Climate Modeling System**

A Thesis
Presented to
The Academic Faculty

by

Qian Tan

In Partial Fulfillment
of the Requirements for the Degree
Doctor of Philosophy

School of Earth and Atmospheric Sciences
Georgia Institute of Technology
April 2004

**Investigations of the Emissions and Fate of
Anthropogenic Air Pollutants from East Asia
Using Regional On-line and Off-line
Chemistry-Climate Modeling System**

Approved by:

William Chameides, Committee Chair

Yuhang Wang

Robert Dickinson

Rodney Weber

Armistead Russell

Date Approved: 6 April 2004

To Daozhen, my dearest grandmother ..

ACKNOWLEDGEMENTS

Sincere gratitude goes to my advisor, Prof. William L. Chameides, for his persistent guidance, help, and encouragement throughout my graduate study. His scientific knowledge and thoughtful insight have made working with him being a fulfilling and invaluable experience for me.

I would also like to thank my committee members, Prof. Robert Dickinson, Prof. Armistead Russell, Prof. Yuhang Wang, and Prof. Rodney Weber, for their interests in my research and helpful comments and suggestions on this thesis.

Many thanks to my collaborators: Dr. Chao Luo, Dr. Fillipo Giorgi, Dr. Yun Qian, Ms. Yan Huang, Dr. Xunqiang Bi, Dr. Yongtao Hu, who help me to set up the modeling systems used in this work; Dr. David Streets, Dr. Tao Wang, Dr. Jin Xu, Dr. Michael Bergin, Dr. Karsten Baumann, who provide data as well as valuable suggestions to this study.

Appreciation also goes to my friends: Dr. Hongbin Yu, who was the supervisor of my class back in college, and Wang Chen are my first and best friends in Atlanta, their friendship and encouragements help me go through lots of hardship and difficulties; Allison Steiner, Yan Huang, Jing Zhang, Nicholas Meskhidze, Daniel Cohan, Mi Zhou, Qing Yang, Ping Jing, as well as many other friends make my study at Georgia Tech an enjoyable experience.

Finally, I am very grateful to my family, from my grandparents to my nephew, especially my parents and my husband, for their unconditional love, understanding, and support through these years.

TABLE OF CONTENTS

ACKNOWLEDGEMENTS	iv
LIST OF TABLES	viii
LIST OF FIGURES	x
SUMMARY	xiv
CHAPTER I INTRODUCTION	1
1.1 Emission Inventories from East Asia	2
1.2 Recent and Future Trend of Anthropogenic Emissions from East Asia	4
1.3 Impacts of Anthropogenic Emissions	8
1.3.1 Air quality and human health.	8
1.3.2 Regional climate	11
1.3.3 Economical and ecological consequences	14
1.3.4 Outflow of anthropogenic emissions to other regions	16
1.4 The Role of Numerical Models in the Assessment of Anthropogenic Emissions	17
1.4.1 Numerical models.	17
1.4.2 Chemical transport models (CTMs).	18
1.4.3 Regional scale models	20
1.4.4 Modeling system used in this work	21
1.5 Outline of This Thesis	22
CHAPTER II BUDGET AND EXPORT OF ANTHROPOGENIC SO_x FROM EAST ASIA DURING CONTINENTAL OUTFLOW CONDITIONS	25
2.1 Introduction	25
2.2 Model Description	26
2.2.1 Emissions	29
2.2.2 Gas-phase chemical conversion	29
2.2.3 Heterogeneous reactions	29

2.2.4	Large-scale cloud processing	31
2.2.5	Convective cloud processing	32
2.2.6	Below-cloud scavenging	35
2.2.7	Dry deposition	36
2.3	Model Simulations	36
2.3.1	Simulated SO _x distributions and comparison with observations	37
2.3.2	East Asian SO _x budget and export	45
2.4	Discussion and Conclusion	52
CHAPTER III AN EVALUATION OF THE TRACE-P EMISSION INVENTORIES FROM CHINA USING A REGIONAL MODEL AND CHEMICAL MEASUREMENTS		54
3.1	Introduction	54
3.2	Climate-Chemistry Modeling System	57
3.2.1	Model description	57
3.2.2	Emission inventory	59
3.2.3	Meteorological conditions	62
3.2.4	Model results	64
3.3	Observations	64
3.4	Model-Measurement Comparison	71
3.4.1	Test runs with increased emissions	74
3.4.2	Estimate of the spatial extent of the required emissions increase	77
3.5	The Characteristics of the Missing CO Sources	80
3.5.1	Trajectories of high CO plumes	80
3.5.2	Statistical analysis of high-resolution measurements	85
3.5.3	Scenarios that would provide the missing CO emissions	88
3.6	Conclusion	92
CHAPTER IV CONCLUSION		93
4.1	Major Results	93
4.1.1	Distribution and budget of sulfur compounds in East Asia	93

4.1.2	Evaluation of East Asia anthropogenic emission inventories	95
4.2	Future Research Plan	96
4.2.1	Fully coupling of regional climate and chemical transport model.	96
4.2.2	Global-regional interaction studies	96
4.2.3	Interaction of anthropogenic-natural air pollutants.	97
APPENDIX A	— REGIONAL CHEMISTRY MODEL	98
REFERENCES	125
VITA	145

LIST OF TABLES

Table 1	Total Energy Consumption (quadrillion btu) and Carbon Dioxide Emission (Mt C) by Developing Countries in Asia, China and Their Contribution to the Global Budget.	5
Table 2	Estimated Anthropogenic Emissions of Air Pollutants from China since 1975.	7
Table 3	Ambient Air Quality Standards of China and United States, as well as Recommendations by World Health Organization (WHO). . . .	10
Table 4	The Number of Registered Motor Vehicles (thousands) in China since 1978.	12
Table 5	Comparison of Model-Simulated and Observed SO ₂ Concentrations (ppbv)	41
Table 6	Comparison of Simulated and Observed SO ₄ ²⁻ ($\mu\text{g m}^{-3}$)	41
Table 7	Comparison of Simulated and Aircraft measured SO ₂ (pptv) and SO ₄ ²⁻ (pptv)	42
Table 8	Arithmetic Mean of Measured and Model Simulated Gaseous and Particulate Species at Linan in November, 1999.	68
Table 9	Measured and Model Simulated Geometric Mean of Gaseous Species Concentration (ppb) and CO to SO ₂ Ratios at Linan, China in November, 1999.	75
Table 10	Comparison of Geometric Mean of Model Simulated Particle Concentration ($\mu\text{g}/\text{m}^3$) with Measurements Made at Linan, China in November 1999.	75
Table 11	Description of Various Test Runs.	76
Table 12	Comparison of Simulated Geometric Mean of the Gas and Aerosol Concentration together with Their Ratios from Different Test Runs with Geometric Mean of Measured Photochemically Aged Air. . . .	78
Table 13	Percentage of Increase in Model-Calculated CO and Particulate C (PC) Concentration at Linan for Different Model Test Runs.	79
Table 14	Factor Loadings for Multivariate Analysis of High-Resolution CO, SO ₂ , and NO _y Measurements from Linan	85
Table 15	Summary of Estimated Anthropogenic Emissions within Our Model Domain (Tg) Based on <i>Streets et al.</i> [2003].	100

Table 16	Tropospheric Ozone Budgets for Circa 1990 Conditions from a Sample of Global 3-D CTMs since 1996	104
Table 17	Global Budgets (Tg S/yr) of Major Sulfur Compounds for a Sample of Global Three Dimensional Climate-Chemistry-Aerosol Models since 1991	105
Table 18	Average of Surface Roughness Length	114
Table 19	Major Components of Surface Resistance	120

LIST OF FIGURES

Figure 1	Current and projected trend of anthropogenic emissions from East Asia [<i>IPCC Spatial Report of Emissions Scenarios (SRES)</i> , 2000]. The A2 scenario projects a very heterogeneous world and preserves local identities. It results in the highest global population, while attempting to predict upper limits on future anthropogenic emissions. The B2 scenario predicts an intermediate level of economic development and focuses on local to regional sustainability.	9
Figure 2	Spatial coverage of our modeling system. '.' is the center of each model grid. Color patches are the landuse derived from Global Land Cover Characterization (GLCC) 30" dataset.	23
Figure 3	Spatial domain for model calculations. Also indicated: six subregions used to study the sulfur budget ('1' = China (including Mongolia); '2' = South Russia/East Kazakhstan; '3' = Southeast Asia; '4' = Korea (including both North and South Korea); '5' = Japan; and '6' = Ocean); the PEM-West B flight tracks within our model domain for which SO ₂ and/or SO ₄ ²⁻ data were available (****); and the region from which model calculated concentrations were used to compare to PEM-West B observations (red and blue dots for SO ₂ and red dots for SO ₄ ²⁻).	28
Figure 4	Averaged monthly SO _x emissions (in gS/m ² /month) during February to April, 1995.	30
Figure 5	Monthly averaged (February to April) model-calculated SO _x concentrations (in ppbv) at the surface.	38
Figure 6	Monthly averaged (February to April) model-calculated SO _x concentrations (in ppbv) at 500 hpa.	39
Figure 7	Model-calculated and observed monthly average sulfate wet deposition rate (g SO ₄ ²⁻ /m ² /month). The model results are depicted by the color-coding and represent an average of the deposition rates calculated for the months of March and April. The numbers in the square brackets represent the model-calculated averages for the appropriate 10° x 10° grid (delineated by the dashed lines) in the figure. The numbers without parentheses/brackets are the 10° x 10° grid averages of the observed wet deposition rates for March, April, and May, 1993 reported by <i>Ding et al.</i> [1995]. The smaller numbers in the parentheses indicate the number of stations used to calculate the observed averages for each grid box.	44
Figure 8	Fate of SO _x emission by month and process. LS = large scale clouds, Cb = convective clouds.	46

Figure 9	Monthly averaged (February to April) rate of SO_x export by model boundary and chemical form.	48
Figure 10	Sulfur flux (in $\mu\text{gS}/\text{m}^2/\text{s}$) through the east boundary of the domain, averaged from February to April.	49
Figure 11	Percent contribution by each of the 6 subregions to the total area of the model domain, total SO_x emissions, deposition, and percent of total emission exported.	51
Figure 12	Spatial distribution in the annual average emission rate of CO, SO_2 , and particulate carbonaceous in 2000. It is interpolated from the TRACE-P inventory [<i>Streets</i> , 2003] to our model domain.	60
Figure 13	Contributions of various source-types to the total SO_2 , CO, and Particulate C emissions from China in the TRACE-P emission inventory of <i>Streets et al.</i> [2003].	61
Figure 14	Average temperature, T (K) and humidity, Qv (kg/kg) at the surface and 500 hpa during November, 1999 from the NCEP Reanalysis data and the RegCM simulation.	63
Figure 15	Time series of temperature, T(k), humidity, Qv(kg/kg), wind vector, u and v (m/s), and wind speed, w (m/s) per 6 hour during November, 1999, at Linan from measurements made at the site (T and Qv only), and from interpolation of the surrounding grids from the NCEP reanalysis data and RegCM simulations.	65
Figure 16	Monthly averaged distribution in the model-simulated CO, SO_2 , Particulate SO_4^{2-} , and Particulate C concentration during November, 1999.	66
Figure 17	Model-calculated and observed pollutant concentrations as a function of time at Linan during the November, 1999. Concentrations for gas-phase species (CO and SO_2) are hourly-averages, and concentrations of particulate species (sulfate and carbonaceous) are 24-hour averages. Observed concentrations were obtained from <i>Wang et al.</i> [2002] for gas phase species and from <i>Xu et al.</i> [2002] for the particulate species.	67

Figure 18	Location of the Linan sampling site (30° 17'N, 119° 45'E, 132 m) superimposed over a surface elevation map of the model domain. Also indicated: three major source areas: Beijing, (40° 02'N, 116° 10'E), Shanghai(31° 14'N, 121°29'E), and the Sichuan Basin (~ 28-32°N, 103-107°E); and four Subregions used to study the impacts of emission at different spatial scales on the model-calculated concentrations of species at Linan. The subregions are Subregion A, a 600 km × 600 km area centered at Linan; Subregion B, a 1200 km × 1200 km area centered at Linan; Subregion C, a north-south corridor that includes Beijing; and Subregion D, an east-west corridor that includes the Sichuan Basin.	70
Figure 19	Distribution of percentiles (10%, 25%, 50%, 75%, and 90%) of measured [<i>Wang et al.</i> , 2002] and model-calculated CO and SO ₂ concentrations in November 1999 at Linan, where 'a' and 'b' are derived from measurements and model simulations for the whole month, 'c' is the photochemically aged air (defined in the text) selected from measurements, 'd' is the model simulations for the local afternoon.	73
Figure 20	Scatter plot of hourly-averaged observed and model-calculated CO and SO ₂ concentrations in photochemically-aged air during the afternoon hours in November, 1999. Model results are illustrated for the Standard Model and the 2 CO test run with CO emissions doubled. Also indicated are linear regressions of CO-SO ₂ for each dataset. Three data points with the highest observed CO concentrations and for which back trajectories were calculated are surrounded by dotted square.	81
Figure 21	Two-day back-trajectories for three air masses at Linan (square) with the highest recorded hourly-averaged CO concentrations ('*' denotes the location of the air masses every 6 hour). The back trajectories were calculated with the NOAA ARL HYSPLIT model (www.arl.noaa.gov). Also indicated are locations of power plants in China (with the size of the circles being proportional to the capacity of the plant), and the metropolitan areas of Shanghai and Hangzhou (triangles).	83
Figure 22	Modeled error (dCO = Observed (CO) - Model (CO)) (ppb) as a function of observed SO ₂ concentration (ppb).	84
Figure 23	The probability distribution function (PDF) of CO -SO ₂ correlation coefficients, and average CO and SO ₂ concentrations (in ppbv) for each correlation coefficient bin for values of the as a function of the time interval, n, varying from 5 to 241 minutes.	87

Figure 24	The average confidence level of the CO-SO ₂ running correlation as a function of the time interval, n. Confidence levels calculates using the student's t-test.	89
Figure 25	Aerodynamic resistance based on different parameterizations. Where 'Walcek 86' is based on <i>Walcek et al.</i> , 1986; 'Hogstrom 88': <i>Hogstrom</i> , 1988; 'Holtslag 90': <i>Holtslag</i> , 1990.	111
Figure 26	Calculated aerodynamic resistance as a function of stability for different land surface by using typical surface roughness length and friction velocity [<i>Jacobson</i> , 1999]. Where 'Walcek 86' is based on <i>Walcek et al.</i> , 1986; 'Hogstrom 88': <i>Hogstrom</i> , 1988; 'Holtslag 90': <i>Holtslag</i> , 1990.	112
Figure 27	Interpolation of surface resistance components during the seasonal transitions. The start and end point of the seasonal transition is defined for different latitude based on the climatology of East Asia. If the resistance at one end is very large, i.e. 10^{12} s/m, which means the uptake pathway is not existed, then 'Exponential' interpolation is applied. If the resistances at both beginning and end of transition time period are smaller than 10^{12} , then 'Linear' interpolation is applied. See detailed description in Equation 46 and text.	120
Figure 28	Time series of model calculated aerodynamic resistance (Ra), surface resistance (Rs), and dry deposition velocity (Vd) at a rural site during November 1999, where 'Run 1' and 'Run 2' are model test runs by using landuse data from different sources. In 'Run 1', the rural site is categorized as crop forest mosaic, in 'Run 2', it is categorized as forest. (See text for more detail).	122
Figure 29	Monthly arithmetic mean and geometric mean of model calculated and measured NO _y (ppb) concentration at a rural site in China. Solid line denotes the measurement, dashed line is the model run with NO ₂ dry deposition velocity calculated followed that by <i>Ganzeveld et al.</i> , 1995, dot-dashed lines are model results by 'Run 1' and 'Run 2' in which the NO ₂ deposition velocity are calculated by using <i>Wesely's</i> [1989] scheme.	124

SUMMARY

The work presented in this thesis document reflects the results of a study carried out to better quantify the magnitude and fate of the anthropogenic air pollutants emitted from East Asia.

Simulations of anthropogenic sulfur compounds by a regional on-line coupled chemistry-climate model suggest that large portions of East Asia have high SO_x concentrations, and most subregions within East Asia are net exporters of SO_x ($\text{SO}_2 + \text{SO}_4^{2-}$) (i.e. the anthropogenic S emissions from the region are greater than the deposition to the region). Among them, China is responsible for $\sim 85\%$ of the total emissions, and $\sim 50\%$ of its total emitted SO_x is exported to locations outside its borders.

During the later winter to early spring when the continental outflow conditions predominate, about 20% of the total emitted SO_x within the investigated area has been exported to North Pacific Ocean based on our model simulations. Those exported anthropogenic SO_x from East Asia (mainly in the form of SO_4^{2-}) is likely large enough to perturb the sulfate aerosol concentration over the North Pacific Ocean.

Our investigation by integrating numerical simulations through a regional off-line full chemistry transport model, which is driven by the meteorological conditions calculated by a regional climate model, with field measurements of both gaseous and particulate species at a rural site adjacent to the largest industrialized area in China suggests that CO emissions from China, especially eastern China are likely underestimated by $\sim 50\%$ in the current East Asia anthropogenic emission inventories. In

addition, a 60-90% underestimation of particulate carbonaceous emission in the inventories is suggested. Further statistical diagnoses, together with the back-trajectory analysis show that the missing CO sources are likely associated with SO₂ sources that are already accounted for in the current inventories. This in turn suggests the emission factors of coal-combustors used in the current inventories are likely underestimated.

CHAPTER I

INTRODUCTION

Over the past several decades, East Asia has undergone rapid economic development and urbanization [*US CIA*, 2003; *United Nations*, 1996], and, as a result, has now become one of the major sources of anthropogenic air pollutants for the globe [*US DOE*, 2003; *IPCC SREC*, 2000]. These pollutants are believed to be responsible for significant effects on air quality, climate, and other important environmental resources and the accumulated ecological, social, and economic costs of these effects on local, regional, and even intercontinental scales appear to be significant [*China SEPA*, 2003; *IPCC*, 1996, 2001; *World Bank*, 1997]. This thesis documents research carried out to better quantify the magnitude of the pollutant emissions from East Asia and their fate.

Emissions of anthropogenic air pollutants are closely tied to economic development, industrialization and urbanization. While these types of activities might be having global-scale effects on our environment, they are, at least at the present time, occurring on spatial scales that are more appropriately characterized as regional (i.e., spatial scales of 1000's of kilometers). For example, about 75% of the world's consumption of commercial energy occurs in three regions of the northern mid-latitudes comprising about 23% of the earth's land surface [*Chameides et al.*, 1994]. These regions are: (i) Eastern North America (25-50°N, 105-60°W) ; (ii) Europe (36-70°N, 10°W-90°E); and (iii) East Asia (25-45°N, 100-146°E).

Of the three regions mentioned above, the one located in East Asia is perhaps the most intriguing from both a scientific and policy viewpoint. This region of the globe is undergoing rapid economic growth. Especially interesting is China, the world's

most populous nation, with one of the world's most rapidly developing economies [United Nation, 1996; US CIA, 2003]. From a scientific point-of-view, the rapid economic growth of the region affords the opportunity to observe and study a region and its interaction with the remote troposphere as the peoples within that region evolve from a largely agrarian society to a modern industrially-based and urbanized economy. Moreover, the high population densities of much of East Asia suggest that the magnitude of the evolving anthropogenic impacts is relatively large and thus perhaps more easily discernible and analyzed. The importance from a policy point-of-view arises from the fact that, according to some projections, pollutant emissions from East Asia may already or will soon eclipse those from North America and Europe [e.g., Galloway, 1989; Galloway et al., 1994; Wolf and Hidy, 1997; van Aardenne et al., 1999; Streets and Waldhoff, 2000a; IPCC, 2000; US DOE, 2003]. Understanding the future trajectory of the global environment necessitates a thorough understanding of the magnitude and fate of these pollutants and the fraction and chemical form of the pollutants that are transported into the remote troposphere (e.g., the North Pacific Ocean).

1.1 Emission Inventories from East Asia

Robinson and Robbins [1970ab] were among the earliest investigators to attempt to systematically quantify the emissions of primary air pollutants such as oxides of sulfur (SO_x = sulfur dioxide (SO_2) and particulate sulfate (SO_4^{2-}) and nitrogen (NO_x = nitric oxide (NO) and nitrogen dioxide (NO_2)) on global scales. Subsequent investigators have attempted to improve these early efforts through the use of improved data and enhanced spatial resolution [Kellogg et al., 1972; Granat et al., 1976; Varhelyi, 1985; Dignon and Hameed, 1989; Spiro, et al., 1992; Benkovitz et al., 1996]. However, even as recently as the end of the 1980's, these global emissions inventories were gridded with relatively coarse resolution (e.g, the inventory of Dignon and Hameed [1989]

had a resolution of $5^\circ \times 5^\circ$), and this precluded more detailed regionally-focused assessments.

Detailed studies aimed specifically at quantifying anthropogenic emissions from East Asia began in early 1990's by Japanese scientists when it was realized that air pollutants from the region were increasing rapidly in an inhomogeneous pattern and the existing global emission inventories did not appear to be sufficiently accurate nor to have sufficient spatial and temporal resolution to assess the impact and fate of those emissions [Fujita, *et al.*, 1991; Kato and Akimoto, 1992]. By the mid-1990's detailed multi-species emission inventories with high spatial resolution began to be available to the scientific community. For example, Akimoto [1994] produced an inventory that provided the spatial distribution of SO₂, NO_x, and CO₂ emissions from fuel combustion and industrial activities in Asia on 1° x 1° grid for 1975, 1980, and 1987. Arndt [1997] developed a more comprehensive SO₂ emission inventory with 1 degree resolution using the RAINS-ASIA model to support the study of acid deposition of East Asia. As part of the China-MAP program [Chameides, 1995] which aimed at investigating the impacts of rapid industrialization and urbanization on the environmental vitality of the region, Streets [2000a, 2001c] developed a detailed emission inventory of major air pollutants, including SO₂, NO_x, CO, black carbon, non-methane volatile organic compounds (NMVOC) for 1990 and 1995 and predicted their trend up to 2020.

More recently, in order to correctly reflect the spatial and temporal emission profiles of sources of sources that were operating during the time period of the field campaign, Streets [2003] developed an emission inventory of gaseous and primary aerosols for year 2000 for use in National Aeronautics and Space Administration (NASA) Transport and Chemical Evolution over the Pacific (TRACE-P) Mission [Jacob *et al.*, 2003] and the National Science Foundation (NSF)/National Oceanic and Atmospheric Administration (NOAA) Asian Pacific Regional Aerosol Characterization Experiment

(ACE-Asia) [Huebert *et al*, 2003]. It is probably the most comprehensive and certainly the most current inventory of anthropogenic emissions from East Asia. It quantifies emissions for 9 chemical species, SO₂, NO_x, CO₂, CO, CH₄, non-methane volatile organic compounds (NMVOC), black carbon (BC), organic carbon (OC) and NH₃, and includes separate emission rates for all major contributing sources, including industry, residential, transportation, biomass burning, power plants, and international ship track. Biomass burning (forest fire, savanna/grassland fire and burning of crop residues in the field after harvest) is included since those 'open' burnings are largely related to human activities. The emission data are available for virtually all of East Asia: 64 regions from 60.5°E to 157.5°E, and from 12.5°S to 53.5°N. The data are gridded with various spatial resolutions, from 30'' × 30'' to 1° × 1°.

1.2 Recent and Future Trend of Anthropogenic Emissions from East Asia

The rapid industrialization that has occurred in Asia, especially East Asia, in recent decades has also brought about an increase in energy consumption in the region: an increase that is significant in terms of both the magnitude of energy consumed and its share of the total energy budget of the globe (see Table 1). Over the past decade alone, the total energy consumed by the developing countries of Asia has increased from 15% of the global total in 1990 to 21% in 2001 [US DOE, 2003]. In absolute terms, energy consumption over the 1990's in East Asia increased from 52.5 to 85 quadrillion Btu, with China contributing about half; i.e., 27 quadrillion Btu in 1990 and 39.7 quadrillion Btu in 2001.

In most developing nations, there is a typically a close coupling between economic activity and energy consumption on the one hand and emissions of air pollutants on the other. It is therefore not surprising that emissions from Asia are estimated to have increased dramatically over the later portion of the 20th century. Carbon

Table 1: Total Energy Consumption (quadrillion btu) and Carbon Dioxide Emission (Mt C) by Developing Countries in Asia, China and Their Contribution to the Global Budget.

Energy Consumption	1990	2000	2001	2005	2010	2015	2020	2025
Devp. Asia	52.5	80.5	85.0	92.5	110.1	130.5	151.9	174.6
(%)	15.1	20.2	21.0	21.3	22.9	24.5	26.0	27.0
China	27.0	37.0	39.7	43.2	54.4	65.5	77.6	90.8
(%)	7.8	9.3	9.8	10.0	11.3	12.3	13.3	14
World	348.4	398.9	403.9	433.3	480.6	531.7	583.0	640.1
CO ₂ Emission								
Devp. Asia	1089	1557	1640	1749	2075	2436	2837	3263
(%)	18	24.3	25	25.3	27	28.6	30.3	31.5
China	617	780	832	888	1109	1319	1574	1844
(%)	10.5	12.1	12.8	12.9	14.4	15.5	16.8	17.8
World	5872	6417	6522	6908	7685	8512	9372	10361

Sources: *International Energy Outlook, US DOE [2003]*.

dioxide (CO₂) emissions are probably most closely tied to the generation of energy from the burning of fossil- and bio-fuels and these emissions appear to have undergone a substantial increase. It is estimated that CO₂ from the region have increased from 1089 Mt C or 18% of the global anthropogenic total in 1990, to 1640 Mt C or 25% of the total in 2001 (see Table 1).

In addition to CO₂, the anthropogenic emissions of the more traditional air pollutants from East Asia also appear to have increased substantially since the 1970's. For example, Table 2 summarizes the emission trends of major air pollutants from China over the past decades as estimated by various researchers. The studies yield qualitatively similar results and they all show significant net increases in pollutant emissions since the 1970's. For example, SO₂ emissions from China more than doubled over ~ 20-year period from 5.5 Tg S /yr in 1975 to 13.37 Tg S/yr in 1996 [*Kato and Akimoto, 1992; Streets et al. 2000b*]. Over the same period, global SO₂ emissions were ~ 73 (Tg S/yr) in 1990 (ranging from 60-85 in different studies) [*Rodhe, 1999*]. Anthropogenic NO_x emissions from China increased from 3.9 Tg NO₂/yr (1975) to

11.9-15.0 Tg NO₂/yr (2000) [*Kato and Akimoto, 1992; van Aardenne, 1999; Streets et al., 2003*], while the global anthropogenic NO_x emissions were about 70-80 Tg NO₂/yr in 1980-90 [*Benkovitz et al., 1996; Ehhalt, 1999; Penner et al., 1999*], and ~ 100 Tg NO₂/yr in 2000 [*IPCC SRES, 2000*].

There is however an indication that this trend has not been uniformly upward since the 1970's and that the emissions of some pollutants from China may have actually decreased in the later half of the 1990's. For example, a comparison of the estimates of *Streets* [2003] for emissions from China in 2000 with earlier emissions estimates for 1995 in Table 2 suggests that the emission of SO₂ and BC actually decreased by about 20% in the later half of the 1990's, while those of CO and NO_x remained fairly flat. VOC emissions on the other hand, are estimate to have increased. It is believed that these recent trends have come about as a result of the promulgation of new environmental regulations in China related to the consumption and control of emissions from the burning of coal as well as the slow down of the Chinese economy after 1996-97 [*Sinton and Fridley, 2000; Streets et al., 2001a*].

Despite the estimated recent decreases in pollutant emissions from China, it seems likely that emissions from East Asia will increase in the coming decades. Around 25%-30% of the world's population can be found in East Asia (but less than 10% of the world's land area). Given this high population density, the current state of the technological infrastructure in the region, and the expectations for future economic growth, emission increases seem inevitable unless the nations of the region implement aggressive measures to control them. As indicated in Table 1 and Figure 1, it is projected that the next 25 years will see an almost doubling in the energy consumption and CO₂ emissions from the region. Over the same period, it is expected that emissions of pollutants such as SO₂ and NO_x will also increase, although the magnitude of the increase will depend critically on the degree to which clean technologies and emission controls are adopted in the region. For example the sulfur oxide and nitrogen oxide

Table 2: Estimated Anthropogenic Emissions of Air Pollutants from China since 1975.

	1975	1980	1985	1986	1987	1990	1995	1996	1997	2000	
SO ₂	-	-	-	20.0	-	-	-	-	-	-	<i>a</i>
	10.9	14.6	18.1	19.2	20.8	-	-	-	-	-	<i>b</i>
	-	-	-	-	20.6	-	-	-	-	-	<i>c</i>
	-	-	18.5	19.5	20.8	22.9	26.3	26.7	25.5	-	<i>d</i>
	-	-	-	-	-	23.0	25.2	-	-	-	<i>e</i>
	-	-	-	-	-	21.4	24.3	-	-	-	<i>f</i>
	-	-	-	-	-	-	-	-	-	20.8	<i>g</i>
NO _x	3.9	5.2	6.7	7.2	7.8	-	-	-	-	-	<i>b</i>
	-	-	-	-	-	9.0	-	-	-	15.0	<i>h</i>
	-	-	-	-	-	9.5	12.0	-	-	-	<i>e</i>
	-	-	-	-	-	8.4	12.0	-	13.4	-	<i>i</i>
	-	-	-	-	-	7.6	10.2	-	-	-	<i>f</i>
	-	-	-	-	-	-	-	-	-	11.9	<i>g</i>
CO	-	-	-	-	-	99.42	114.64	-	-	-	<i>e</i>
	-	-	-	-	-	89.75	-	-	-	-	<i>j</i>
	-	-	-	-	-	-	-	-	-	117.88	<i>g</i>
VOC	-	-	-	-	-	-	14.96	-	-	-	<i>j</i>
	-	-	-	-	-	12.1	13.8	-	-	-	<i>f</i>
	-	-	-	-	-	-	-	-	-	17.94	<i>g</i>
BC	-	-	-	-	-	-	1.342	-	-	-	<i>k</i>
	-	-	-	-	-	-	-	-	-	1.056	<i>g</i>
OC	-	-	-	-	-	-	-	-	-	3.39	<i>g</i>

Sources: *a*: Fujita et al., 1991; *b*: Kato and Akimoto, 1992; *c*: Ardn and Carmichael, 1997; *d*: Streets et al., 2000b; *e*: Streets and Waldhoff, 2000a; *f*: Klimont et al., 2001; *g*: Streets et al., 2003; *h*: van Aardenne et al., 1999; *i*: Streets et al., 2001b; *j*: Tonooka et al., 2001; *k*: Streets et al., 2001c

emissions from China are projected to increase to as much as 60.8 Tg SO₂/yr and 35 Tg NO₂/yr, respectively, in 2020 for the high economy increase projection without emission controls [*van Aardenne, 1999; Streets and Waldhoff, 2000*]. According to the Intergovernmental Panel on Climate Change (IPCC) Special Report of Emissions Scenarios (SRES) [2000], East Asia will probably be the largest emitter of CO₂, SO₂, and NO_x, and the second largest of CO by the end of the 21st century.

1.3 Impacts of Anthropogenic Emissions

While East Asia has only just begun its economic and industrial development, the air pollution that has resulted from this development appears to have already caused significant adverse effects on the environment and climate on local and regional scales; in many cases the effects are likely to be felt by economically important ecosystems and resources [*IPCC, 1996, 2001; World Bank, 1997; Chameides, 1999ab; Qian and Giorgi, 2000; Xu, 2001; Menon et al., 2002; Kaiser and Qian, 2002; Meskhidze, 2003*]. Transport of pollutants out of the region has also been well-documented and appears to be having significant impacts on the North Pacific Ocean, North America, and beyond [*Andreae et al., 1988; Prospero and Savoie, 1989; Parrish et al., 1992; Talbot et al., 1997; Jaffe et al., 1997, 1999, 2003; Jacob et al., 1999; Liu et al., 2003; Jaegle et al., 2003*].

1.3.1 Air quality and human health.

Among the negative consequences of the industrial development, degradation in air quality is perhaps most evident. Air pollution has long been recognized as a critical problem in China. According to a 1998 World Health Organization (WHO) report on air quality in 272 cities worldwide, seven of the world's ten most polluted cities are in China. Based on an evaluation by the Chinese government, two-thirds of the 343 cities and counties monitored in China are polluted and two-thirds of these are moderately to severely polluted [China SEPA, 2003]. Ambient concentration of

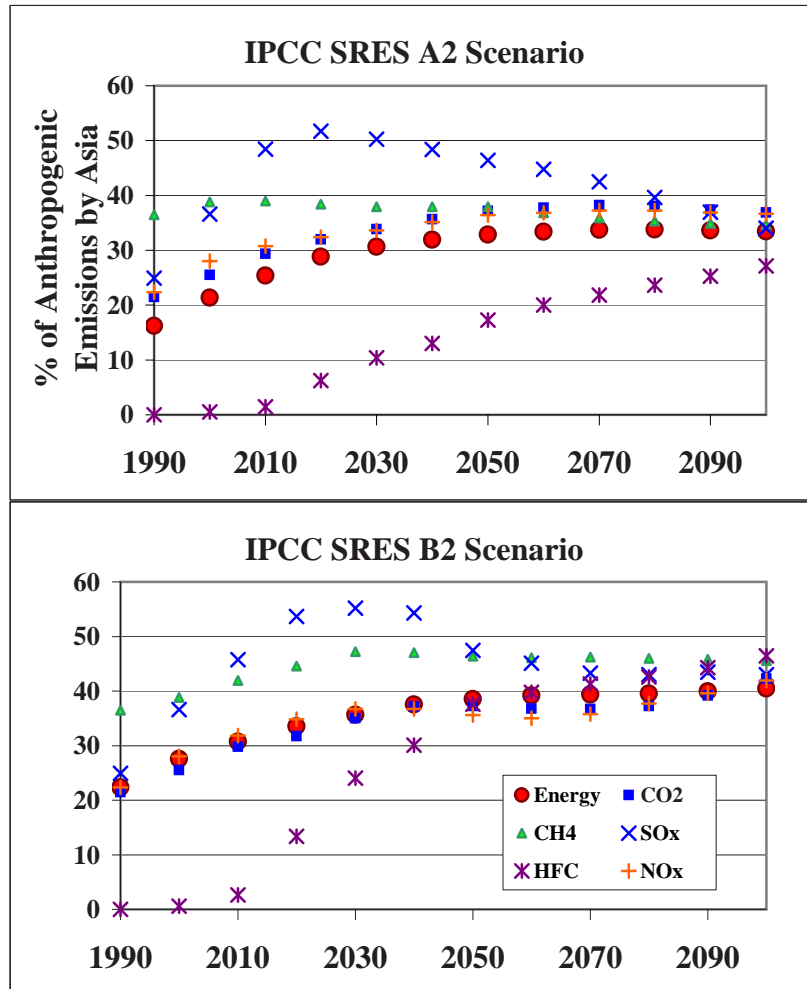


Figure 1: Current and projected trend of anthropogenic emissions from East Asia [IPCC *Spatial Report of Emissions Scenarios (SRES)*, 2000]. The A2 scenario projects a very heterogeneous world and preserves local identities. It results in the highest global population, while attempting to predict upper limits on future anthropogenic emissions. The B2 scenario predicts an intermediate level of economic development and focuses on local to regional sustainability.

Table 3: Ambient Air Quality Standards of China and United States, as well as Recommendations by World Health Organization (WHO).

Species	China EPA ^{a-1}	China EPA ^{a-2}	US EPA ^b	WHO ^c
CO	5240*	3500*	9000 [@]	8730 [@]
O ₃	100 ⁺	80 ⁺	80 [@]	50-60 [@]
SO ₂	35	21	30	14-21
NO ₂	42	21	53	80*
PM 10	150	100	50	70*
TSP ^d	300	200		150-230

Units: CO, O₃, SO₂, and NO_y : ppb; PM_{2.5} and PM₁₀: $\mu\text{g}/\text{m}^3$

Sources: ^a: China State Environmental Administration (SEPA) Ambient Air Quality Standard, where '1' for the industrial areas and heavy traffic areas, '2' is for the rural areas and residential urban areas, <http://www.zhb.gov.cn> (in Chinese).

^b: US Environmental Protection Agent (EPA) National Ambient Air Quality Standards (NAAQS). <http://www.epa.gov/air/criteria.html>

^c: World Health Organization (WHO) Air Quality Guidelines. <http://www.who.int/inf-fs/en/fact187.html>

^d: Total suspended particulates

Notes: the standard is the annual average unless otherwise notified.

*: Daily average

@: 8-hour average

⁺: 1-hour average

total suspended particulate (TSP) and sulfur dioxide (SO₂) in China are among the world's highest: most of the cities and counties in China monitored for TSP (with a national average of 289 $\mu\text{g}/\text{m}^3$) far exceed the WHO guideline (60–90 $\mu\text{g}/\text{m}^3$) and some cities can be as high as 10 times, while half of the cities monitored for SO₂ are above WHO guideline [*China SEPA*, 2003, *World Bank*, 1997]. Due to the severity of air pollution in China, the regulatory standard for ambient air quality of PM 10 promulgated by the China State Environmental Protection Administration (SEPA) is two-three times higher than that of the United States Environmental Protection Agent (EPA) and WHO [China SEPA, US EPA, WHO] (Table 3).

Air pollution is thought to be one of the significant risk factors for respiratory diseases, such as chronic obstructive pulmonary disease (COPD), lung cancer, pulmonary

heart disease, and bronchitis, and these diseases are the leading causes of death in China [US State Department, 2004; World Resources 1998-1999]. The World Bank [1997] estimated in the 1990's that approximately 178,000 deaths in China, (7% of all deaths in urban areas), and 346,000 hospitalizations related to respiratory problems could have been prevented each year if the air quality of China had met its second class (or moderate) ambient air pollutant standards.

Similar to that observed in developed countries [NRC, 1991], the air pollution problems in China are not only limited to the urban areas. Since late 1970, the number of vehicles in China has been growing at an annual rate of nearly 13%. If the number of various vehicles in 1978 is used as the unit, '1', the total passenger automobiles were 3.1 in 1990 and 33 in 2000, while total motorcycles were 33.4 in 1990, 299.3 in 2000, 343.7 in 2001. The increased emission of NO_x and other ozone precursors caused by large expansion of vehicles usage appears to be a significant factor in the accumulation of high concentrations of ground-level ozone in rural areas in China [*Chameides et al.*, 1999a; *Luo et al.*, 2000]. The high rates of coal consumption in China appears to be causing highly acidic precipitation in large parts of southern China, i.e. 30% of China's land area [*Galloway et al.*, 1987; *Wang and Wang*, 1995; *Hao and Liu*, 1997; *Streets et al.*, 1999]. Severe regional haze and smog are often observed from central to east China [*Chameides et al.*, 1999b; *Xu et al.*, 2002]. Other examples include the images by the Moderate Resolution Imaging Spectroradiometer (MODIS) on board of various NASA Earth Observing System (EOS) [<http://modis.gsfc.nasa.gov>, MODIS image gallery].

1.3.2 Regional climate

In order to identify a human-induced climate change, there are two required steps. Firstly, detection, i.e. the observed climate change must be out of the range

Table 4: The Number of Registered Motor Vehicles (thousands) in China since 1978.

Year	1978	1980	1985	1990	1995	2000	2001
Automobile	259.0 (1.0)	350.8 (1.4)	794.5 (3.1)	1621.9 (6.3)	4179.0 (16.1)	8537.3 (33.0)	9939.6 (38.4)
Truck	1001.7 (1.0)	1299.0 (1.3)	2232.0 (2.2)	3684.8 (3.7)	5854.3 (5.8)	7163.2 (7.2)	7652.4 (7.6)
Special	97.7 (1.0)	133.1 (1.4)	184.7 (1.9)	206.9 (2.1)	366.8 (3.8)	388.5 (4.0)	428.4 (4.4)
Tractor			1783.5 (1.0)	4625.8 (2.6)	5919.1 (3.3)	8209.2 (4.6)	8260.2 (4.6)
Motorcycle	126.0 (1.0)	180.2 (1.4)	946.0 (7.5)	4212.8 (33.4)	13719.3 (108.9)	37717.9 (299.3)	43307.7 (343.7)
Others	104.3 (1.0)	125.3 (1.2)	615.8 (5.9)	410.5 (3.9)	1226.9 (11.8)	3962.7 (38.0)	3932.8 (37.7)

Source: *China Statistical Year Book 2002*.

Notes: numbers in parenthesis are factors of increase compare with the vehicle number in 1978. (Statistics of 'Tractor' started from 1985.)

of the internal variation of climate system itself, or it is statistically unusual. Secondly, attribution, i.e. the climate change is caused by human activities instead of natural forces [IPCC, 2001]. Because of the complexity of the climate system, detection is largely a statistical process, while attribution requires both statistics and climate-model simulations. The model simulations are needed to demonstrate that the observed climate trends are consistent with and therefore potentially attributable to a specific human-induced effect.

There is now compelling evidence from both observational and modeling perspectives that increased anthropogenic emissions of greenhouse gases as well as the aerosol particles and their precursors from East Asia are affecting the climate system. These climate effects arise from perturbations to earth-atmosphere energy budget, including the fluxes of solar and infrared radiation, as well as to the hydrological cycle and the general circulation [Wang and Gong, 2000; Zhai and Ren, 1999; Yu et al., 2001; Qian and Giorgi, 2000; Kaiser and Qian, 2002; Xu, 2001; Menon et al., 2002]

Both warming and cooling trends have been observed in different parts of East Asia. Analysis of instrumental records together with historical documents and proxy data indicate that a warming trend, about 0.5K/100 year, has occurred in most of eastern Asia over the last hundred years [*Wang and Gong, 2000*]. This trend is comparable to the mean global warming, i.e. 0.4 to 0.8°C [*IPCC, 2001*]. More specifically, the observed average minimum temperature generally increased and the diurnal temperature range (DTR) generally decreased in the last several decades over a large part of East Asia: trends that are consistent with those expected from the impacts of increased greenhouse gases [*Zhai and Ren, 1999; Yu et al., 2001*]. The trends in observed maximum daytime temperature and mean temperature over East Asia, on the other hand, vary regionally and seasonally. These variations appear to arise from the competing effects of warming from greenhouse gases and absorbing aerosols and cooling from scattering aerosols, i.e. the greenhouse vs. the whitehouse effects [*Zhai and Ren, 1999; Wang and Gong, 2000; Qian and Giorgi, 2000; IPCC, 2001*]. The trends are spatially non-uniform because aerosols have shorter lifetimes and therefore larger spatial gradients and seasonal variations than greenhouse gases. For example, statistically significant cooling trends have been observed in both average temperature (-0.1 K/yr) and daily maximum temperature (-0.14 K/yr) over southeast China, especially the Sichuan Basin, i.e. $\sim 103^{\circ} - 107^{\circ}E, 28^{\circ} - 33^{\circ}N$. At the same time this region shows the largest increases in aerosol loading, or aerosol extinction coefficient and the largest decreases in sunshine duration [*Qian and Giorgi, 2000; Kaiser and Qian, 2002*]

In addition to temperature changes, anthropogenic pollutants may also be driving an unusual shift in precipitation patterns over the region. During the summer of a normal year, the monsoonal rainy belt shifts northward as the season progresses, bringing critical precipitation to the northern part of East Asia, where the surface water resources are highly limited, and then retreats southward and dissipates. In

recent decades, however, the monsoonal rainy belt has begun its southward retreat earlier in the season causing droughts in northern China and floods in southern China. On the basis of an analysis of historical records of drought/flooding patterns in east China by *Wang and Zhao* [1987], *Xu* [2001] concluded that this unusual pattern of ‘north drought with south flooding’ in east China during the past two decades is the most intense since AD 950, and, therefore, probably out of the range of internal climate changes.

Xu [2001] suggests that the major cause of this unusual shift in the monsoonal circulation and precipitation is the high loading of sulfate aerosols over the region, which reduces the solar surface-heating. *Menon et al.*, [2002], on the other hand, found that their global model was able to simulate the observed trend in both temperature and precipitation over the region if the effects of absorbing black carbon was included in their model. They therefore argued that there are significant effects of absorbing aerosols, i.e., black carbon (BC), on the large scale circulation and hydrological cycles of the region. BC has particularly high concentration in East Asia and mainly originates from anthropogenic sources.

1.3.3 Economical and ecological consequences

Degradation of the environment caused by the rapid industrial developments in East Asia, and especially China, has had some significant cost to the resource base and economy of the region. It has been estimated, for example, that pollution costs the Chinese economy about 7-10 % of its GDP (Gross Domestic Production) each year [US State Department, 2004; World Bank 1997]. Of particular interest is the continued viability and self-sufficiency of China’s agricultural sector: China has 22% of the world’s population living on just 7% of the world’s arable land [World Bank, 1997], and significant portions of this land (especially in the north) experience severe water stress [*IPCC*, 2001].

The recent increases in flood and drought discussed above have caused numerous loss of lives especially in the southern flooded area and severe damages to the nation's agriculture and economy. According to official Chinese government reports, 3656 people have been killed by the floods, the second worst to hit the country in more than 130 years. The floods have left 14 million people homeless, affected 240 million people, destroyed 5 million houses, damaged 12 million houses, flooded 25 million hectares of farmland, and caused over \$ 20 billion (US) in estimated damages [*US NOAA*, 1998].

In addition to the problems related to the shift in the monsoonal precipitation patterns discussed above, several recent studies have indicated that agricultural lands in China are exposed to potentially harmful amounts of phytotoxic pollutants such as ozone and acid rain, and these may be having a significant negative impacts on overall crop yields in the region [*Mauzerall and Wang*, 2001; *Chameides*, 1999a; *Streets et al.*, 1999]. Crop yields in China may also be depressed as a result of the reduction and alteration in the character of solar radiation reaching the earth's surface caused by regional haze [*Chameides*, 1999b; *Cohan et al.*, 2002].

Beside adverse effects on agriculture, wide spread acid deposition and elevated ozone concentrations may also cause harmful impacts on other unmanaged but important ecosystems, including forests, ranges, and waters. For example, soil acidification is likely to have long-term impacts on ecosystems: it is believed to be the cause of the extensive dieback of forests in Central Europe over the past decades [*World Bank*, 1997].

There may even be a linkage between ocean productivity and air pollution from East Asia. In a recent study of the biogeochemical cycle of iron in East Asia, *Meskhidze et al.* [2003] found that a significant fraction of the iron in dust particles from the deserts of East Asia can be mobilized to bioavailable forms if the dust storm tracks are infused with pollutant plumes that contain high levels of SO₂ from

the urban/industrial centers along the east coast of China. This bioavailable iron can then be deposited into remote regions of the North Pacific Ocean and trigger phytoplankton blooms. Interestingly, if correct this would imply that a decrease in SO₂ emissions in China would depress ocean productivities and C-uptakes.

1.3.4 Outflow of anthropogenic emissions to other regions

Previous ground- and airborne-based studies have shown that the outflows of anthropogenic pollutant plumes from East Asia can be exported to the North Pacific Ocean when the appropriate meteorological conditions exist. These conditions include relatively low levels of stagnation, so that pollutants emitted in the boundary layer can be vented to the free troposphere, but infrequent precipitation events to limit the wet removal of pollutants, as well as significant westerly winds capable of advecting pollutants from their source regions to the marine atmosphere. In general, conditions of this nature are most common over East Asia in the spring [Duce *et al.*, 1980; Prospero and Savoie, 1989; Merrill, 1989]. During the spring, outflows from East Asia can rapidly move pollutant (as well as mineral dust) plumes from China to the remote regions of the North Pacific Ocean and on to North America within 5-6 days [Kritz, 1990; Jaffe *et al.*, 1999, 2003]. Field experiments and modeling studies have documented the significant impact these plumes can have on the chemical composition of the remote North Pacific Ocean and, in extreme cases, even the continental United States. [Andreae *et al.*, 1988; Levy and Moxim, 1989; Parrish *et al.*, 1992; Talbot *et al.*, 1997; Jaffe *et al.*, 1999, 2003; Jacob *et al.*, 1999; Xu *et al.*, 1999]. It has been estimated using global models that about 10% of the total anthropogenic sulfur from East Asia is transported to the neighboring ocean annually [Chin *et al.*, 2000b], while the outflow can be as large as 20-30% during the winter and spring [Xu *et al.*, 1999; Tan *et al.*, 2002]. Jaegle *et al.* [2003] suggested that 17% of the O₃ and 48% of the CO in the northeast Pacific troposphere originated from East Asian emissions. Additionally,

Lagrangian back-trajectory analysis and satellite observations also provide evidence of long range transport of mineral dust and air pollutants from East Asia. One object of this thesis has been to re-examine the estimates of Chin et al. [2000b] using a higher resolution regional modeling system.

1.4 The Role of Numerical Models in the Assessment of Anthropogenic Emissions

Due to the reasons stated above, there is a compelling need to assess the magnitude and possible effects of anthropogenic emissions from East Asia. Because of the myriad of complex, non-linear, and interacting processes that ultimately determine the fate and effects of air pollutants, numerical models, especially three-dimensional coupled climate/chemical-transport models, are pivotal in carrying out this assessment.

1.4.1 Numerical models.

Numerical modeling is based on the original ideas of Norwegian hydro-dynamist *V. Bjerknes* in 1904 [*Friedman*, 1989] and British scientist *Lewis F. Richardson* [1922]. In the intervening years since this pioneering work, the explosion in computational technologies has facilitated the use of numerical models and they have now become a standard tool for weather forecasting, air quality assessments, and climate simulations [*Chaney*, 1950; *Phillips*, 1956; *Smagorinsky, et al.*, 1965; *Manable, et al.*, 1975; *Anthes and Warner*, 1978; *Anthes*, 1987; *Chang*, 1989; *Rind and Lerner*, 1996; *Kiehl, et al.* 1996; *Grell, et al.* 1996; *Byun and Ching*, 1999; *Rind et al.*, 1999; *Michalakes*, 2001; *Collins et al.*, 2003; *IPCC*, 1990, 1992, 1996, 2001]. Suffice to say, the development of modeling tools capable of assessing the impacts of human activities on the regional/global climate and air quality represents a major scientific challenge to the community of atmospheric scientists, as well as an important need for policymakers tasked with designing strategies for mitigating adverse environmental impacts.

Ideally, a model should include all physical-chemical mechanisms, as well as related biological and geological processes, including their interactions and feedbacks, and these mechanisms and processes should be treated using the fundamental equations and relationships that describe them. But due to the complexities of the earth-climate-atmospheric chemical system and limitations on computational resources, such a comprehensive simulation of the atmosphere is not realistic. Current models address these limitations by ignoring processes that are deemed to have small or negligible impacts on the model results and by adopting parameterizations that provide reasonable but not fundamental representations for some of the relevant processes and mechanisms.

1.4.2 Chemical transport models (CTMs).

Numerical simulations of air pollutants within a 3-dimensional and time dependent framework are carried out using Chemical Transport Models (CTMs) [*Raynolds et al.*, 1973, 1974; *Carmichael and Peter*, 1980; *Peters and Jovanis*, 1979; *Chang et al.*, 1987; *Carmichael et al.*, 1991; *Odman and Ingram*, 1996; *Russell*, 1997; *Levy et al.*, 1997; *Roelofs and Lelieveld*, 1997; *Wang et al.*, 1998; *Crutzen et al.*, 1999; *Byun and Ching*, 1999; *Wild and Prather*, 2000; *Horowitz et al.*, 2003]. These models typically have modules that treat pollutant emissions, transport, chemical conversion, and removal. In most current-day CTMs, the transport module is driven using meteorological fields that are specified or input into the model. These fields can be generated from an off-line global climate or general circulation model (GCM) (e.g., *Wang et al.*, [1998]; *Horowitz et al.* [2003]); from re-analyzed observed wind fields (e.g., *Bey et al.*, [2001]), or from a mesoscale meteorological model (e.g. *Byun and Ching*, 1999; *Klonecki et al.*, 2003). Using GCM's results as inputs is most useful for addressing long-term trends and impacts since the wind fields are climatological, while using reanalysis data or mesoscale model results are most useful for simulating

and evaluating model performance during specific episodes (e.g, during a field campaign) since the wind fields represent actual conditions that occurred. Both types of approaches are used in current global CTMs (eg. NCAR/MOZART-2 [Horowitz *et al.* 2003]; MATCH-MPIC [Lawrence *et al.*, 1999]).

Because the aforementioned models have no coupling of the gas and particulate tracer fields calculated in the CTM back to the meteorological/climatological fields, these models are unable to directly assess the impact of atmospheric chemistry on climate. One approach that has been used to deal with this limitation is to use the chemical fields derived in a CTM as input into a subsequent climate simulation to estimate the climate forcing (eg. Tanre *et al.*, 1984; Kiehl and Briegleb, 1993; Boucher and Anderson, 1995; Kiehl and Rodhe, 1995; Haywood *et al.*, 1995; Haywood *et al.*, 1997; Myhre *et al.*, 1998). However, this approach is limited by its inability to account for positive or negative feedbacks between chemistry and climate (see for example, Feichter *et al.*, 1996; Giorgi and Mearns, 1999]

To fully treat the coupled climate/atmospheric chemistry system one must use a model that simulates both the climatological and chemical processes simultaneously. Such on-line climate/chemical models have been developed and used, especially in the context of global simulations (e.g., Taylor and Penner, 1994; Feichter *et al.*, 1996; Koch *et al.*, 1999; Kiehl *et al.*, 2000; Adams *et al.*, 2001; Koch *et al.*, 2001; Jacobson, 2001), however because of the aforementioned limitations in computational resources, the chemical mechanism included in the model and the number of chemical species simulated by the model generally represent simplified versions of those used in the more traditional off-line CTMs (for example using prescribed or parameterized free radical fields from off-line CTMs).

1.4.3 Regional scale models

For the purpose of climate studies, the initial numerical models were often regional in scale because of the limitations on computational resources. But since the 1960's, general circulation models (GCMs) with global coverage have been the primary tool used in climate studies. With reliable projections of future external climatic forcings, chemical species emissions, land-use changes, and other related parameters (solar activities, volcanic activities, etc.), coupled global climate/chemical transport models should be able, at least in principle, to simulate future global climatic and chemical conditions.

GCMs that run at current resolutions of 200-500 km appear to be capable of simulating the global mean climate states. Because of the coarse resolution of these global models, however, they can produce biases in simulated regional climate variability with apparent errors of as much as $\pm 5^{\circ}\text{C}$ in temperature, and -40% to +60% in precipitation [Leung *et al.*, 2003; IPCC, 2001]. In a recent integrated assessment of the economic impacts on agriculture from climate change, significantly different results were obtained from climate change scenarios derived from different models with differing spatial scales (300km vs. 50km) (Mearns 2003). IPCC (2001) suggested that higher resolution models will likely provide more realistic response of the climatic system on regional scales to changes in forcing, especially for regions with high elevation, complex coastlines, or complex landuse patterns. East Asia is one such region: it includes the highest mountain range, the Himalayas, and highest plateau, Tibet, as well as areas with complex mixtures of crop land, forest, grass, lakes, and bare land. In addition most of the anthropogenic emissions within the region have large spatial gradients, with major sources clustered in relatively small urban and suburban areas.

One approach that can be used to address the need for higher resolution in regions such as East Asia (and the approach adopted in this thesis) is to make use a limited

area regional scale model. Because the model does not attempt to simulate the entire globe, it makes it possible to increase the spatial resolution without overtaxing the computational requirements. Of course the disadvantages of such models is their requirement for appropriate boundary conditions and their inability to simulate the interactions between the regional- and global scales. These disadvantages can be addressed, at least in principle, by nesting a regional model inside a global model. However, such a two-way nesting that allows for feedbacks in both directions between a global and regional model has yet to be accomplished.

Regional scale models have been widely implemented in a multitude of studies focused on meteorology, weather forecasting, and air quality [*Anthes, 1972; Anthes and Warner, 1978; Anthes, 1987; Chang, 1989; Grell, 1996; Byun and Ching, 1999; Michalakes, 2001*].

The development of a regional climate model began at the National Center for Atmospheric Research (NCAR) [*Dickinson et al., 1989; Giorgi and Bates, 1989*]. NCAR Regional Climate Model (RegCM) was initially built upon the PSU/NCAR Mesoscale Model version 4 (MM4) with modifications and augmentations of various parameterizations to make it appropriate for longer-term climate simulations and to make it capable of being nested inside the NCAR Community Climate Model (CCM). In subsequent years the model has been updated and further improved (see for example, Giorgi et al., 1993, 1999, 2002), and modules have been added to make it possible to study climate-chemistry interactions. Some of these additions were completed as part of this thesis and are documented in subsequent chapters.

1.4.4 Modeling system used in this work

In this work, the results of model simulations are presented and analyzed that have been generated using the modeling system that was initially developed in the

China-MAP project (<http://www-wlc.eas.gatech.edu/chinamap.html>). This modeling system is regional in spatial scale with a domain that covers much of East Asia (see Figure 2). The system is a hybrid of the various types of climate and CTM systems described above. It makes use of: 1. a modified version of the NCAR RegCM [*Giorgi et al.*, 1993 ab, 1999, 2002] with new algorithms for the treatment of the emissions, transport, chemical transformations, and removal of gas-phase and particulate-phase sulfur oxides is used to quantify the fate and budgets of the anthropogenic sulfur emissions of East Asia in 1995; and 2. a modified version of the Regional Acid Deposition Model or RADM [*Luo et al.*, 2000], a regional CTM with detailed and comprehensive algorithms for the treatment of relevant gas- and particulate-phase species. The RegCM is used to generate the meteorological fields used to drive RADM as well as to directly assess the budget and fate of sulfur oxidized emitted from East Asia. The RADM is used to provide a detailed simulation of the gas- and particulate-phase chemistry of the atmosphere overlying China to compare to chemical measurements made at rural site in China and thereby assess the accuracy of the pollutant emissions inventory recently developed by Streets [2003].

1.5 Outline of This Thesis

This thesis focuses on better understanding and quantifying the budget and fate of anthropogenic pollutants from East Asia. Specifically, the following scientific questions are addressed:

1. What is the spatial distribution of the concentrations and deposition patterns of anthropogenic pollutants over East Asia and the western North Pacific Ocean?
2. Can an on-line coupled regional climate-chemistry model (with simplified chemical algorithms) simulate the observed concentrations and deposition rates of sulfur oxides over East Asia and the western North Pacific Ocean?
3. What is the budget of anthropogenic sulfur oxides from East Asia? What

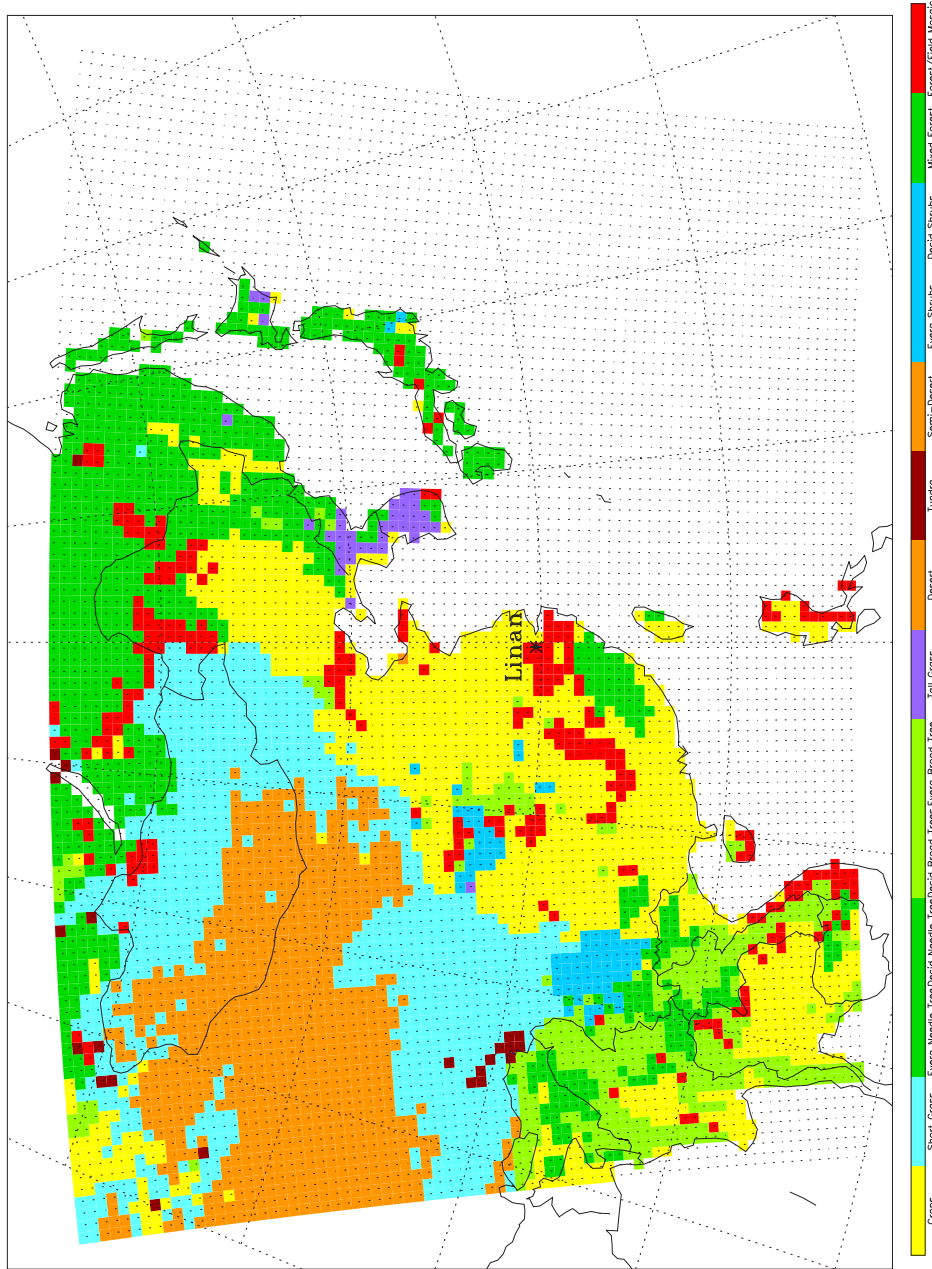


Figure 2: Spatial coverage of our modeling system. 'x' is the center of each model grid. Color patches are the landuse derived from Global Land Cover Characterization (GLCC) 30" dataset.

fraction of the sulfur oxides that are emitted end up being exported out of the region?
Are the nations of East Asia net exporters or importers of sulfur oxide pollution?

4. How accurate are current-day emission inventories for the major air pollutants emanating from East Asia?

5. Using a combination of regional model simulations and simultaneous gas-phase and particulate-phase measurements at a rural site in China, what constraints can be placed on pollutant emission rates from East Asia?

6. To the extent that current emission inventories from East are inaccurate, how can model simulations and measured data be used to identify the nature of these inaccuracies and how they might be removed in future inventories?

This thesis is organized into 4 chapters:

Chapter 2: Examination of the budget and export of anthropogenic SO_x (SO_2 and particulate sulfate) emitted from East Asia during the late winter/early spring when continental outflow conditions dominate.

Chapter 3: Evaluation of the anthropogenic emissions inventories from East Asia and diagnosis of possible additional sources.

Chapter 4: Conclusions of this study and future research plan.

CHAPTER II

BUDGET AND EXPORT OF ANTHROPOGENIC SO_x FROM EAST ASIA DURING CONTINENTAL OUTFLOW CONDITIONS

2.1 Introduction

There is increasing evidence that the trace chemistry of the atmosphere is changing on hemispheric and even global scales [NRC, 1998]. Of particular concern are perturbations in the concentrations and distributions of sulfate aerosols. These aerosols affect the solar irradiance reaching the earth's surface and, as a result, can influence the climate [Charlson *et al.*, 1992; Penner *et al.*, 1994; IPCC, 1996; Schwartz, 1996; Schwartz and Andrea, 1996], visibility [Husar *et al.*, 2000] and photosynthesis rates [Chameides *et al.*, 1999b]. They may also adversely affect human health [Dockery and Pope, 1994].

While sulfate aerosols are produced naturally in the atmosphere, for example from the oxidation of dimethylsulfide [Cox and Sheppard, 1980; Atkinson *et al.*, 1984; Chatfield and Crutzen, 1984; Berresheim *et al.*, 1996], they are also produced as a result of anthropogenic activities [Charlson *et al.*, 1990; Charlson *et al.*, 1991; Berresheim *et al.*, 1996; Rodhe, 1999]. Anthropogenic sulfate arises primarily from the oxidation of anthropogenic sulfur dioxide (SO₂), which in turn comes primarily from the burning of fossil fuels. As noted in Chapter 1, East Asia is an especially large source of sulfur oxide emissions.

Recent model calculations indicate that SO_x emissions from East Asia (and more specifically China) are already having significant regional environmental consequences due to haze production [Chameides *et al.*, 1999b; Cohan *et al.*, 2002]. And climate trend analyses suggest that they may also be perturbing regional climate [Qian and Giorgi, 2000; Kaiser and Qian, 2002, and see Chapter 1]. Other model calculations indicate that these same emissions may soon have non-negligible effects upon Northern Hemispheric and even global particulate matter concentrations [Berntsen *et al.*, 1996; Berntsen and Karlsdottir, 1999; Elliott *et al.*, 1997; Mauzerall *et al.*, 1997; Kasibhatla *et al.*, 1997; Bey *et al.*, 1999; Jaffe *et al.*, 1999; Carmichael *et al.*, 1998; Jacob *et al.*, 1999; Wilkening *et al.*, 2000; Phadnis and Carmichael, 2000a]. Of particular concern in this regard are the export of pollutants from East Asia during the late winter/early spring, when continental outflow to the North Pacific Ocean is at its height [Merrill *et al.*, 1989; Talbot *et al.*, 1997]. To better quantify the rate at which sulfur oxides from East Asia is exported, we have carried out model simulations of the emissions, chemical conversion, removal, and transport of anthropogenic SO_x over East Asia and the western North Pacific Ocean during February, March, and April using the China-MAP regional coupled climate/chemical transport modelling system.

2.2 Model Description

Our simulations were carried out using a modified version of the coupled regional climate/chemical transport model described by Qian *et al.* [1999]. The model uses the NCAR Regional Climate Model (RegCM) described by Giorgi *et al.* [1993a, 1993b, 1999] with on-line algorithms to treat the emission, gas-phase, aqueous-phase, heterogeneous chemical processing, wet and dry deposition, and transport of sulfur oxides (SO_x). NCAR RegCM was built upon NCAR-Pennsylvania State University Mesoscale Model Version 4 (MM4), and several physics parameterizations were modified for long-term climate simulation. Detailed description of model and its validation

are included in *Giorgi et al.* [1993a, 1993b, 1999]. The model treats SO_x as two coupled chemical species: gaseous SO_2 and sulfate aerosol (SO_4^{2-}). In the model in its current form, SO_4^{2-} is treated as a monodisperse, externally mixed aerosol with a nominal diameter of $0.1 \mu\text{m}$. The model domain covers a horizontal grid of $60 \text{ km} \times 60 \text{ km}$ cells on a Lambert conformal projection over a domain spanning coordinates: 48.42°N , 84.42°E ; 48.66°N , 154.4°E ; 14.09°N , 99.43°E ; and 14.21°N , 140.1°E (see Figure 3). The dynamical portion of the model (i.e., RegCM) is driven by lateral meteorological boundary conditions from the analysis of observations from the European Center for Medium-Range Weather Forecasts (ECMWF) for the 1995 period.

The chemical transport algorithms in the model solve two coupled prognostic equations for the time rate of change in the mixing ratios of SO_2 and SO_4^{2-} as a function of location:

$$\frac{\partial \chi_i}{\partial t} = E_i - V \nabla \chi_i + F_{H,i} + F_{V,i} + T_{gas,i} + T_{hetero,i} + T_{ls,i} + T_{conv,i} + T_{below-cloud,i} + T_{dep,i} \quad (1)$$

where χ_i is the mixing ratio (in units of kg/kg) for the i^{th} species (i.e., $i = \text{SO}_2$ or SO_4^{2-}), E_i is surface emission rate of the i^{th} species; the second term on right hand side is horizontal and vertical advection; $F_{H,i}$ and $F_{V,i}$ are horizontal and vertical turbulent diffusion, respectively; $T_{gas,i}$ is the chemical tendency of the i^{th} species due to gas phase reactions; $T_{hetero,i}$ is the tendency due to heterogeneous reactions; $T_{ls,i}$ and $T_{conv,i}$ are the tendencies of the i^{th} species due to processing by large-scale and convective clouds, respectively; $T_{below-cloud,i}$ is the rate of removal by below-cloud scavenging; and $T_{dep,i}$ is the dry deposition rate. The advection and turbulent diffusion terms for SO_2 and SO_4^{2-} in Equation(1) were specified using the modules within RegCM that are used to calculate advective and turbulent transport for water vapor. The formulations used for each of the other terms in Equation (1) are briefly discussed below. For more details the reader is referred to *Giorgi et al.* [1993a,b] and *Qian et al.* [1999], as well as the references cited therein.

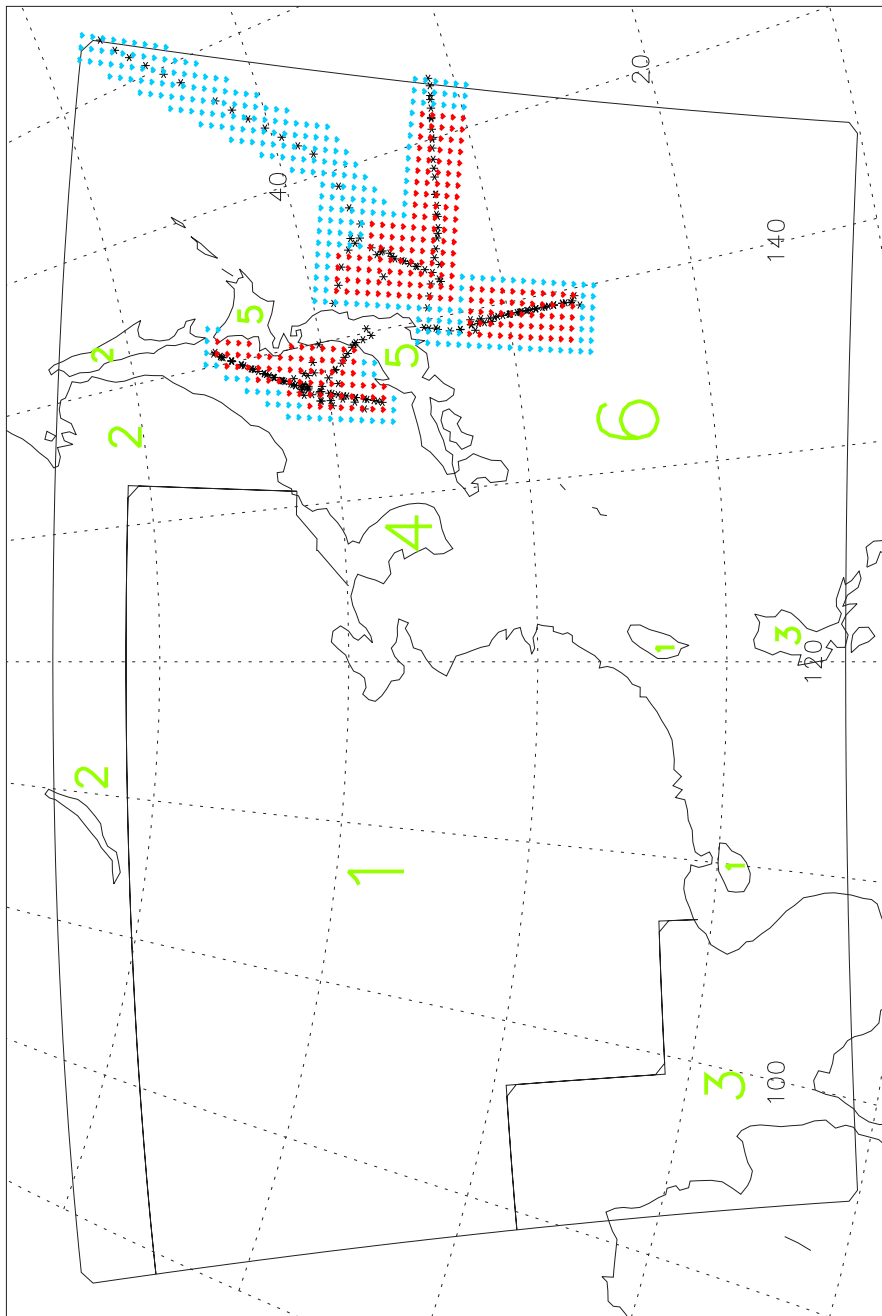


Figure 3: Spatial domain for model calculations. Also indicated: six subregions used to study the sulfur budget ('1' = China (including Mongolia); '2' = South Russia/East Kazakhstan; '3' = South Korea; '4' = Southeast Asia; '5' = Japan; and '6' = Ocean); the PEM-West B flight tracks within our model domain for which SO_2 and/or SO_4^{2-} data were available (****); and the region from which model calculated concentrations were used to compare to PEM-West B observations (red and blue dots for SO_2 and red dots for SO_4^{2-}).

2.2.1 Emissions

As our focus is on the fate and export of anthropogenic SO_x from East Asia, we only consider anthropogenic sources of these compounds. Figure 4 illustrates the averaged monthly SO_x emissions during the simulation period. Gridded monthly averaged emissions of SO_x over China were obtained from the 1995 emission inventory of *Streets and Waldorf* [1999]. SO_x emissions over the non-Chinese portion of the domain were interpolated from the Global Emissions Inventory Activity (GEIA) inventory [Penner *et al.*, 1994]. Of the total SO_x emissions, 98% was assumed to be in the form of SO_2 and 2% in the form of SO_4^{2-} .

2.2.2 Gas-phase chemical conversion

The $T_{gas,i}$ terms in Equation (1) are used to represent the rate of conversion of SO_2 to SO_4^{2-} that is triggered by the gas-phase reaction between SO_2 and the OH radical [Calvert and Stockwell, 1983]. Thus,

$$T_{gas,\text{SO}_2} = -T_{gas,\text{SO}_4^{2-}} = -n(\text{OH}) k_{\text{OH},\text{SO}_2} \chi_{\text{SO}_2} \quad (2)$$

where $n(\text{OH})$ is the OH number density and $k_{\text{OH},\text{SO}_2}$ is the effective second order rate constant for the reaction [DeMore *et al.*, 1994]. In the calculations presented here, appropriate values for $n(\text{OH})$ as a function of time and location were specified using the results of the China-MAP chemical transport model simulations of East Asia of Luo *et al.* [2000].

2.2.3 Heterogeneous reactions

Following Kasibhatla *et al.* [1997] we have included an additional pathway for the conversion of SO_2 to SO_4^{2-} that is nominally intended to account for the effect of heterogeneous reactions with pre-existing aerosols. The reaction was assumed to only occur within the boundary layer and to result in a 2-day lifetime of SO_2 against

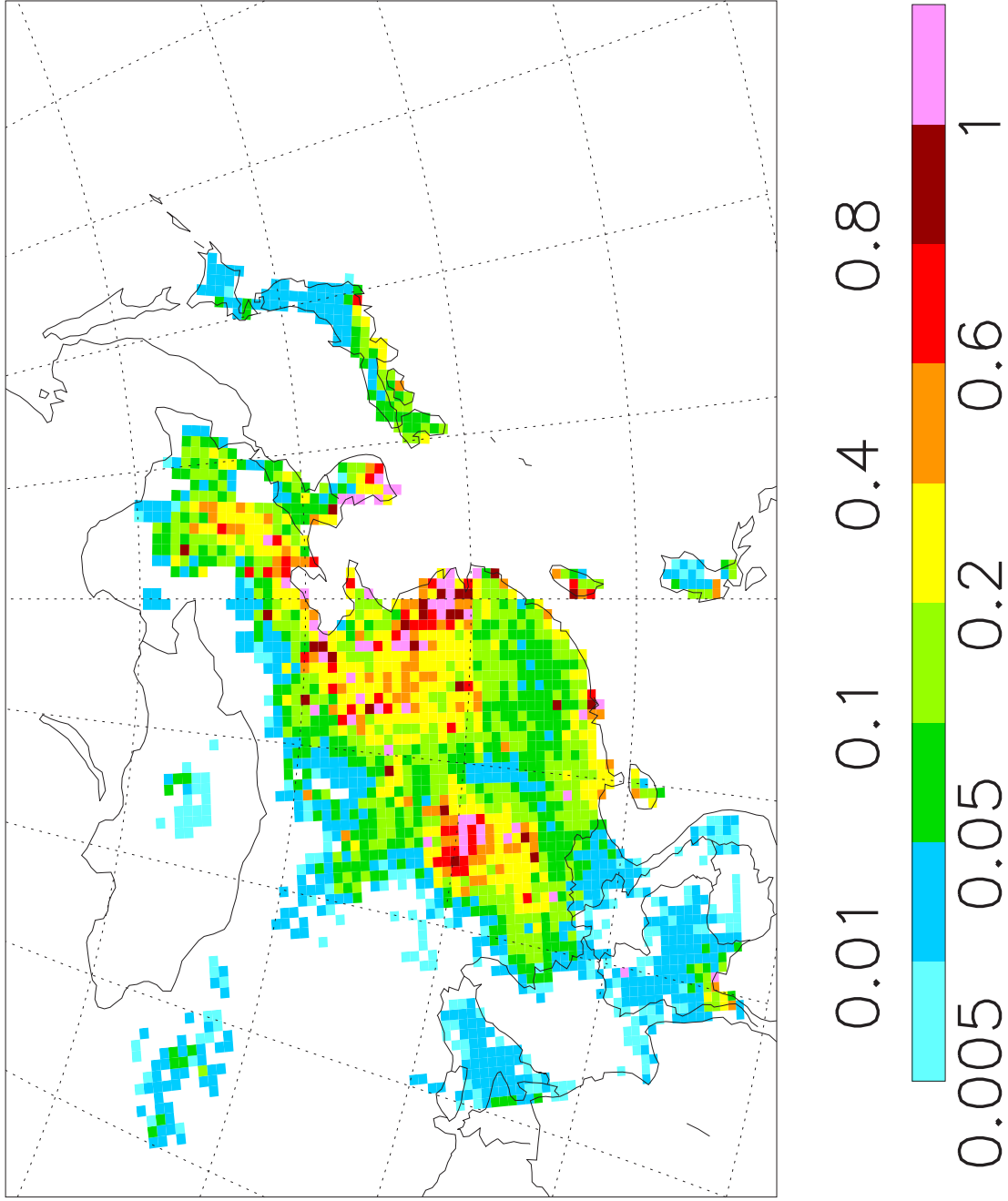


Figure 4: Averaged monthly SO_x emissions (in $gS/m^2/month$) during February to April, 1995.

reaction with aerosols within the boundary layer. Hence, within the boundary layer,

$$T_{hetero,SO_2} = -T_{hetero,SO_4^{2-}} = -6.0 \times 10^{-6} \chi_{SO_2} \quad (3)$$

and above the boundary layer,

$$T_{hetero,SO_2} = -T_{hetero,SO_4^{2-}} = 0 \quad (4)$$

2.2.4 Large-scale cloud processing

The RegCM treats two types of clouds: large-scale or resolvable-scale clouds and convective clouds. Following *Kasibhatla et al.* [1997], we assume that the processing of SO₂ within clouds is controlled by the rate at which SO₂ is oxidized within cloud water. Further assuming that the aqueous-phase oxidation of dissolved SO₂ is initiated by reaction with dissolved H₂O₂, [*Koch et al.* 1999; *Chin et al.* 2000a; *Adams et al.* 2001] and that the process is limited by the availability of H₂O₂ and SO₂ rather than by mass transport between the aqueous- and gas-phases. The aqueous oxidation by O₃ is neglected for it has been shown to be a less important pathway [*Rasch et al.*, 2000]. It follows that the SO₂ tendency within large-scale clouds is given by

$$T_{ls,SO_2} = frac_{ls} [exp(\frac{-w_L dt}{360}) - 1] min(\chi_{SO_2}, \chi_{H_2O_2}) \quad (5)$$

where $frac_{ls}$ is the fraction of the grid box that contains large scale clouds (i.e., 1 except where convective clouds are also present, then 0.7), w_L is the liquid water content of the cloud as calculated by the dynamical portion of the model for the appropriate grid box and time step (see [Giorgi,1993a,b]), the number 360 in the denominator of the exponential function was adapted from *Chameides* [1984] to give an appropriate rate of oxidation as a function of w_L , and dt is the model time step (i.e., about 3 minutes). It should be noted that the assumption of oxidant limitation on S(IV) in-cloud conversion has a relatively minor impact on our results. For example, if we assume no oxidant limitation, regardless of the SO₂ concentration, the sulfate concentration over urban areas is increased by at most 20%, and the total amount of

sulfate deposition over the model domain and sulfate export from the model domain are increased and decreased, respectively, by about 6%.

The oxidation of dissolved SO_2 within cloud water leads to the production of SO_4^{2-} . However, a fraction of this in-cloud-generated SO_4^{2-} , along with the ambient SO_4^{2-} that is entrained into the cloud, is removed by precipitation. Observations suggest that in-cloud scavenging coefficients for sulfate particles are essentially equal to unity [Hegg and Hobbs, 1983; Seinfeld and Pandis, 1998]. We therefore assume that all SO_4^{2-} within the clouds is dissolved in cloud water, and when the cloud water evaporates, the SO_4^{2-} not rained out is returned to the atmosphere as aerosol. Hence, the tendency for SO_4^{2-} within large-scale clouds is given by

$$T_{ls,SO_4^{2-}} = [\exp(-r_{rem}dt) - 1] [frac_{ls} \chi_{SO_4^{2-}} - T_{ls,SO_2}] \quad (6)$$

where r_{rem} is the so-called autoconversion frequency for the production of rain from cloud water [Georgi and Chameides, 1986; Georgi et al., 1999].

2.2.5 Convective cloud processing

In addition to chemical processing and wet removal, convective clouds can affect the distribution of SO_x through convective transport. It is important that this process be appropriately simulated here, since convective transport can move SO_x from the boundary layer and lower free troposphere into middle and upper free troposphere where it can be more effectively transported over long distances. We have modified the model of Qian et al. [1999] to more accurately account for this process. Our treatment assumes that convective transport and wet removal of SO_x by convective clouds closely follows that of water vapor and thus makes use of many of the same algorithms used in RegCM to treat water vapor in convective clouds. By way background, we briefly discuss how the RegCM simulates water vapor in convective clouds before we present the specific algorithms used to treat the processing of SO_x within these clouds.

2.2.5.1 Treatment of Water Vapor in Convective Clouds

Because of their horizontal scale, convective clouds are not resolved by the RegCM, as is the case for most regional and global models. Parameterizations must therefore be used to describe the relevant convective cloud processes using the variables simulated by the model [Arakawa, 1993]. Currently the RegCM's treatment of convective clouds is based on the Kuo scheme [Kuo, 1974; Anthes *et al.*, 1987], which is, in turn, based on the assumption that convective clouds form when a sufficient amount of water vapor converges in an unstable vertical column of air.

For each vertical column in the model grid and at each time step, S_{qv} , the rate of water vapor convergence, is calculated as:

$$S_{qv} = \sum_{column} qv_{tendency} \quad (7)$$

where qv is the mixing ratio of water vapor, and $qv_{tendency}$ is the tendency of water vapor at a given model height caused by horizontal advection. If S_{qv} is larger than a critical value (taken to be $3.0 \times 10^{-5} kgm^{-2}s^{-1}$, [Anthes *et al.*, 1987]) and the atmospheric stratification is unstable, then a convective cloud is activated within the model in that vertical column for that time step.

The converged water vapor, S_{qv} , within a column that has an active convective cloud is partitioned by the model into two components. One component is removed as precipitation, and the other is redistributed back to the atmosphere. The partitioning function P_{convg} is defined as the portion of the converged water vapor that is redistributed back to the atmosphere and is calculated as:

$$P_{convg} = 2(1 - \overline{RH}), \quad \text{when } \overline{RH} \geq 0.5 \quad (8)$$

$$P_{convg} = 1.0, \quad \text{when } \overline{RH} < 0.5 \quad (9)$$

where \overline{RH} is the column averaged relative humidity. The amount of water vapor returned to each vertical layer, z_k , within the column is given by

$$[H_2O \text{ vapor detrained from cloud at level } z_k] = P_{convg} S_{qv} w(z_k) \quad (10)$$

where $w(z_k)$ is a vertical weighting factor that is, in turn, a function of relative humidity [Anthes, 1977]. Thus, T_{conv,H_2O} , the water vapor tendency due to the precipitation in the convective cloud at level z_k is given by

$$T_{conv,H_2O} = P_{conv} S_{qv} w(z_k) \quad (11)$$

2.2.5.2 Convective Cloud Algorithms for SO_x

Given that the transport, conversion and removal of SO_x in convective clouds are closely related to the behavior of water vapor, we have chosen to parameterize the behavior of these species using a scheme closely related to the Kuo-scheme for water vapor discussed above.

We first calculate the total amounts of SO_2 and SO_4^{2-} that are entrained into a convective cloud at vertical level z_k by assuming that the amount of tracer that enters the cloud is proportional to the amount of water vapor that enters the cloud and the relative concentrations of the tracer and water vapor at that level. Thus,

$$En(z_k)_i = qv_{tendency} \left(\frac{\chi_i}{qv} \right) \quad (12)$$

and

$$S_i = \sum_{cloud_base}^{cloud_top} En(z_k) \quad (13)$$

where $En(z_k)$ is the rate at which tracer 'i' is entrained into the cloud at the z_k vertical level and S_i is the column integrated amount of tracer 'i' entrained into the cloud.

For SO_2 , a fraction of the total amount that is entrained into the cloud is oxidized to SO_4^{2-} and the remainder is redistributed back to the atmosphere as SO_2 with the same vertical weighting as that of water vapor. Following the formulation adopted for large-scale clouds in Section 2.3, the fraction, P_{oxid} , of the entrained SO_2 that is oxidized is given by

$$P_{oxid} = 1. - \exp(-T_{cumulus} w_L / 360) \quad (14)$$

where $T_{cumulus} = 30min$, is the typical lifetime of a mature stage of convective cloud [Rogers,1989] and $w_L = 2 \text{ g/m}^3$ is the assumed liquid water content of a convective cloud [Giorgi and Chameides, 1986].

From the above equations, it follows that the tendency for SO_2 at vertical level z_k due to convective clouds can be expressed as:

$$T_{conv,SO_2} = -En(z_k)_{SO_2} + S_{SO_2} (1 - P_{oxid}) w(z_k) \quad (15)$$

Similarly, the tendency for SO_4^{2-} in convective clouds is given by:

$$T_{conv,SO_4^{2-}} = -En(z_k)_{SO_4^{2-}} + S_{SO_4^{2-}} P_{conv} w(z_k) + S_{SO_2} P_{oxid} P_{conv} w(z_k) \quad (16)$$

where the first term on the right-hand-side represents the loss of SO_4^{2-} due to cloud entrainment, the second term represents the amount of the entrained SO_4^{2-} that is returned to the atmosphere and the last term is the amount of SO_2 that is oxidized within the cloud and redistributed into the atmosphere as SO_4^{2-} .

2.2.6 Below-cloud scavenging

Our parameterization for below cloud removal is based on that of *Levine and Schwartz* [1982]. The tendency for SO_2 is specified as

$$T_{below-cloud,SO_2} = -6.5 \times 10^{-5} Precip^{0.68} \chi_{SO_2} \quad (17)$$

where $Precip$ is the below cloud precipitation rate (in mm hr^{-1}).

Sulfate aerosols are generally found in the accumulation model (i.e. sub-micron to micron diameter range). *Dentener and Crutzen* [1993] suggested that these type of aerosols can be represented with a log-normal distribution having a number mean diameter of $0.078 \mu\text{m}$ and standard deviation 2.0. The calculation of *Dana and Halesand* [1976] suggests that the rainout rate constant for such an aerosol distribution is about 0.01 mm^{-1} normalized to the precipitation rate. If we assume a typical

large-scale precipitation rate of 2 mm h^{-1} [Balkasiet *et al.*, 1993], the lifetime of accumulation mode aerosols in the precipitation column is about 50 hours. This suggests that aerosols of this size are not effectively scavenged by falling raindrops, and thus we assume that

$$T_{\text{below-cloud}, \text{SO}_4} = 0 \quad (18)$$

To the extent that below-cloud scavenging of sulfate aerosols is important, this assumption would cause us to under-predict sulfate wet deposition.

2.2.7 Dry deposition

Dry deposition rates for SO_x are parameterized using dry deposition velocities. For SO_2 , the dry deposition velocities over land are set at 0.25, 0.27, and 0.30 cm s^{-1} for the months of February, March, and April, respectively. The values were estimated using data from CASTNET [Clean Air Status and Trends Network]. And it is 0.8 cm s^{-1} over water. For SO_4^{2-} , a constant deposition velocity of 0.2 cm s^{-1} was specified throughout.

2.3 Model Simulations

To assess the fate and export of anthropogenic SO_x from East Asia during late winter/early spring outflow conditions, we carried out a series of 3 $\frac{1}{3}$ month simulations using conditions appropriate for the period spanning February 1 1995 to May 10, 1995. Since the focus of our study is on the fate of anthropogenic emissions from East Asia, we preclude any influence of emission from other regions by adopting boundary value for both SO_2 and SO_4^{2-} at their nominal background levels (i.e., 10 pptm). At the start of the model simulation, the concentrations of SO_2 and SO_4^{2-} were set to background levels throughout the model domain. The model was then run for 3 months with the appropriate levels and distribution of anthropogenic SO_x emissions. At the end of the third simulation-month (i.e., April), the anthropogenic emissions

were then turned off and the model was run until SO_x concentrations returned to their background levels, generally this required about 10 days of simulation. The budget of the SO_x emitted into the model domain was assessed by calculating the fractions of the emissions from each month and for all three months combined that were dry- and wet-deposited on to the model domain, as well as that exported out of the model domain to the north, east, south, and west. The budget was further refined by quantifying the fractional amounts of SO_x emitted from and deposited into each of 6 subregions of the model domain (i.e., China, South Russia and East Kazakhstan, Southeast Asia, Korea, Japan, and Ocean). The spatial extent of each subregion is illustrated in Figure 3.

2.3.1 Simulated SO_x distributions and comparison with observations

The average model-calculated distributions in SO_2 and SO_4^{2-} at the surface and at 500 hpa (i.e., 5-6 km) are illustrated in Figures 5 and 6, respectively. Surface SO_2 concentrations are closely related to their emission sources. Large gradients exist between industrialized regions and remote ones. SO_4^{2-} , on the other hand, is spread over a larger domain with smaller gradients. Over high emission regions, SO_2 concentrations decrease rapidly with altitude, over two orders of magnitude between the surface and 500 hpa. SO_4^{2-} has a much smaller vertical gradient, about factor of 10-20 decrease in the same vertical extension.

Tables 5 and 6 compare our model calculated surface concentrations for SO_2 and SO_4^{2-} with the limited data available for these species from non-urban surface-monitoring sites within the model domain and general period of the simulation. The observed concentrations span a range of more than an order of magnitude for SO_2 (i.e., 0.1 to 15 ppbv) and SO_4^{2-} (i.e., 2 to 28 $\mu\text{g m}^{-3}$). With a few notable exceptions, the model-simulated concentrations fall within a factor of 2 or less of the observed values. These exceptions include rather large model overestimates of SO_2 at the Long

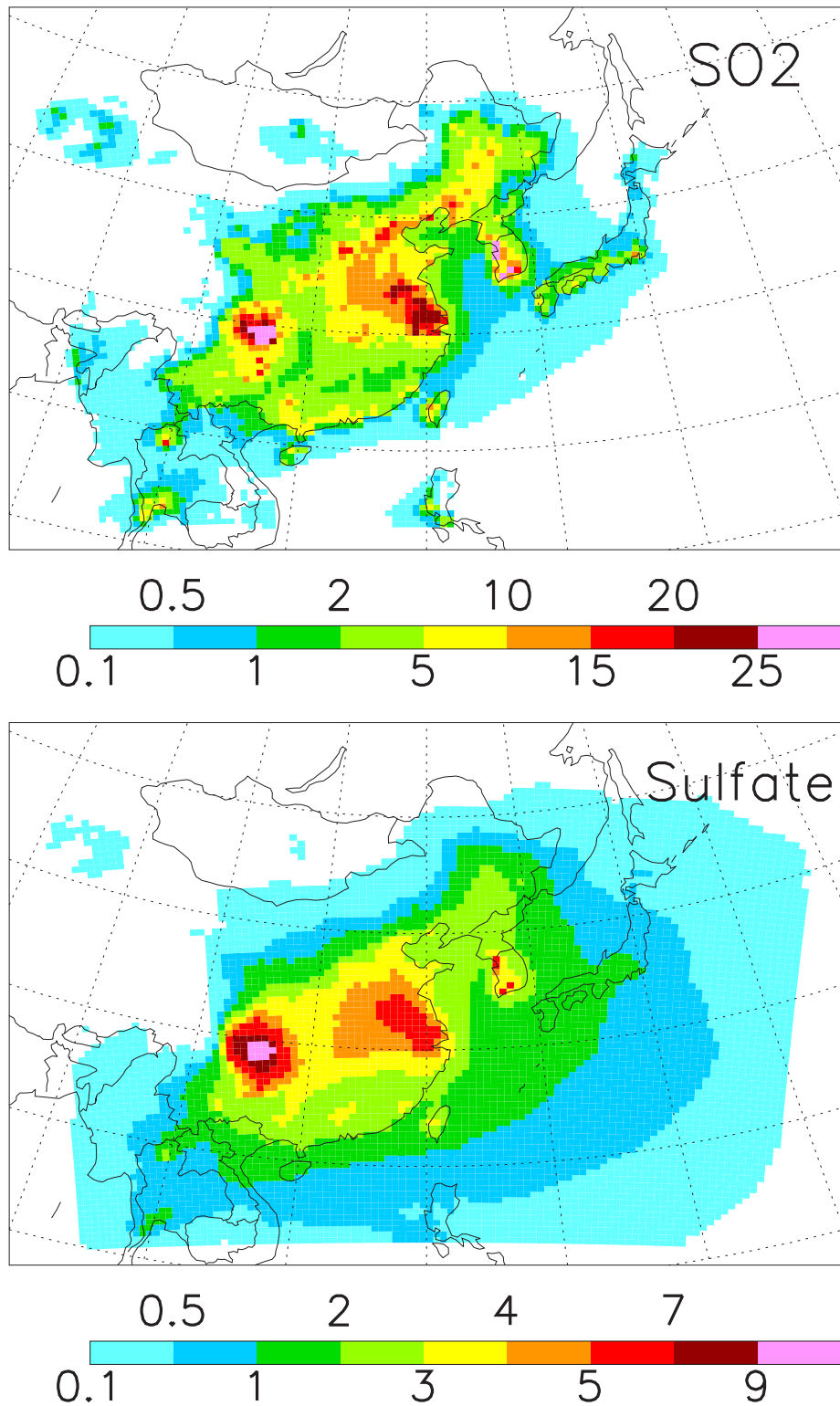


Figure 5: Monthly averaged (February to April) model-calculated SO_x concentrations (in ppbv) at the surface.

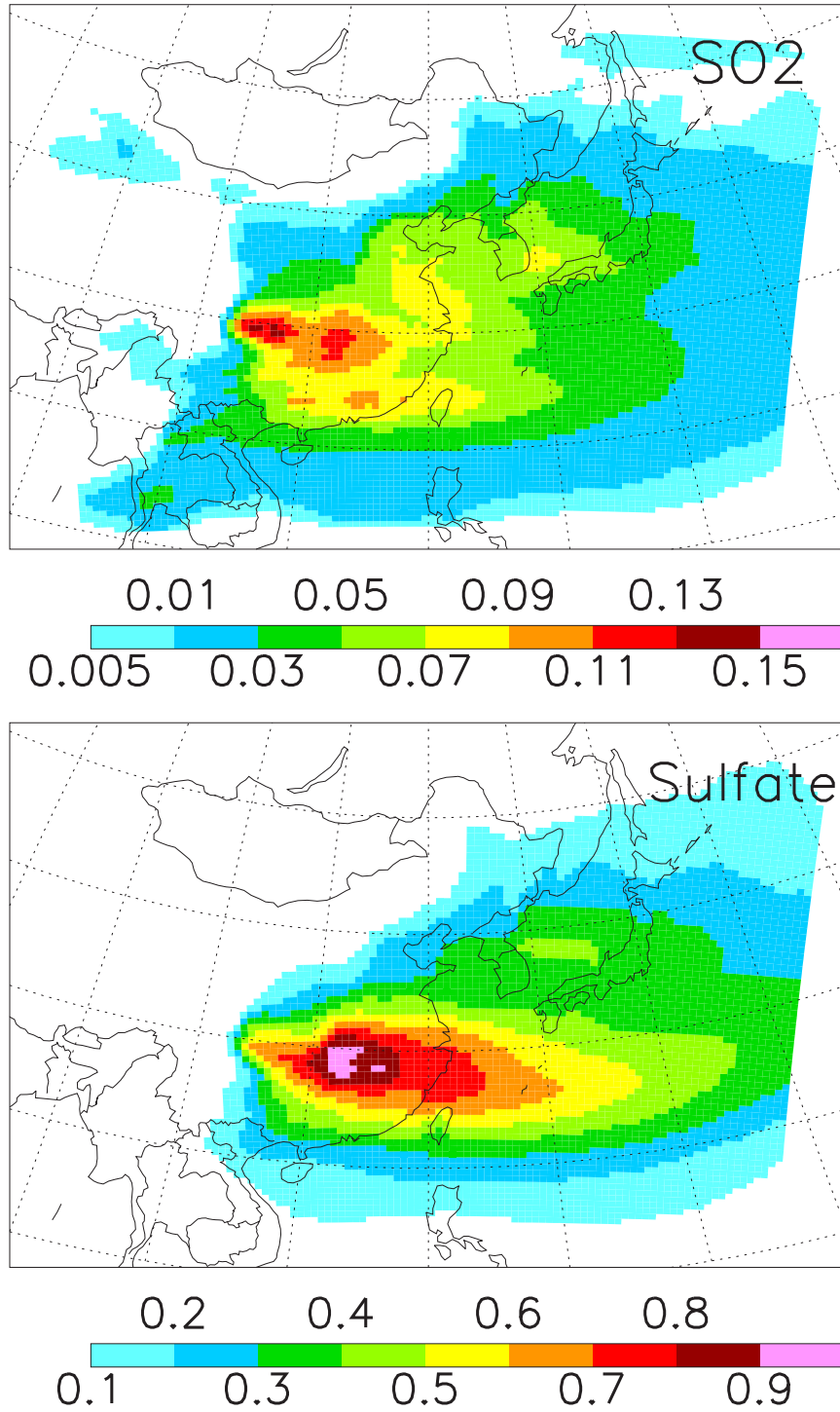


Figure 6: Monthly averaged (February to April) model-calculated SO_x concentrations (in ppbv) at 500 hpa.

Feng and Waliguan sites (see Table 1). Both of these sites are located outside the region where most of the pollutant SO_x is located in our model. This suggests that the discrepancy might have been caused by overly rapid dispersal of pollutants in the model. However, this is not consistent with the fact that the model-calculated SO_4^{2-} at Long Feng was more than a factor of 2 less than the observed SO_4^{2-} (see Table 2). At Taen, which is located off the west coast of Korea, our model overestimates the measured concentrations reported for both SO_2 and SO_4^{2-} . However, the reported measured values from Taen represent only those concentrations observed under meteorological conditions that minimized the impact of emission from the Korean continental and thus are likely lower than the actual monthly means. Perhaps most critical for our assessment of the rate of export of SO_x from East Asia is the fact that the model-calculated SO_x concentrations agree reasonably well with the easternmost sites with relevant data (i.e., Okinawa and Cheju).

In Table 7, we compare our model results with airborne observations of SO_2 and SO_4^{2-} made in the western North Pacific Ocean in March 1994 during PEM-West B [Thornton *et al.*, 1999; Davis *et al.*, 2000; Talbot *et al.*, 1997]. The observed SO_x concentrations listed in Table 3 are based on measurements made during the experiment within our model domain (the flight tracks used to make these measurements (SO_2) are illustrated in Figure 3). These measurements were first divided by altitude into three vertical layers (0 -1 km, 1 - 6 km, and above 6 km) and then averaged. The model-calculated SO_x concentrations listed in Table 7 are averages of the results obtained for the month of March over the region of the model domain that roughly corresponds to the flight tracks used in PEM West B (see Figure 3). From Table 7 we see that the model-calculated SO_2 concentrations are less than the observed SO_2 for all three vertical levels. The under-prediction is only about 25% in the 0 - 1 km layer, but grows to about 50% in the highest vertical level. The model-calculated SO_4^{2-} concentrations are reasonably close to the observations (i.e. within about 20%)

Table 5: Comparison of Model-Simulated and Observed SO₂ Concentrations (ppbv)

Location*	Model	Simulat. Month	Observ.	Observ. Time	Source
Lin An	17	February	13	February, 1995	<i>a</i>
	12	March	15	March, 1995	<i>a</i>
	11	April	14	April, 1995	<i>a</i>
Long Feng	7	February	1	February, 1995	<i>a</i>
	4	March	1	March, 1995	<i>a</i>
	3	April	1	April, 1995	<i>a</i>
Qing Dao	15	February	25	February, 1995	<i>a</i>
	10	March	13	March, 1995	<i>a</i>
	9	April	13	April, 1995	<i>a</i>
Cheju	1	March	1	March, 1994	<i>c</i>
	0.4	April	~ 1	April, 1994	<i>c</i>
Taen	2	April	1-2	April, 1998-99	<i>d</i>
Waliguan	0.7	March	0.1	March, 1995	<i>b</i>
	0.6	April	0.2	April, 1995	<i>b</i>

Source: *a*: Yan, et al., [1997]; *b*: Yu, et al., [1996]; *c*: Chen, et al., [1997]; *d*: Kim, et al., [2001]

*: Lin'An (30°N,120°E), Long Feng (45°N,128°E), Qing Dao (36°N,121°E), Cheju (34°N,126°E), Taen (37°N,126°E), Waliguan (36°N,101°E)

Table 6: Comparison of Simulated and Observed SO₄²⁻ (μg m⁻³)

Location*	Model	Simulat. Month	Observ.	Observ. Time	Source
Lin An	17	February	14	February 21-28, 1994	<i>a</i>
	12	March	16	March, 1992-94	<i>a</i>
	11	April	28	April, 1995	<i>b</i>
Long Feng	4	April	9	April 1995	<i>b</i>
Cheju	7	February	7	February, 1992-94	<i>a</i>
	5	March	4	March, 1992-94	<i>a</i>
Taen	5	April	~ 2	April, 1998-99	<i>c</i>
Hong Kong	6	February	9	March, 1992-94	<i>a</i>
	5	March	9	March, 1992-94	<i>a</i>
Okinawa	4	February	5	February, 1992-94	<i>a</i>
	3	March	3	March, 1992-94	<i>a</i>

Source: *a*: Arimoto, et al., [1997]; *b*: Yan, et al., [1997]; *c*: Kim, et al., [2001].

*: Lin An (30°N,120°E), Long Feng (45°N,128°E), Cheju (34°N,126°E), Taen (37°N,126°E), Hong Kong (22°N,114°E), Okinawa(27°N,128°E)

Table 7: Comparison of Simulated and Aircraft measured SO₂ (pptv) and SO₄²⁻ (pptv)

Altitude	SO ₂		SO ₄ ²⁻	
	Model ^a	Observation ^b	Model ^c	Observation ^d
0-1km	180	240	379	414
1-6km	115	190	279	233
above 6km	13	26	43	96

Source: Thornton et al., 1999; Davis, 2000; Talbot et al., 1997.

^a: Averaged model results from March over the red and blue dotted area in Figure 3; this area chosen to overlap with the PEM-West B flight listed in footnote 'b'.

^b: Geometric mean of observed SO₂ from PEM-West B flights during March 4, 5, 6, 7, 11 and 13, 1994. See Figure 3 and <http://www-gte.larc.nasa.gov/FM.html> for more details.

^c: Averaged model results from March over red dotted area in Figure 3; this area chosen to overlap with the PEM-West B flight tracks listed in footnote 'd'.

^d: Mean of observed SO₄²⁻ from PEM-West B flights during March 4, 6, 7, 11, 1994. See Figure 3 and <http://www-gte.larc.nasa.gov/FM.html> for more details.

in the lower two levels. Above 6 km, the model-calculated SO₄⁻² is less than the observed concentration by a little more than a factor 2. A likely explanation for the underprediction in both SO₂ and SO₄²⁻ is the fact that our simulations only considered anthropogenic emissions from East Asia. Given the distance of some of the PEM West B flights from the Asian continent, it is likely that the observed SO₂ and SO₄⁻² concentrations from these flights were significantly influenced by other sources such as DMS oxidation and, especially at high altitudes, by volcanic emissions and long range transport. Nevertheless, the results suggest that our model should be able to do a reasonably good job simulating the export of SO_x from East Asia. As we discuss later, our results indicate that most of the export occurs as SO₄⁻² transport between about 2 and 6 km, a vertical region where our model-calculated SO₄⁻² is quite close to the PEM-West B observed concentrations.

In Figure 7 we compare model-calculated wet deposition rates over China to deposition rates reported by Ding et al. [1995] for the spring of 1993 from 81 precipitation

monitoring sites located throughout China (73 of these were located east of the 100°E meridian where most of the anthropogenic SO_x is emitted). To filter out the high level of spatial variability found in this data set, we averaged the data from *Ding et al.* [1995] into 5 individual 10° x 10° grid averages using geometric means), and it is these averages that are presented in Figure 7. When we consider the deposition over the eastern portion of China, the model-calculated and observed deposition rates are in good agreement. The geometric mean of the observed deposition rates for the five 10° x 10° grid boxes is 0.12 g SO₄⁻²/m²/month and the model-calculated mean for the same spatial domain is also 0.12 g SO₄⁻²/m²/month. The geometric of deposition rates observed at 73 sites east of the 100°E meridian is 0.10 g SO₄⁻²/m²/month. However, while the overall observed and model-calculated deposition rates are in good agreement, inspection of Figure 7 indicates that there are some spatial discrepancies. Generally the observations show an overall trend toward decreasing deposition rates as one travels northward from southern China. The model-calculated distribution, on the other hand, predicts a maximum in deposition in central China and decreasing rates to the south as well as the north. A possible cause for this discrepancy is the fact that the dynamical portion of the model itself is not able to accurately reproduce the spatial distribution of precipitation over China [*Giorgi et al.*, 1999]. However, here again it is relevant to note that for the purpose of accurately predicting SO_x export from East Asia it is more critical that the model correctly simulate the overall SO_x deposition rate than the spatial distribution of the deposition. It is also relevant to note that the spatial distribution in sulfate deposition over China calculated here and illustrated in Figure 7 is quite similar to that obtained by *Xu and Carmichael* [1999] from the Acid Deposition Module in RAINS-ASIA (Regional Acidification Information and Simulation System).

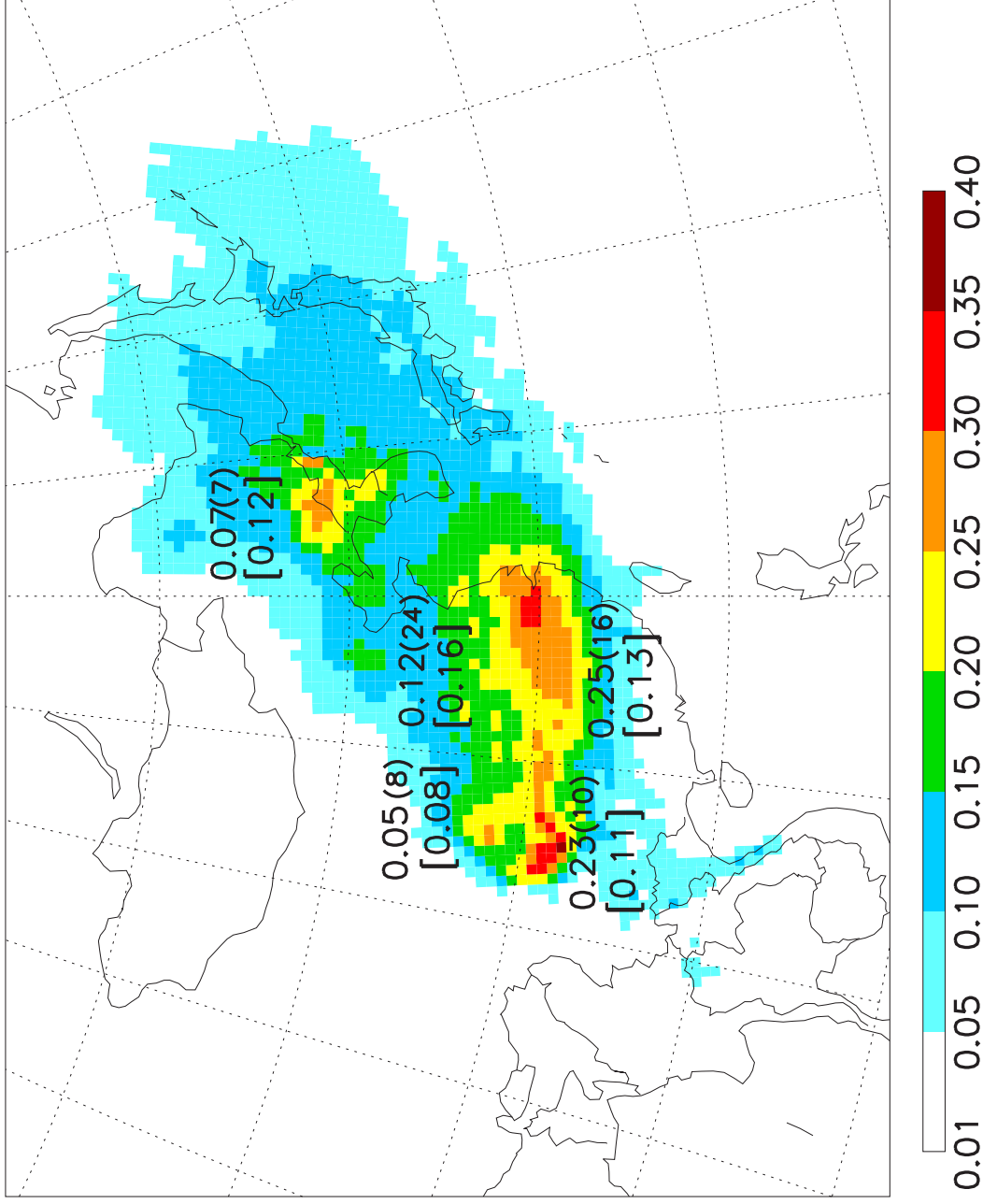


Figure 7: Model-calculated and observed monthly average wet deposition rate ($\text{g SO}_4^{2-} / \text{m}^2 / \text{month}$). The model results are depicted by the color-coding and represent an average of the deposition rates calculated for the months of March and April. The numbers in the square brackets represent the model-calculated averages for the appropriate $10^\circ \times 10^\circ$ grid (delineated by the dashed lines) in the figure. The numbers without parentheses/brackets are the $10^\circ \times 10^\circ$ grid averages of the observed wet deposition rates for March, April, and May, 1993 reported by *Ding et al.* [1995]. The smaller numbers in the parentheses indicate the number of stations used to calculate the observed averages for each grid box.

2.3.2 East Asian SO_x budget and export

During the months of February, March, and April, a total of 1.39, 1.32, and 1.24 Tg of S are emitted into our model domain, respectively. Figure 8 illustrates the ultimate fate of these emissions. On average we see that roughly 35% of the total emissions is returned to the model domain by wet deposition from large-scale clouds and a similar amount is returned by dry deposition. Another approximate 10% is returned by wet deposition from convective clouds. The remaining 20% is exported out of the model domain. Note also that there is relatively little change in the SO_x budget over the 3-month simulation period. The most significant change appears to be a slight increase in SO_x removal by clouds as the simulation progressed from February to April because of increased rainfall within the period. (In both observations and our model-calculations, the transition from winter to spring is generally accompanied by a weakening in the continental high-pressure system lying over the East Asian subcontinent. This leads to a decrease in atmospheric stability and an increase in precipitation over the model domain.) However, this increase in wet removal is largely compensated for by a decrease in dry removal, and, as a result, there is little change in the net rate of SO_x export over the 3 months.

Because of the increase in precipitation over the simulation period, wet deposition becomes increasingly important in the sulfur budget as we progress from February to the end of April. Thus the ratio of wet deposition to dry deposition is 1.0 in February, 1.3 in March and 1.75 in April. By comparison, *Xu and Carmichael* [1999] predicted a decrease in the ratio of wet-to-dry deposition over Asia from February to April (i.e., 1.6 in February, 1.2 in April). One possible reason for this discrepancy is the fact that while we assumed that SO_2 emissions in Northern China decreased from February to April, *Xu and Carmichael* [1999] assumed constant emissions. Because precipitation is small in Northern China in February, the relatively high North-China SO_2 emissions assumed in our model during February would tend to cause a relatively small ratio of

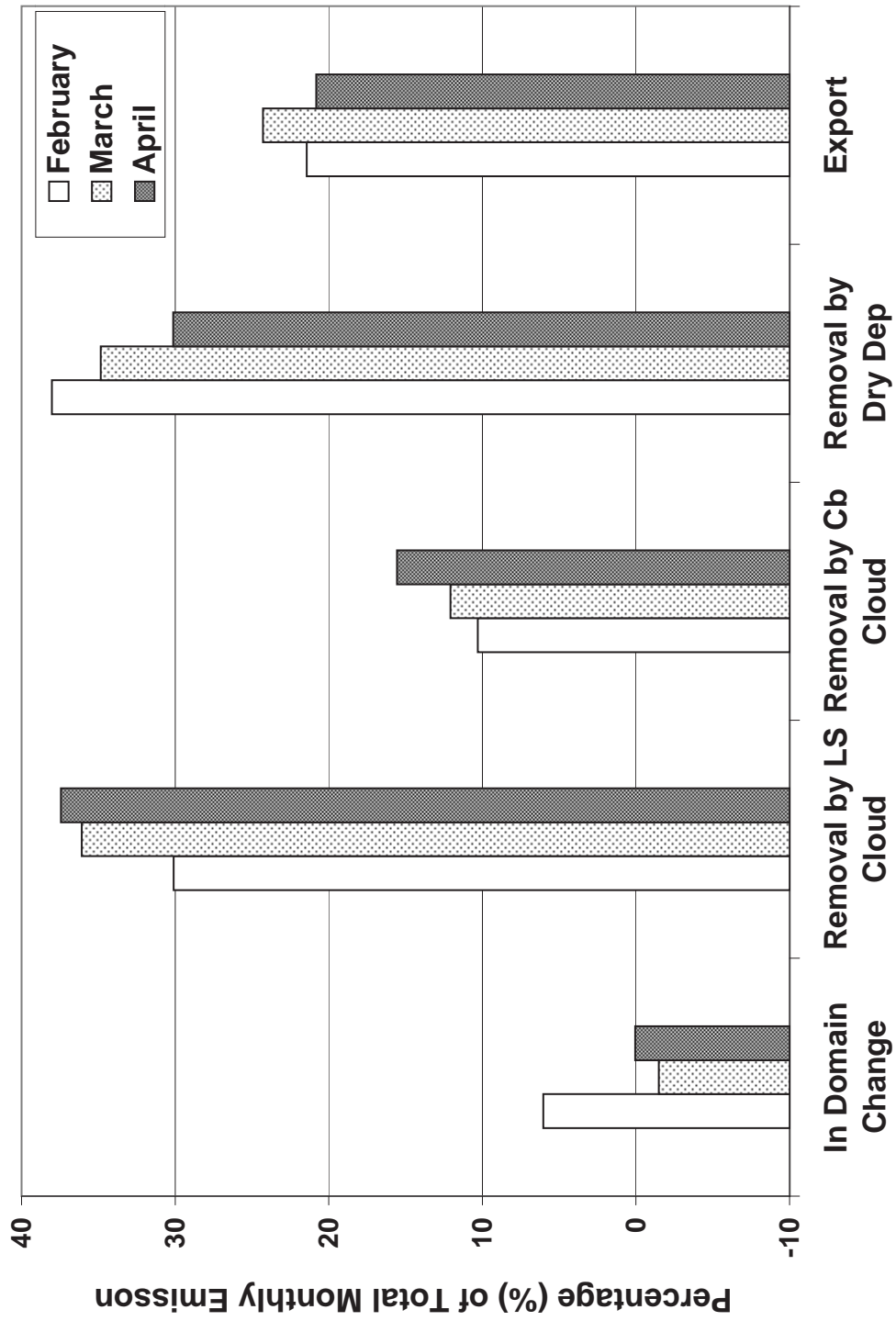


Figure 8: Fate of SO_x emission by month and process. LS = large scale clouds, Cb = convective clouds.

wet-to-dry deposition as compared to that obtained by *Xu and Carmichael* [1999]. It should also be noted that the domain of the *Xu and Carmichael* [1999] model included the Indian subcontinent, while ours did not. Since April tends to be an extremely hot and dry month over India, this would favor relatively small wet-to-dry deposition ratios when compared to those obtained from our model.

2.3.2.1 Morphology of the SO_x Export

Figure 9 categorizes the SO_x exported from the model domain for each of the three months of the simulation as a function of both chemical form (i.e., SO_2 or SO_4^{2-}) and the model boundary through which the export was calculated to have occurred. Inspection of the figure reveals that the vast majority of the SO_x -export occurred in the form of SO_4^{2-} and was accomplished by advection through the eastern boundary of our model domain (i.e., into the North Pacific Ocean). These results are not surprising: (i) given the relatively fast rates of SO_2 -to- SO_4^{2-} conversion generally found in the atmosphere [*Walcek et al.*, 1990; *Seinfeld and Pandis*, 1998], one would expect to find most of the exported SO_x in the form of SO_4^{2-} ; and (ii) since the prevailing winds between $20^\circ N$ and $50^\circ N$ during the simulation period are westerly, most of the export would be expected to be through the eastern boundary of the model domain.

Since SO_4^{2-} is generally longer-lived when it is present in the free troposphere than when it is in the boundary layer, it is also interesting to consider the altitude dependence of the SO_x export. Figure 10 illustrates this dependence for the case of SO_x -export through the eastern boundary. We see that most of the export occurs in the middle of the free troposphere, around 500 hpa, where the product of SO_x concentration and zonal winds are at a maximum. *Benkovitz et al.* [1994] also noted that the greatest export from North America occurred in the free troposphere.

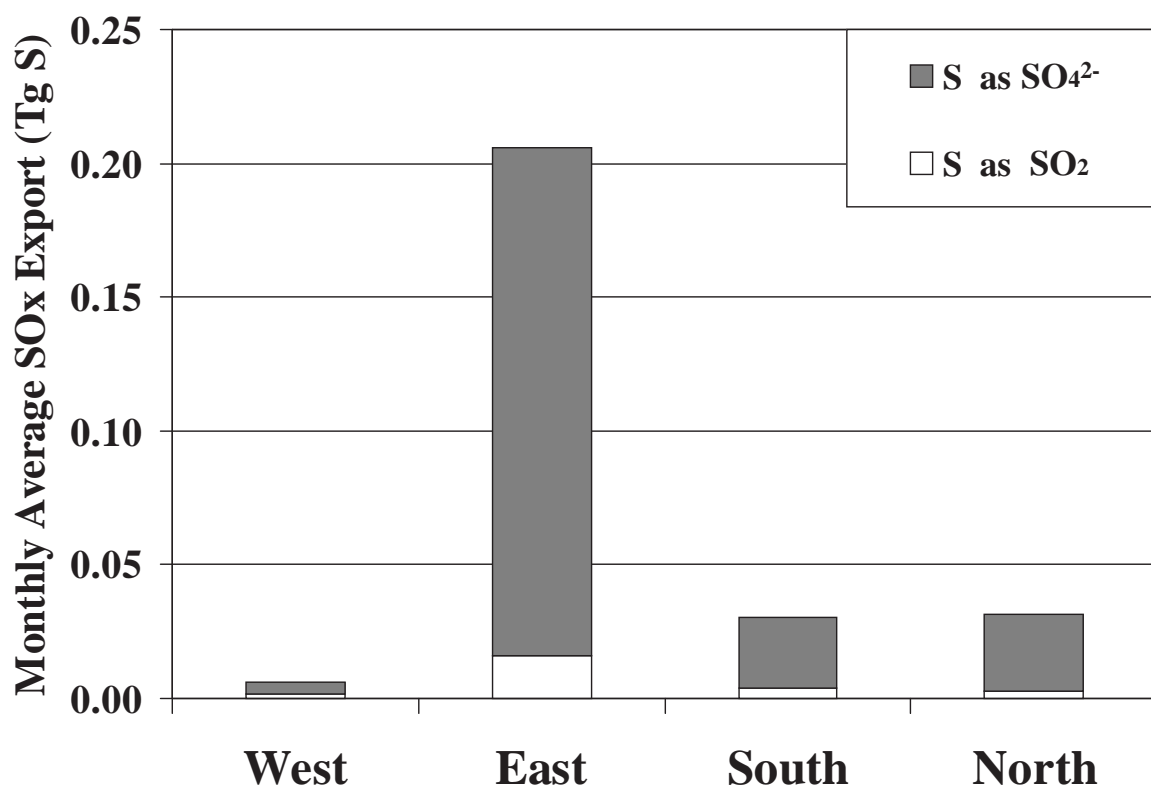


Figure 9: Monthly averaged (February to April) rate of SO_x export by model boundary and chemical form.

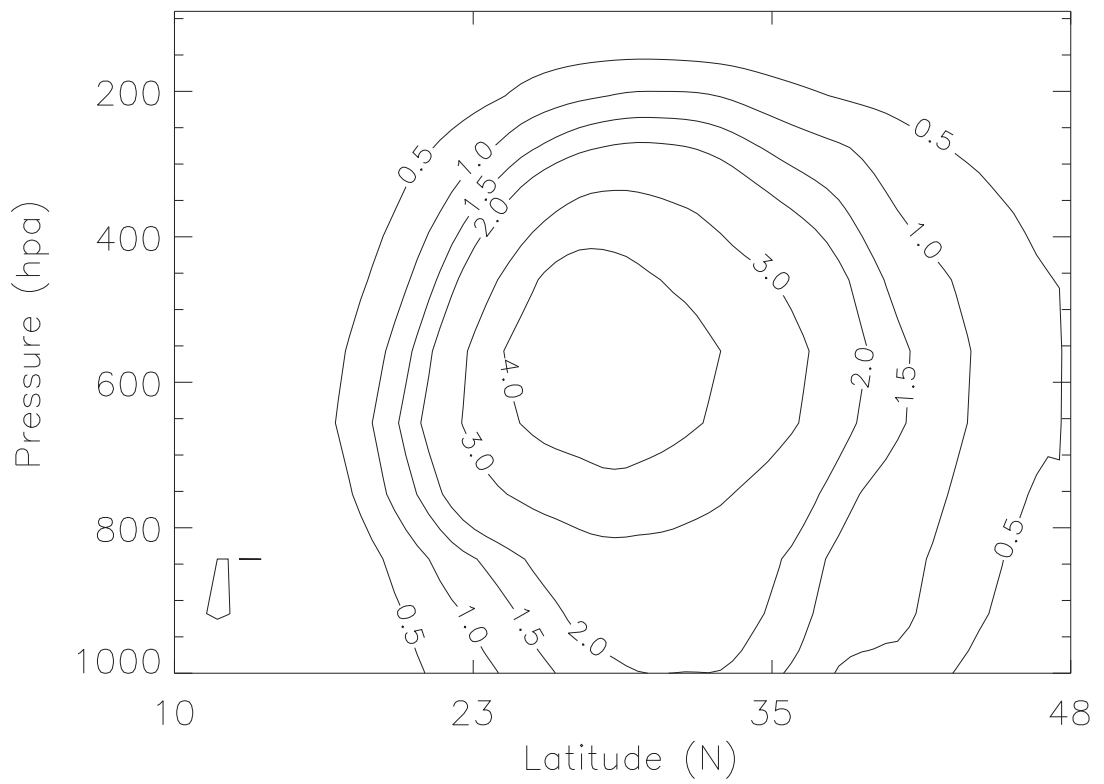


Figure 10: Sulfur flux (in $\mu\text{gS}/\text{m}^2/\text{s}$) through the east boundary of the domain, averaged from February to April.

2.3.2.2 *Intra-regional exchange of SO_x*

The transport and subsequent deposition of pollutants such as SO_x can trigger environmental concerns at the regional and national level, especially if the transport occurs across political boundaries. In this section we address this issue by considering the sources and sinks of anthropogenic SO_x within 6 subregions of the model domain. These subregions were chosen by first dividing the model domain into a continental and an oceanic portion and then further dividing the continental portion into five subregions on the basis of either national and/or regional identities. As indicated in Figure 3, the resulting 6 subregions are: (i) China (including Mongolia); (ii) South Russia/East Kazakhstan; (iii) Southeast Asia; (iv) Korea (including both North and South Korea); (v) Japan; and (vi) Ocean. We calculated sulfur emission from and deposition into each of the subregion.

Figure 11 summarizes the contributions of each subregion to the overall emission and deposition of SO_x over the 3-month simulation period. We find that China is, by far, the largest player in the overall budget of anthropogenic SO_x. China is estimated to be responsible for about 85% of the total emissions. On the other hand China receives back a little more than 45% of the total emissions in the form of wet and dry deposition. Thus we estimate that China exports almost 50% of its emissions to locations outside its borders during the late winter and early spring when continental outflow conditions predominate.

While three of the other four continental subregions (Southeast Asia, Korea, and Japan) are responsible for much smaller amounts of SO_x emissions, they are all, nevertheless, calculated to be net exporters of anthropogenic SO_x (i.e., the S emissions from the region are greater than the depositions to the region). This is even true of Korea and Japan, even though they are both situated 'downwind' of China during the simulated period. Moreover, while the South Russia/East Kazakhstan subregion is calculated to be a net importer of SO_x during the simulation period, this result is

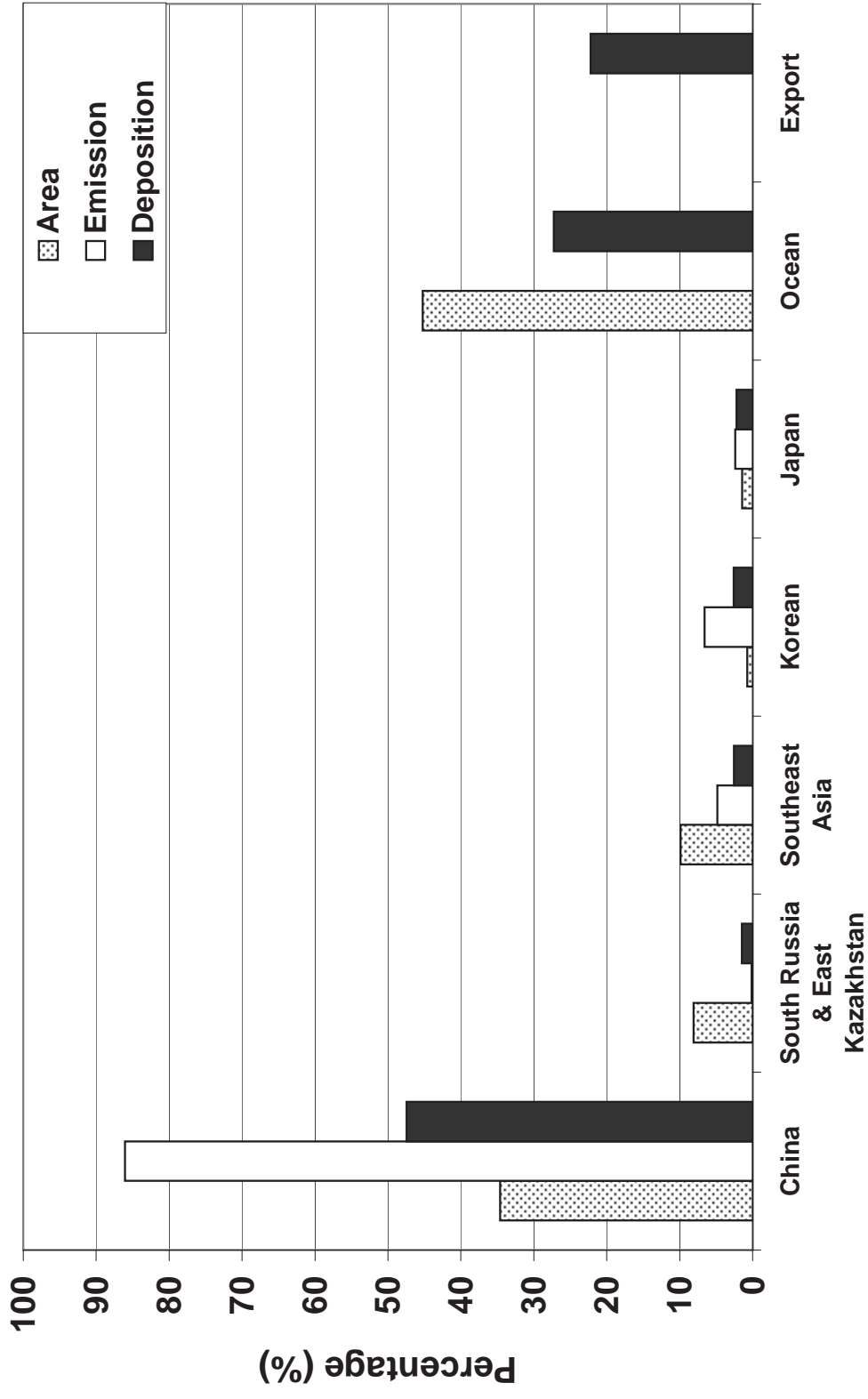


Figure 11: Percent contribution by each of the 6 subregions to the total area of the model domain, total SO_x emissions, deposition, and percent of total emission exported.

somewhat misleading. Note in Figure 3 that only small portions of Russia and Kazakhstan are included in our model domain, and, by setting the boundary conditions for SO_x at background levels in our simulations, we essentially precluded any import of SO_x from more northerly locales in the two nations.

Finally, note in Figure 11 that we estimate that about 50% of the total SO_x emissions is exported out of the continental subregions. A little more than one-half of this exported fraction is deposited in the ocean subregion of our model domain and the remainder is exported out of the model domain. *Xu and Carmichael* [1999] estimate about 30% of the sulfur emission, both natural and anthropogenic, from Asia is transported out of domain in winter and spring. By contrast, *Chin et al.* [2000b] estimated that, on an annual bases, only about 11% of anthropogenic sulfur emitted in eastern Asia is transported to the neighboring oceans. Our export rate is in their range and reflects our focus on the high continental outflow season, February to April, of the East Asia.

2.4 Discussion and Conclusion

Regional model simulations of the emission, transport, and deposition of anthropogenic SO_x from East Asia suggest that about 20% of the SO_x emitted from the region is exported during the late winter/early spring when continental outflow conditions predominate. Most of this exported SO_x is in the form of SO_4^{2-} and occurs through the eastern boundary of our model domain (i.e., into the North Pacific Ocean) and in the middle portion of the free troposphere.

On a mass basis, we estimate that about 0.17 Tg of S as SO_4^{2-} and 0.03 Tg of S as SO_2 are transported each month from the East Asian subcontinent to the North Pacific Ocean during the late winter/early spring period. By comparison, estimates of the natural source of S to the North Pacific from emissions of dimethylsulfide range from about 0.1 to 0.3 Tg per month [cf., *Bates et al.*, 1987; *Chen et al.*, 1999]

and the total global sources of S due to natural processes have been estimated at about 2 - 3.5Tg of S per month [*Berresheim et al., 1996*]. It should be borne in mind, however, that not all of the sulfur from natural emission is converted to sulfate aerosol [*Berresheim et al., 1996*]. The SO_x-export from East Asia, on the other hand, was found to have been mostly SO₄²⁻ and to be in the free troposphere, where SO₄²⁻ tends to be longer lived and stronger zonal winds favor more rapid transport. Thus it would appear that the export of anthropogenic SO_x from East Asia during the late winter and early spring is probably large enough to significantly perturb sulfate aerosol concentrations over the North Pacific Ocean and perhaps even on larger and more global scales.

While China was found to be the largest contributor to the export of SO_x from East Asia, all the nations/continental subregions of East Asia were found to be net exporters of SO_x and thus they all bear some responsibility for the SO_x-export during continental outflow conditions.

An encouraging implication of China's large role in SO_x export from East Asia is the fact that it is now believed that SO_x emissions from China have reached their peak and will be declining in the coming decades [*Streets and Waldhoff, 1999; van Aardenne et al., 1999*]. Thus it seems reasonable to expect that SO_x export from East Asia will also be declining in the coming decades. A potential complication to this scenario arises from the fact that most of export occurs within the mid-troposphere. For example, if the strength of convective transport over East Asia should increase in the coming decades due to climate change, it could offset some of the potential reductions in SO_x export that might be expected from decreases in SO_x anthropogenic emissions. Measurements of the altitude profile of SO₄²⁻ within the East Asian plume as it advects into the North Pacific could provide some insight into this conjecture.

CHAPTER III

AN EVALUATION OF THE TRACE-P EMISSION INVENTORIES FROM CHINA USING A REGIONAL MODEL AND CHEMICAL MEASUREMENTS

3.1 Introduction

In order to assess the possible impacts of anthropogenic pollutants on local, regional, and global scales, an accurate and comprehensive emission inventory is needed. However, several recent studies indicate that significant inaccuracies may exist in the inventory for pollutant emissions from East Asia, and especially for that of carbon monoxide (CO) [*Kasibhatla et al.*, 2002; *Kiley et al.*, 2003; *Palmer et al.*, 2003; *Carmichael et al.*, 2003]. CO pollution arises primarily from the incomplete combustion of fossil fuel and biomass. It is also produced from the oxidation of anthropogenic and natural hydrocarbons. The abundance of CO has large impact on the oxidizing capacity of the Earth's atmosphere, therefore it will indirectly affect the lifetime of other air pollutants and greenhouse gases [*Logan et al.*, 1981; *Seinfeld and Pandis*, 1998].

Kasibhatla et al. [2002] applied an inverse modeling technique using a global chemistry model (GEOS-CHEM) and NOAA/CMDL background CO measurements, and concluded that CO emissions estimated by the EDGAR/GEIA inventory [*Olivier et al.*, 1996] from fossil fuel and biofuel combustion in East Asia are underestimated by a factor of 1.5, or 110-140 Tg/yr, and that CO emissions from biomass burning are

underestimated by a factor of 2 or 60 Tg/yr. More recently, *Kiley et al.* [2003], *Palmer et al.* [2003], and *Carmichael et al.*[2003] concluded, on the basis of a comparison between model calculations and TRACE-P airborne measurements over the western North Pacific Ocean near the coast of China, that CO emissions from East Asia are underestimated by the TRACE-P inventory prepared by *Streets et al.* [2003]; this later inventory is similar to the Asian part of the GEIA inventory. The posteriori CO emission inventory derived by *Palmer et al.* [2003] has an additional 60 Tg/yr of emissions from fossil and biofuel burning in China over that of the TRACE-P emission inventory; this represents a factor of 1.5 increase in CO emissions from these sectors. On the other hand, *Carmichael et al.* [2003] concluded that the underestimate in CO emissions arose from domestic sources in central China, and they estimate that these emissions need to be increased in the TRACE-P inventory by a factor of 3-5.

Thus, while there appears to be a consensus among previous investigators that CO emission from East Asia are underestimated, there are significant differences in the magnitude of the underestimate and in the identity of the sources that are responsible for these additional emissions. In this study we use simultaneous measurements of gas and particulate matter pollutants at Linan, a rural site in China, during November, 1999 [*Wang et al.*, 2002; *Xu et al.*, 2002] in combination with a regional climate/chemistry model to evaluate the TRACE-P emission inventory for CO, SO₂, and particulate carbonaceous matter (PC).

Our approach has a number of aspects that set it apart from the aforementioned studies. *Kasibhatla et al.* [2002] used a global model and globally-distributed measurements of CO at CMDL background monitoring sites. *Palmer et al.* [2003] also used a global model, but, instead of globally-distributed measurements, TRACE-P measurements made during a number of flights off the coast of China during February-April, 2001. *Carmichael et al.*, [2003] also used the TRACE-P measurements, but

in this case a regional model. The study of *Kiley et al.* [2003] is based on inter-comparison of four global and three regional models. In our case, we use a regional model, similar to that of *Carmichael et al.*, [2003], but, in contrast to all the other investigators, make use of more detailed and continuous chemical measurements from a site within one of the most populated and industrialized regions of China. While this might make our results more susceptible to local influences, it makes them less dependent on uncertainties related to the simulation of long-range transport and chemical transformations, and it minimizes the confounding influence of emissions from other regions of the globe. Moreover, unlike the investigators who used the TRACE-P measurements, our approach makes use of an entire month of near-continuous observations. This perhaps makes our results less susceptible to the influences of episodic anomalies. Uncertainties related to the simulation of transport and meteorological phenomena are further reduced by the availability of simultaneous data on multiple gaseous and particulate species. This allows us to compare model-calculated and observed ratios of species concentrations in addition to their absolute concentrations, and concentration ratios should be less dependent upon transport and meteorological influences.

As noted above, our analysis focuses on the month of November. We chose this month since this was the only time when simultaneous measurements of both gaseous and particulate species were made at the Linan site, and the availability of both gaseous and particulate measurements provides a valuable constraint for evaluating the model results. However, there are other advantages to our November focus. Regional air pollution episodes over eastern China are frequent and severe during this month [*Luo et al.*, 2000]. During November, the influence of dust storms and boreal fires tends to be at a minimum and the dominant wind flow out of the northwest minimizes the influx of pollutants from biomass burning in Southeast Asia. This allows us to use the data to focus on pollutant emissions from China. Moreover,

the climatology over China during month of November tends to be characterized by relatively stable conditions and relatively little precipitation. This reduces model uncertainties related to the simulation of convective transport, cloud processing, and wet deposition.

3.2 Climate-Chemistry Modeling System

3.2.1 Model description

Our simulations make use of a modified version of the regional three-dimensional coupled climate-chemistry modeling system used by *Chameides et al.*, [1999ab, 2002a], *Luo et al.* [2000], *Giorgi et al.* [2002]. The modeling system consists of two components: the aforementioned NCAR Regional Climate Model (RegCM2) [*Giorgi*, 1993 ab, 1999, 2002] which provides the meteorological fields that drive a chemical transport model; and an enhanced version of Regional Acid Deposition Model (RADM) [*Luo et al.*, 2000]. RegCM is built upon the PSU/NCAR MM4 and is equivalent to the hydrostatic version of the current MM5 with additional and modified versions of several parameterizations needed for long-term climate simulations. RADM was originally developed by *Chang et al.* [1987]. The version we used is based on the one used and evaluated for East Asia by *Luo et al.* [2000] with a number of updates and modifications as described below. More detailed description of the RegCM and RADM can be found in above references.

Our model domain for RegCM is the same that mentioned in Chapter 1 and 2, which covers the major part of East Asia, i.e. ~ 80 - 160° E in east-west direction and 10 - 55° N in the south-north direction with $60\text{km} \times 60\text{ km}$ horizontal grid cells on a Lambert conformal projection and 15 vertical levels on σ coordinates that top-off at 80 hpa. Five of the vertical layers are within the planetary boundary layer. The RADM model domain is slightly smaller than that of RegCM, since the outmost domain in RegCM is the region where RegCM simulation is nudging to the large scale

lateral boundaries. Prior to simulating the gas and aerosol distribution of November, 1999, both RegCM and RADM are run for a two month spin-up period.

In this study we made several modifications to the version of RADM used by *Luo* [2000]. The photochemical reaction rates have been updated based on *Sander* [2003]. RADM now uses the same vertical resolution as RegCM, i.e., 14 layers instead of 6 as in *Luo et al.* [2000]. The dry deposition of species is calculated using a resistance-in-series module that accounts for seasonal variations in land-surface character and the specific physical/chemical properties of the depositing tracer species [*Walcek et al.*, 1986; *Wesely*, 1989; *Walmsley and Wesely*, 1996]. Some improvements to the original deposition scheme of *Wesely* [1989] include calculating the aerodynamic resistance based on *Jacobson* [1999] and *Byun et al.* [1999], the surface resistance over tundra based on *Jacob et al.* [1992], the surface resistance of NO₂ based on *Ganzeveld* [1995], and the surface resistance of SO₂ over snow based on *Valdez*[1987] and *Ganzeveld* [1998]. Our model calculated dry deposition velocities are within the range of observed velocities [*Ganzeveld et al.* 1998 and reference within] and comparable to other regional and global models results: EPA Model-3 [*Hu et al.*, 2003], GO-CART [*Chin et al.*, 2000a], and ECHAM [*Ganzeveld, et al.*, 1998]. A detailed description of the chemical transport model used in this study, as well as the modifications we have made to the model, has been documented in the Appendix A.

In the previous applications of the modeling system (eg. *Luo et al.*, 2000), RADM and RegCM used different land-cover/land-use datasets. In order provide consistency between the models, the Global Land Cover Characterization (GLCC) 30'' dataset is used to derive the land surface types for our model domain and used as inputs to both RegCM and RADM. (The two models require different landuse categorizations, and so somewhat different aggregations were used.)

3.2.2 Emission inventory

Estimates of anthropogenic emissions of air pollutants that were specifically focused on East Asia began in the early 1990's and have been continuously improved [Fujita, et al., 1991; Kato and Akimoto, 1992; Akimoto and Narita, 1994; Arndt and Carmichael, 1997; Klimont et al., 2001; Streets et al., 2000ab, 2001abc]. Most recently, Streets et al. [2003] developed an emission inventory of gaseous and primary aerosols for the year 2000 for NASA TRACE-P [Jacob et al., 2003;] and the NSF/NOAA ACE-Asia experiments [Huebert et al., 2003]. It is one of the most comprehensive and updated study of anthropogenic emissions from East Asia to date. The inventory includes all major sources of pollutants for essentially the entire East Asian region on various spatial scales. In our model simulations, we made use of the TRACE-P inventories provided with resolution of $1^\circ \times 1^\circ$ and the $30' \times 30'$, and obtained similar results. The calculations presented here used the $1^\circ \times 1^\circ$ inventory.

Figure 12 illustrates the spatial distribution of the TRACE-P CO, SO₂, and particulate carbonaceous (PC) aerosols emissions interpolated to our model grid and Figure 13 illustrates the total CO, SO₂, and PC emissions by source type or sector. The spatial distribution of the CO, SO₂, and PC emissions are quite similar, with large sources located near the major urban-industrial centers (e.g., Beijing, Shanghai, Chengdu). However, because significant amounts of CO are emitted by biomass burning, domestic sources, and transport-related sources, their emissions tend to be somewhat more disperse than that of SO₂, whose emissions are dominated by point sources. This will turn out to be an important distinction in our later discussion on the identity of the additional sources of CO that we conclude are needed to rationalize model simulations with observations.

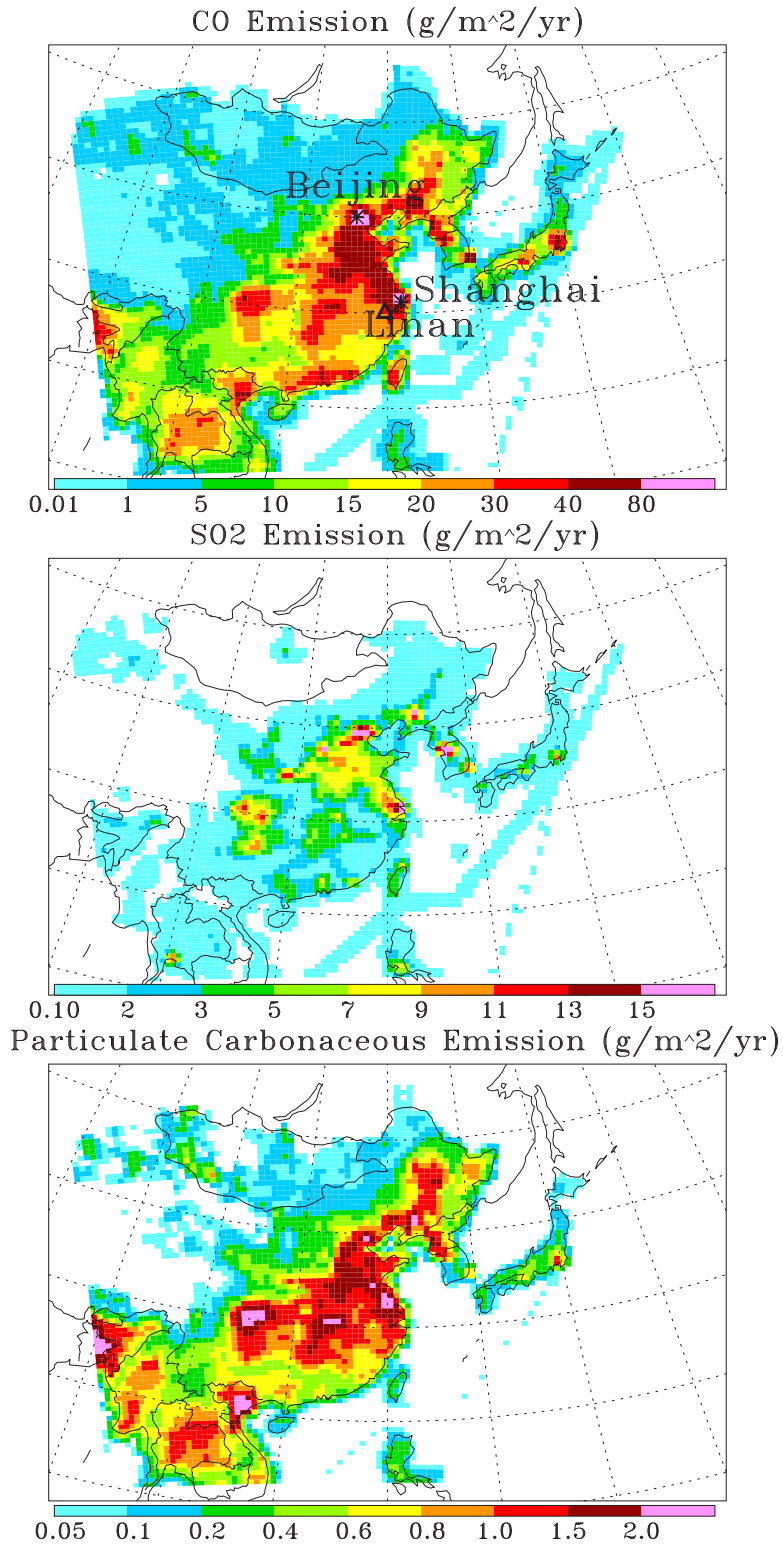


Figure 12: Spatial distribution in the annual average emission rate of CO, SO₂, and particulate carbonaceous in 2000. It is interpolated from the TRACE-P inventory [Streets, 2003] to our model domain.

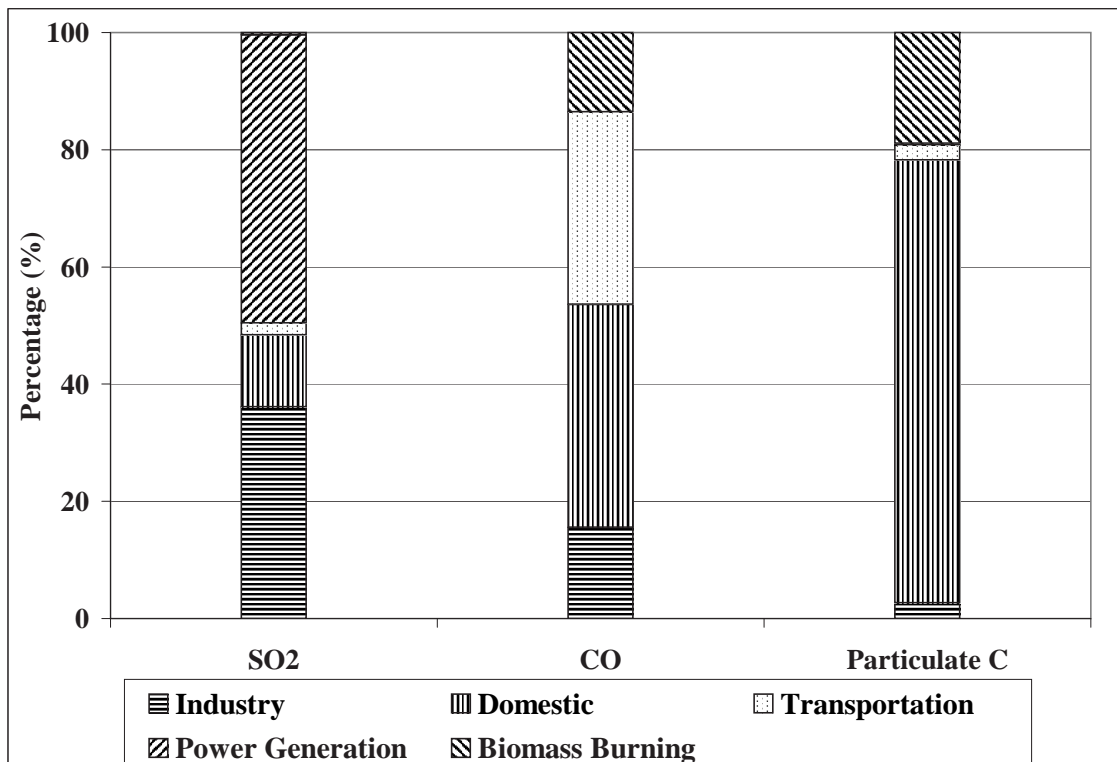


Figure 13: Contributions of various source-types to the total SO₂, CO, and Particulate C emissions from China in the TRACE-P emission inventory of *Streets et al.* [2003].

3.2.3 Meteorological conditions

The meteorological fields needed to drive the RADM simulations are provided by the RegCM. The large-scale boundary and initial conditions used to drive the RegCM simulations are obtained from the NCEP reanalysis data provided by the NOAA-CIRES Climate Diagnostics Center, Boulder, Colorado, USA, from their Web site at <http://www.cdc.noaa.gov/>. These data are available 4 times per day on a $2.5^\circ \times 2.5^\circ$ grid at the surface and different pressure levels.

Figure 14 illustrates the monthly averaged NCEP and RegCM simulated temperature (T) and humidity (Qv) fields at the surface and 500 hpa over our model domain for November 1999. In general, the RegCM simulations reproduced the monthly-averaged spatial distribution of the NCEP reanalysis data over both the surface and mid-troposphere. One noticeable difference is that the simulated temperature and humidity over central to south China are slightly lower than those of NCEP. These differences maybe due, at least in part, to differences in the topographies used for the NCEP and RegCM grids.

Figure 15 illustrates the time series of temperature, humidity, wind components (u and v), and wind speed (w) measured at the sampling site, Linan, during November, 1999, as well as the values appropriately interpolated to the Linan site's location from NCEP-Reanalysis data and RegCM simulations. The RegCM simulated temperature and Qv generally follow the trend of the two set of measurements. During the early November, however, the RegCM temperature is several degrees lower than both measurements. RegCM winds agree with NCEP data quite well in both magnitude and directions with some fluctuations. One significant difference is on November 15, when the NCEP wind speed is much larger than that of RegCM simulation. We checked the NCEP data and found that there was a strong frontal system, with meridional winds (v) as high as 20 m/s, just off the coast of China, i.e. about 150-200 km away from Linan. Since the original NCEP data have a horizontal resolution of 2.5° (i.e.

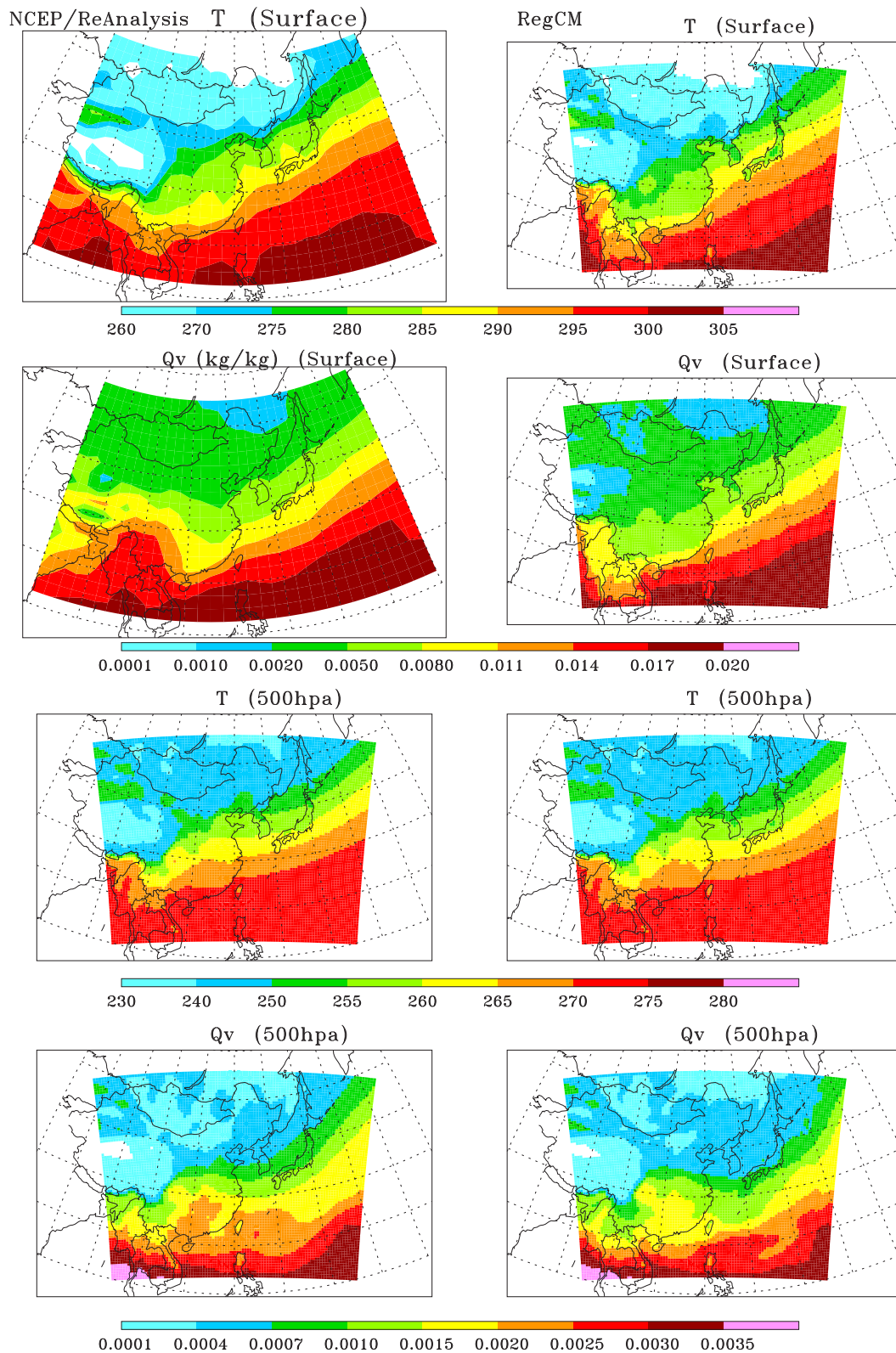


Figure 14: Average temperature, T (K) and humidity, Q_v (kg/kg) at the surface and 500 hpa during November, 1999 from the NCEP Reanalysis data and the RegCM simulation.

~ 240 km), the high v -value at Linan in the NCEP data may reflect errors produced from the interpolation of coarsely gridded data to a specific point.

In summary, while episodic inconsistencies exist between the RegCM simulations and the meteorological observations, it appears that the RegCM provides a reasonable reproduction of average conditions during the month of November, 1999 (see Figure 14). This suggests that the RegCM-RADM modeling system used here will not be able to accurately simulate the day-to-day variations in pollutant concentrations at a specific grid point in the model domain. On the other hand, if other aspects of the modeling system are accurate, it should be able to do a reasonable job on longer weekly to monthly time scales. This was in fact found to be the case when this modeling system's ability to simulate ozone pollution episodes over East Asia was evaluated by *Luo et al.*, [2000].

3.2.4 Model results

Figure 16 illustrates the monthly averaged CO, SO₂ and particulate C during November, 1999 simulated by RADM. Their spatial distributions generally follow the pattern of their emissions (Figure 12). In Figure 17 we plot the time series of gaseous and particulate species simulated by RADM at Linan, and Table 8 lists the monthly-averaged model simulated concentrations for a number of key gaseous pollutants. Figure 17 and Table 8 also include measured concentrations, these are discussed below.

3.3 Observations

An intense field campaign to monitor the concentrations of gaseous and aerosol species was carried out at a rural site, Linan, in the Yangtze Delta of China in November 1999. Gaseous species, including SO₂, CO, NO_{*y*}, and O₃ were measured by *Wang et al.* [2002], and aerosol mass and composition were measured by *Xu et al.* [2002].

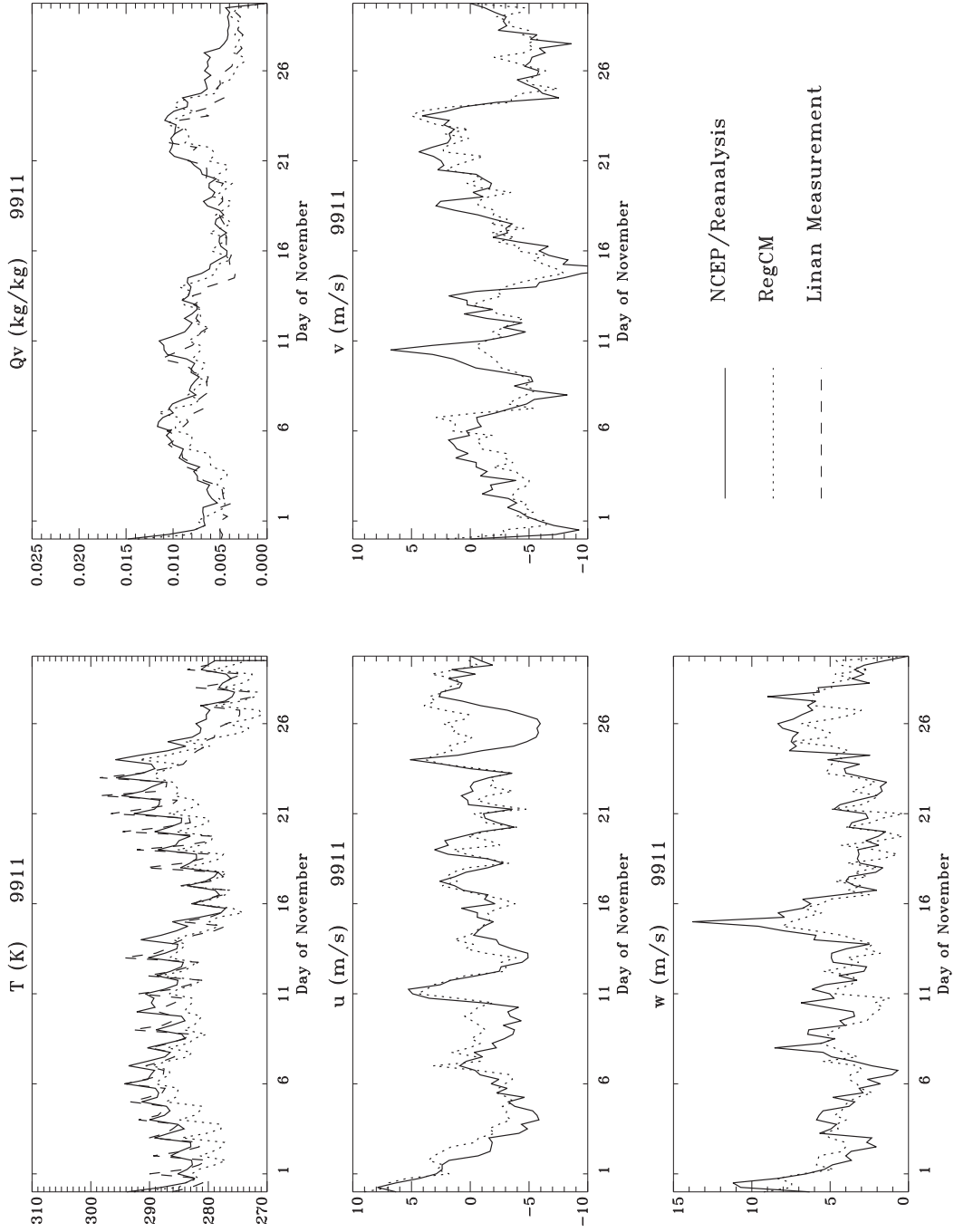


Figure 15: Time series of temperature, T (k), humidity, Q_v (kg/kg), wind vector, u and v (m/s), and wind speed, w (m/s) per 6 hour during November, 1999, at Linan from measurements made at the site (T and Q_v only), and from interpolation of the surrounding grids from the NCEP reanalysis data and RegCM simulations.

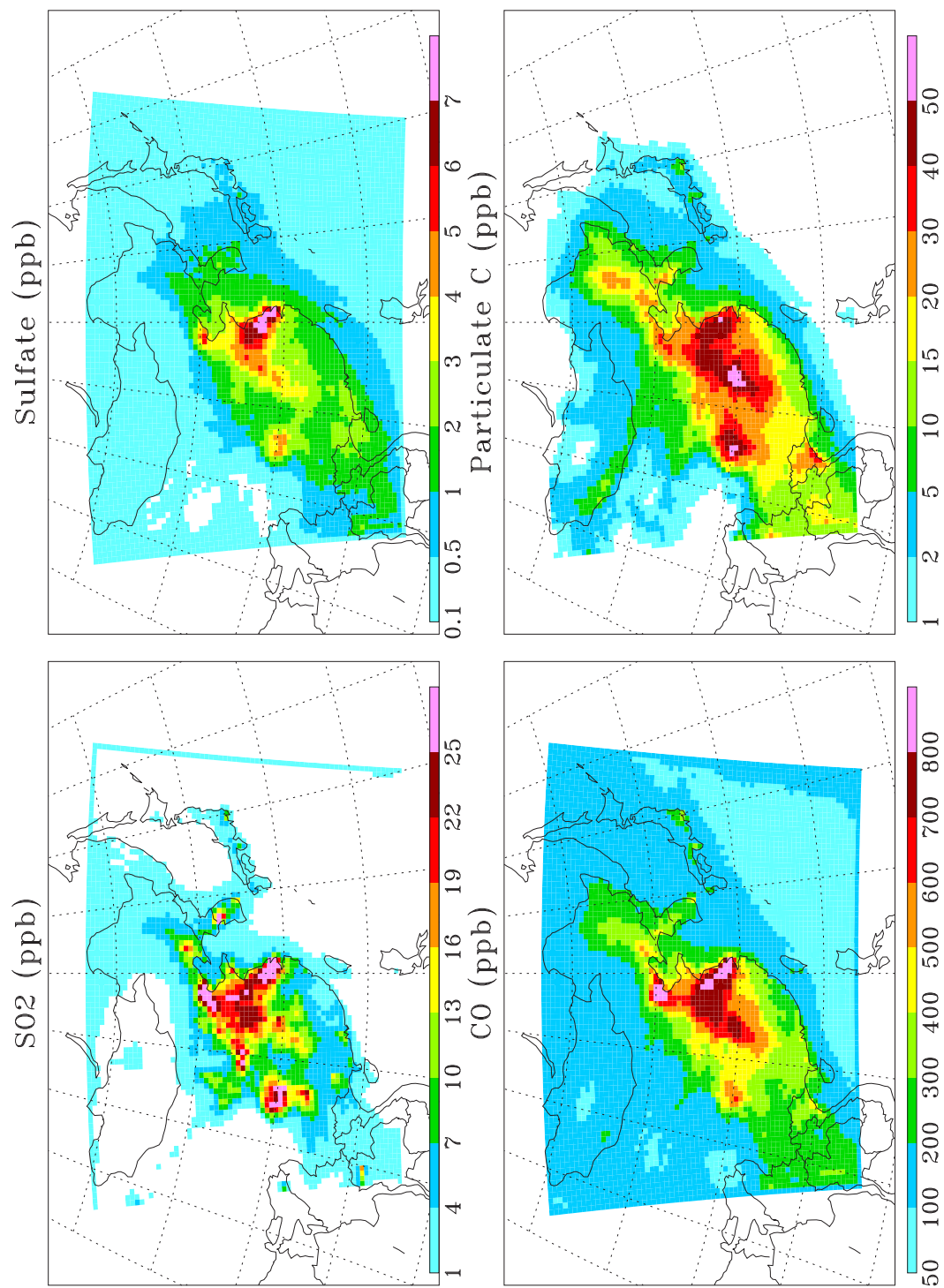


Figure 16: Monthly averaged distribution in the model-simulated CO, SO₂, Particulate SO₄²⁻, and Particulate C concentration during November, 1999.

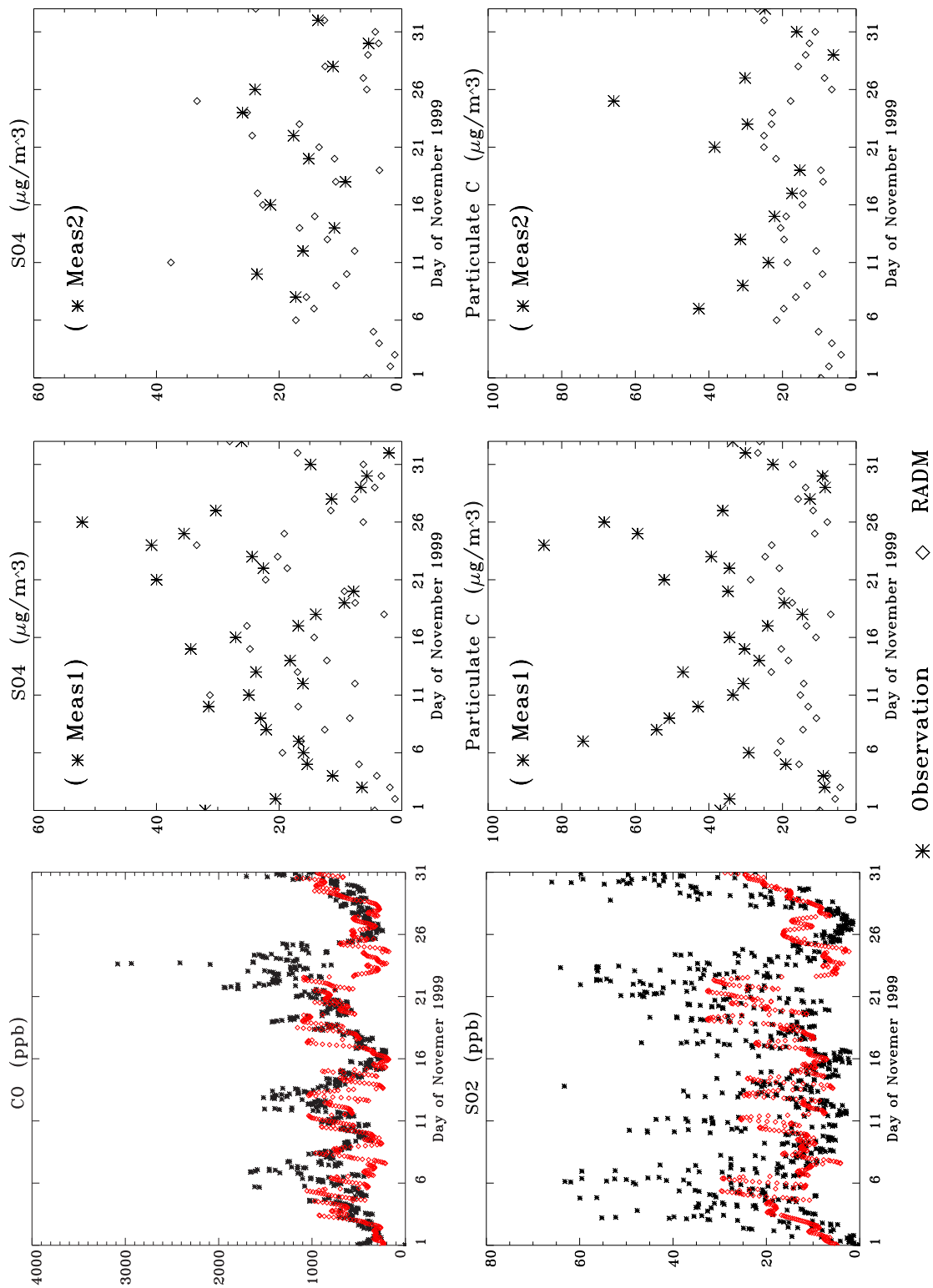


Figure 17: Model-calculated and observed pollutant concentrations as a function of time at Linan during the November, 1999. Concentrations for gas-phase species (CO and SO₂) are hourly-averages, and concentrations of particulate species (sulfate and carbonaceous) are 24-hour averages. Observed concentrations were obtained from *Wang et al.* [2002] for gas phase species and from *Xu et al.* [2002] for the particulate species.

Table 8: Arithmetic Mean of Measured and Model Simulated Gaseous and Particulate Species at Linan in November, 1999.

Species	Measurement ^a	Model ^b		
CO	763	587		
O ₃	33.4	24.7		
SO ₂	19.8	14.8		
NO _y	12.2	17.2		
	Meas_1 ^c	Model ^d	Meas_2 ^c	Model ^d
SO ₄ ²⁻	21.2	13.4	16.3	14.6
NO ₃ ⁻	7.74	3.5	5.94	3.8
NH ₄ ⁺	8.56	6.05	7.52	6.62
PC	35.0	15.8	28.2	16.7

units: CO, O₃, SO₂, and NO_y : ppb; SO₄²⁻, NO₃⁻, NH₄⁺, and PC : $\mu\text{g}/\text{m}^3$

^a Monthly average of hourly measurement by Wang et al., 2002.

^b Monthly average of model results.

^c Monthly average of daily measurements by Xu et al., 2002, where 'Meas_1' and 'Meas_2' are two sets of measurements made by different instruments and covered slightly different time period: 'Meas_1' included 33 24-hour filter samples taken over a period spanning Oct. 29 - Dec. 1, 1999, 'Meas_2' included 27 24-hour filter samples taken from Nov. 4 - Nov. 30, 1999.

^d Average of model simulations over the same time period as aforementioned 'Meas_1' and 'Meas_2'.

In this work we use the measurements of CO, SO₂, and particulate SO₄²⁻ and carbon to compare to our model simulations in order to assess the accuracy of the TRACE-P emissions inventory for CO, SO₂, and carbonaceous aerosols. Because of uncertainties in the measurements of reactive nitrogen by *Wang et al.* [2002] (see for example, NARSTO, 2000), we do not consider the NO_y measurements made at Linan and do not address issues related to the emission inventory for NO_x. Because of uncertainties in the division of particulate carbon emissions and ambient concentrations to organic C and elemental C (see for example, *Chameides and Bergin*, [2002b]), we only consider the sum of all particulate carbon in our analyses.

The Linan observatory (30.4° N, 119.7° E, 132m) is surrounded by crop fields and plantations which is typical of rural areas in east China. As illustrated in Figure 18, the station is 40-50 km west to Hangzhou (population ~ 1 million), and about 200 km southwest of Shanghai, the largest city of China with a population ~ 12 million. Even though Linan is considered a rural site, it often experiences air pollution episodes that cause significant spikes in the concentrations of CO, SO₂, NO_y, O₃, and particulate matter [*Chameides et al.*, 1999a; *Luo et al.*, 2000; *Wang et al.*, 2002; *Xu et al.*, 2002]. This was clearly the case in November, 1999. As illustrated in Figure 17, the period was marked by a number of occasions when CO exceeded 1 ppmv and SO₂ exceeded 50 ppbv. The monthly average concentrations of pollutants at Linan were also quite high (see Table 8). The average CO at Linan was ~ 760 ppb for November 1999. By contrast the average CO at 36 northern hemisphere NOAA/CMDL background sites is only 111 ppb for the same month (<http://www.cmdl.noaa.gov/>). The average SO₂ of 19.8 ppb at Linan is higher than averaged annual mean SO₂ concentration measured at urban, suburban, and rural sites in United States (<http://www.epa.gov/airtrends/index.html>). At the same time, the PM_{2.5} and PM₁₀ mean concentration measured at Linan of 90 μg/m³ and

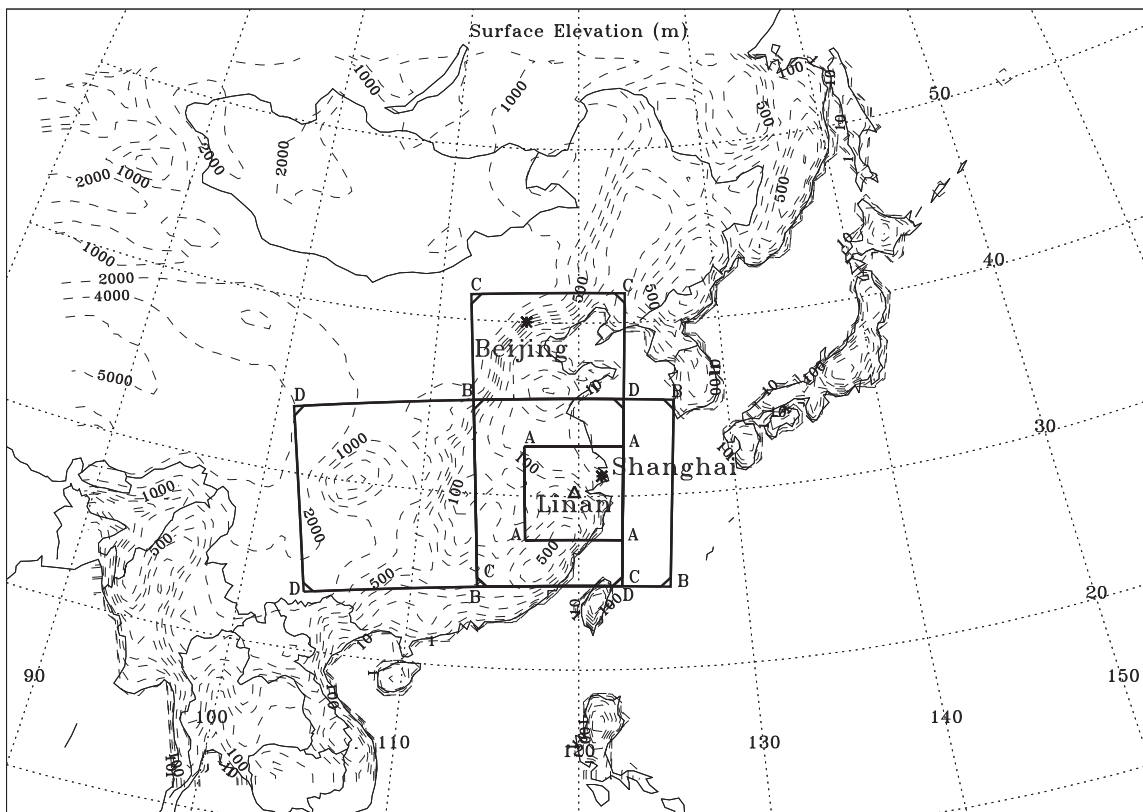


Figure 18: Location of the Linan sampling site ($30^{\circ} 17'N$, $119^{\circ} 45'E$, 132 m) superimposed over a surface elevation map of the model domain. Also indicated: three major source areas: Beijing, ($40^{\circ} 02'N$, $116^{\circ} 10'E$), Shanghai ($31^{\circ} 14'N$, $121^{\circ} 29'E$), and the Sichuan Basin ($\sim 28-32^{\circ}N$, $103-107^{\circ}E$); and four Subregions used to study the impacts of emission at different spatial scales on the model-calculated concentrations of species at Linan. The subregions are Subregion A, a $600 \text{ km} \times 600 \text{ km}$ area centered at Linan; Subregion B, a $1200 \text{ km} \times 1200 \text{ km}$ area centered at Linan; Subregion C, a north-south corridor that includes Beijing; and Subregion D, an east-west corridor that includes the Sichuan Basin.

$98 \mu\text{g}/\text{m}^3$ are 5 and 1 times higher than the US EPA NAAQS promulgated to protect human health, i.e. $15 \mu\text{g}/\text{m}^3$ for $\text{PM}_{2.5}$ and $50 \mu\text{g}/\text{m}^3$ for PM_{10} respectively (<http://www.epa.gov/air/criteria.html>). Thus the measurements from Linan provide a database that has been significantly impacted by anthropogenic emission from China and, as a result, well-suited for analyzing the accuracy of pollutant emission inventories for the region.

3.4 *Model-Measurement Comparison*

Inspection of Figure 17 reveals a general qualitative similarity between the model-calculated and observed temporal variations in the concentrations of the gaseous and particulate species of interest during November, 1999. On the other hand, while both observations and model-calculated species exhibit significant day-to-day variability, the timing of the observed concentration spikes does not always correspond to the timing of the model-calculated spikes. Moreover, the model-calculated concentrations generally vary more smoothly with time than do the observed concentrations. As discussed in detail by *Luo et al.* [2000] this is to be expected when comparing day-to-day variations in observations at a specific locale with concentrations calculated using a regional modeling system of the sort used here. In this work, therefore, we focus on a more appropriate comparison: namely between monthly-averaged observed and model-calculated concentrations.

Inspection of Table 8 indicates significant differences in the simulated and observed monthly-averaged concentrations at Linan with the model results well below the observations in all but one case (NO_y). A comparison of the percentile distributions in the modeled and measured concentrations (Figure 19 ab) indicates that much of the model-calculated underestimate arises from the fact that there were a significant number of observations with especially high concentrations that are not reflected in the model simulations. It is quite possible that these discrepancies, especially for the higher percentile concentrations, are due, at least in part, to incommensurability between the model-calculated and measured concentrations [NARSTO, 2000]. While, in our case, the model-calculated concentrations represent averages over a 60 km x 60 km x 70 m grid, the observations are at a single point in space and are thus subject to short-term perturbations caused by local emissions and sub-grid scale meteorological processes. To limit these influences, we make two adjustments to the method used to calculate the observed averaged concentrations: 1. we use geometric means instead

of arithmetic means; and 2. we limit the comparison of gaseous species to the afternoon hours when the air at the sampling site is 'photochemically aged' (i.e., when $O_3 > 35$ ppbv) [Trainer *et al.*, 1993; Parrish *et al.*, 1993]. Since Linan is a rural site, there is little afternoon titration of O_3 by local NO sources, and as a result $\sim 80\%$ of the afternoon data collected at Linan qualify as being photochemically aged. The use of geometric means (measure of central tendency) tends to limit the influence of short-term concentration spikes on the resulting averages, and the requirement for photochemically-aged air during the afternoon increases the probability that the air being sampled is well-mixed and thus more representative of the area surrounding the sampling site [Trainer *et al.*, 1993; Parrish *et al.*, 1993]. (Note that in making the comparison between model-calculated and measured particulate matter concentrations we could not limit the comparison to the afternoon hours or to photochemically-aged air, since the measurements are based on filter samples collected over 24-hour intervals.)

Finally to limit the influence of model uncertainties related to the simulation of the boundary layer and transport, we compare model-calculated and observed ratios of species' concentrations as well as absolute species concentrations. Since chemical species are all impacted by boundary-layer mixing and transport processes equally, the use of ratios should tend to normalize out model errors arising from the inaccurate simulation of these processes and thereby allow us to focus on inaccuracies related to the emission inventories (see for example, Parrish *et al.*, [1991]; Chameides *et al.*, [1992]).

A comparison of the resulting monthly geometric means of measured and model-calculated concentrations and concentration ratios of gaseous and particulate species are presented in Table 9 and Table 10, respectively. In the case of the comparison of particulate concentrations in Table 10, comparisons with two sets of measurements carried out using somewhat different instrumentation and spanning somewhat different time periods: Meas_1 involved analyses of 33 24-hour filter samples taken over a

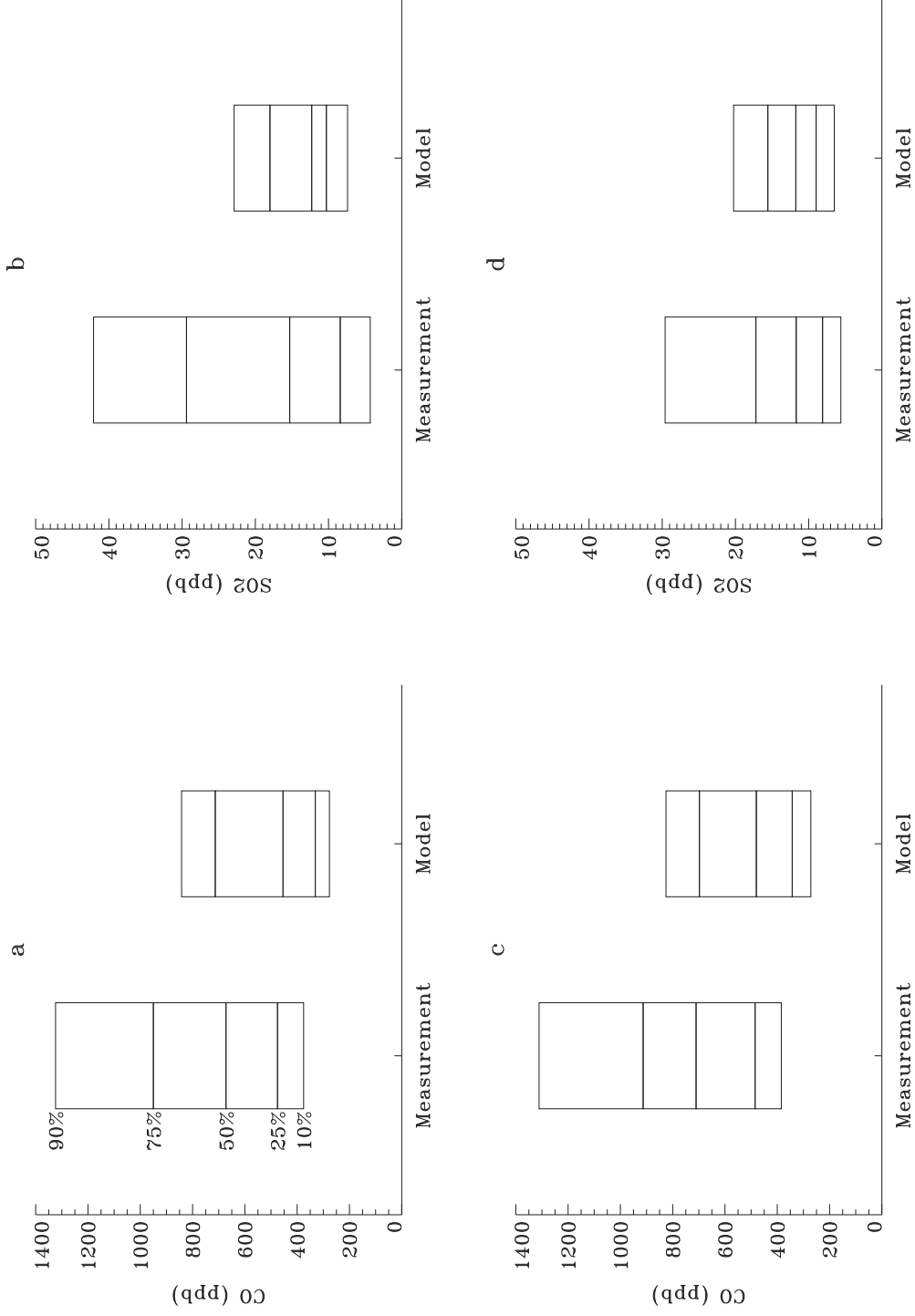


Figure 19: Distribution of percentiles (10%, 25%, 50%, 75%, and 90%) of measured [Wang et al., 2002] and model-calculated CO and SO₂ concentrations in November 1999 at Linan, where 'a' and 'b' are derived from measurements and model simulations for the whole month, 'c' is the photochemically aged air (defined in the text) selected from measurements, 'd' is the model simulations for the local afternoon.

period spanning Oct. 29 - Dec. 1, 1999 while Meas.2 involved analyses of 27 24-hour filter samples taken from Nov. 4 - Nov. 30, 1999. Inspection of the Tables, reveals that while the model-simulated monthly average SO_2 was quite close to the observed average, the model-simulated averages for CO, particulate SO_4^{2-} , and particulate C are all significantly underestimated. When we compare the ratio of CO-to- SO_2 , we find that the model-calculated ratio is $\sim 30\%$ smaller than that of the measurements. Figure 19 illustrates that modeled CO concentration at each percentile range (10, 25, 50, 75, and 90) is smaller than that of measurements while modeled SO_2 is confined in the range of measured values. In the case of the comparison of particulate concentrations, we find better agreement between the model and Meas.2 than between the model and Meas.1. However, in both cases, the underestimate in PC is larger than that of particulate SO_4^{2-} , and the model-calculated ratio of particulate SO_4^{2-} -to-PC ratio is $\sim 30\%$ lower than that of measurements.

3.4.1 Test runs with increased emissions

A modeling system such as the one used here contains a variety of uncertain inputs and parameters that could in principle give rise to the inconsistencies between model-calculated and observed concentrations and concentration ratios discussed above. Examples, include the description of landuse and land cover, the parameterizations for dry and wet deposition, the photochemical mechanism, and boundary layer mixing, as well the pollutant emission rates. We have attempted to examine the sensitivity of our model results to many of these uncertainties, and, with the exception of the emission rates, were unable to find a reasonable adjustment in model inputs and parameterizations that was able to uniformly improve model performance with respect to the observations at Linan. For example, while downward adjustments in OH concentrations can lead to model-calculated CO concentrations that are closer to the observations, they make the simulated SO_2 and SO_4^{2-} concentrations further from

Table 9: Measured and Model Simulated Geometric Mean of Gaseous Species Concentration (ppb) and CO to SO₂ Ratios at Linan, China in November, 1999.

Species	Measurement ^a	Model ^b	Diff (%) ^c
CO	683	479	-30
O ₃	44 ⁺	38	-14
SO ₂	11.5	11.5	0.4
NO _y [@]	10.1	13.2	30.7
CO : SO ₂	59	42	-28.8
ΔCO* : SO ₂	50	33	-34

^a Selected photochemically aged air from measurements by Wang et al., 2002. Photochemically aged air denotes the measurements made at afternoon (12:00 - 18:00) when the ozone is higher than 35 ppb

^b Model simulations for the local afternoon 12:00-18:00.

^c Difference of model simulations is calculated as: Diff (%) = (Model - Measurement) / Measurement *100

⁺ Monthly geometric mean of measured ozone (12:00-18:00).

^{*} CO increment with respect to the background concentration. Measured CO background level is 111 ppb based on monthly average of CO measured at 36 North Hemisphere NOAA/CMDL background sites in November 1999; model uses 100 ppb as background CO level.

[@] Because of uncertainties in the measurements of reactive nitrogen by Wang et al. [2002] (see for example, NARSTO, 2000), we do not consider the NO_y measurements made at Linan and do not address issues related to the emission inventory for NO_x

Table 10: Comparison of Geometric Mean of Model Simulated Particle Concentration (μg/m³) with Measurements Made at Linan, China in November 1999.

	Meas_1 ^a	Model	Diff(%) ^b	Meas_2 ^a	Model	Diff (%) ^b
SO ₄ ²⁻	17.7	10.1	-43	15.0	12.1	-19
NO ₃ ⁻ [@]	5.4	3.3	-40	4.8	3.8	-22
NH ₄ ⁺ [@]	7.1	4.9	-31	6.8	5.7	-16
Particulate C	29.2	14.3	-51	24.6	15.6	-37
SO ₄ ²⁻ : PC	0.61	0.71	16	0.61	0.78	28

^a Measurements made by Xu et al., 2002. 'Meas_1' and 'Meas_2' are described in Table 8.

^c Difference of model simulations is calculated as: Diff (%) = (Model - Measurement) / Measurement *100

[@] Because of uncertainties in the measurements and model simulations of particulate nitrate and particulate ammonium, we do not address issues related to their emission inventory.

Table 11: Description of Various Test Runs.

	Descriptions
STND MOD	Simulations driven by TRACE-P emissions inventory
2 CO MOD	Simulations driven by doubled CO emissions
2 PC MOD	Simulations driven by doubled PC emissions
3 PC MOD	Simulations driven by tripled PC emissions

the observations. Similarly adjustments to the boundary layer mixing heights in the model in order to improve CO, particulate SO_4^{2-} , and PC would have little effect on the CO:SO₂ and particulate SO_4^{2-} :PC ratios and would worsen the simulated SO₂. Increases in dry deposition velocities improve the simulated CO:SO₂ ratio, but do not improve the simulated CO concentration and worsen the simulated concentrations for SO₂, particulate SO_4^{2-} and PC.

Of all the sensitivity tests we carried out, the only adjustment that uniformly improved the model-predicted concentrations of all relevant species and species ratios were the tests involving an increase in the emissions of CO and PC. To illustrate this, we summarize in Table 11 the results of three additional model runs: '2 CO MOD' with CO emissions increased uniformly by factor a 2 and '2 PC MOD' and '3 PC MOD' with PC emissions increased by factors of 2 and 3, respectively. Not surprisingly, since CO and PC are primary pollutants an increase in the emissions of these species leads to an approximate proportionate increase in their model-simulated concentrations, bringing them more in line with the observations. An interesting and somewhat unexpected result is the fact that increasing the PC emissions also leads to an increase in the model-simulated particulate SO_4^{2-} concentrations and brings it closer to the measured value as well. This occurs because the model includes a heterogeneous pathway for converting SO₂ to particulate SO_4^{2-} (see Chameides et al., [2002a]), and, thus an increase in the concentration of PC increases the rate of production of particulate SO_4^{2-} and, in turn, its concentration.

Because the CO and PC concentrations vary in an approximate linear fashion with their emissions, we can use the results summarized in Table 12 to estimate the percentage increase in CO and PC emissions that would be needed to bring the model-simulations into agreement with the observations. For CO, the estimated increase is about 52% (i.e., a factor of 1.52 over the TRACE-P emissions). For PC the increase is 100% for Meas.1 and 60% for Meas.2. If the increase occurred uniformly throughout China and throughout the year, it would correspond to 61 Tg of CO yr⁻¹ and 2.5 - 4.5 Tg of PC yr⁻¹. The underestimates quantified based on this study is within the range of uncertainties suggested by *Streets et al.* [2003] for CO ($\pm 185\%$), BC ($\pm 360\%$), and OC ($\pm 450\%$).

3.4.2 Estimate of the spatial extent of the required emissions increase

Based on the above analysis, we conclude that the CO and PC emissions are underestimated by about 50 and 60-100% respectively. We then estimated the magnitude of the emissions increase that would be needed if that increase were spread over the whole domain. However, our analysis is based on a comparison with measurements at one site, and it may not be appropriate to conclude that the underestimation we inferred from these measurements is applicable to the whole domain. In this section we present model simulations in which we increased CO and PC emissions over four subregions of the model domain surrounding Linan to determine the minimum spatial extent required for the emissions increase. The subregions are in Figure 18: Subregion A comprises a 600 km x 600 km box with Linan at the center; Subregion B a 1200 km x 1200 km box with Linan at the center; Subregion C a 600 km x 1800 km rectangle that includes emissions from Beijing, a major source of pollutants; and subregion D a 2000 km x 600 km rectangle that includes emissions from the Sichuan Basin but not Beijing.

Table 13 summarizes the results of a series of model runs in which CO emissions

Table 12: Comparison of Simulated Geometric Mean of the Gas and Aerosol Concentration together with Their Ratios from Different Test Runs with Geometric Mean of Measured Photochemically Aged Air.

	Meas ^a	STND MOD ^b	2 CO MOD ^b	
CO (ppb)	684	479	848	
SO ₂ (ppb)	11.5	11.5	10.8	
	Meas.1 ^a	STND MOD	2 PC MOD ^b	3 PC MOD ^b
Sulfate($\mu\text{g}/\text{m}^3$)	17.7	10.2	11.8	13.4
PC ($\mu\text{gC}/\text{m}^3$)	29.2	14.3	25.5	36.7
	Meas.2 ^a	STND MOD	2 PC MOD	3 PC MOD
Sulfate($\mu\text{g}/\text{m}^3$)	15.0	12.2	14.2	16.1
PC ($\mu\text{gC}/\text{m}^3$)	24.6	15.6	27.8	39.9
Ratios				
	Meas	STND MOD	2 CO MOD	
CO:SO ₂	60	42	78	
$\Delta\text{CO}:\text{SO}_2$	51	33	69	
	Meas.1	STND MOD	2 PC MOD	3 PC MOD
SO ₂ :Sulfate	0.65	1.13	0.94	0.81
PC: Sulfate	1.65	1.41	2.16	2.74
	Meas.2	STND MOD	2 PC MOD	3 PC MOD
SO ₂ :Sulfate	0.76	0.94	0.79	0.67
PC: Sulfate	1.64	1.28	1.96	2.49

^a 'Meas': gaseous species measured by Wang et al., 2002; 'Meas.1', 'Meas.2': particulate matter measured by Xu et al., 2002

^b Model test runs as defined in Table 4

^c Suggested increment of emissions as a factor of the original TRACE-P inventory.

^d Required additional emissions in Tg/yr if the emission underestimates are throughout China.

Table 13: Percentage of Increase in Model-Calculated CO and Particulate C (PC) Concentration at Linan for Different Model Test Runs.

CO		PC	
Model Run	(%)*	Model Run	(%)*
2 CO MOD ^a	100	2 PC MOD ^a	100
2 CO in Subregion A ^b	75	2 PC in Subregion A	76
2 CO in Subregion B	89	2 PC in Subregion B	91
2 CO in Subregion C	96	2 PC in Subregion C	96
2 CO in Subregion D	91	2 PC in Subregion D	92

^a Test runs that are defined in Table 11.

^b Test runs with emissions of CO or PC doubled just in subregion 'A', 'B', 'C', and 'D', which are defined in Figure 18.

* Relative to increment obtained from '2 CO MOD' or '2 PC MOD' test runs.

and PC were doubled in either the whole model domain or in one of the subregions. We find that increased emissions in Subregion A is responsible for only about 75% of the model-calculated increases in CO and PC concentrations in Linan obtained from a proportionate increases in emissions throughout the whole domain. Further significant increases in the model-calculated concentrations at Linan are obtained by including portions of the model domain to the north of Linan, including Beijing (i.e., Subregion B and C). Inclusion of emission to the west had a negligible effect (cf., results for Subregion D and Subregion B). These results suggest that either: 1. The required emission increases cover a fairly large portion of China (i.e., virtually the entire eastern half of China) although they do not necessarily have to cover all of China and may not include the Sichuan basin; or 2. The emissions increases are constrained to a smaller area around Linan, for example if the increases are within the 360,000 km² area around Linan (Subregion A in Figure 18), then they need to be 30 - 40% larger than inferred from the extrapolation of our model calculations discussed in the previous section.

3.5 The Characteristics of the Missing CO Sources

In this section we use the high resolution, continuous measurements of CO and SO₂ at Linan to gain insights into the characteristics of the missing CO source or sources that we concluded in the previous section are not accounted for in the TRACE-P emissions inventory. (Because particulate matter measurements at Linan were not continuous (i.e., 24-hour filter samples collected on selected days), a similar analysis is not possible for Particulate C emissions.)

3.5.1 Trajectories of high CO plumes

We begin by considering a scatter plot of the measured and model-calculated CO and SO₂ concentrations at Linan (Figure 20). Inspection of the regression lines also included in the figure reveals that the CO-SO₂ regression line for the Standard Model generally underestimates CO for a given SO₂ concentration. The regression line for the 2 CO Test run, on the other hand, overestimates CO. This is consistent with our earlier conclusion that CO emissions need to be increased by a factor of ~ 1.5 to bring the model-results into agreement with the observations.

It is also interesting to note that the observation data points tend to fall into two groups: one group that tends to fall close to the regression line from the Standard Model run, and the other that tends to fall closer to the regression line from the 2 CO Test run. This suggests, perhaps, that: (i) there were times when the sampling site was impacted by a set of CO and SO₂ sources whose magnitudes were consistent with the TRACE-P emissions inventory used in the Standard Model; but (ii) other times when some additional source or sources of CO not accounted for in the TRACE-P emissions inventory were impacting the sampling site. It is for this second set of points that an enhanced CO emissions inventory is needed in the model.

Next consider the three observation data points in Figure 20 with the highest CO concentrations; these data points are surrounded by a dotted box in the figure.

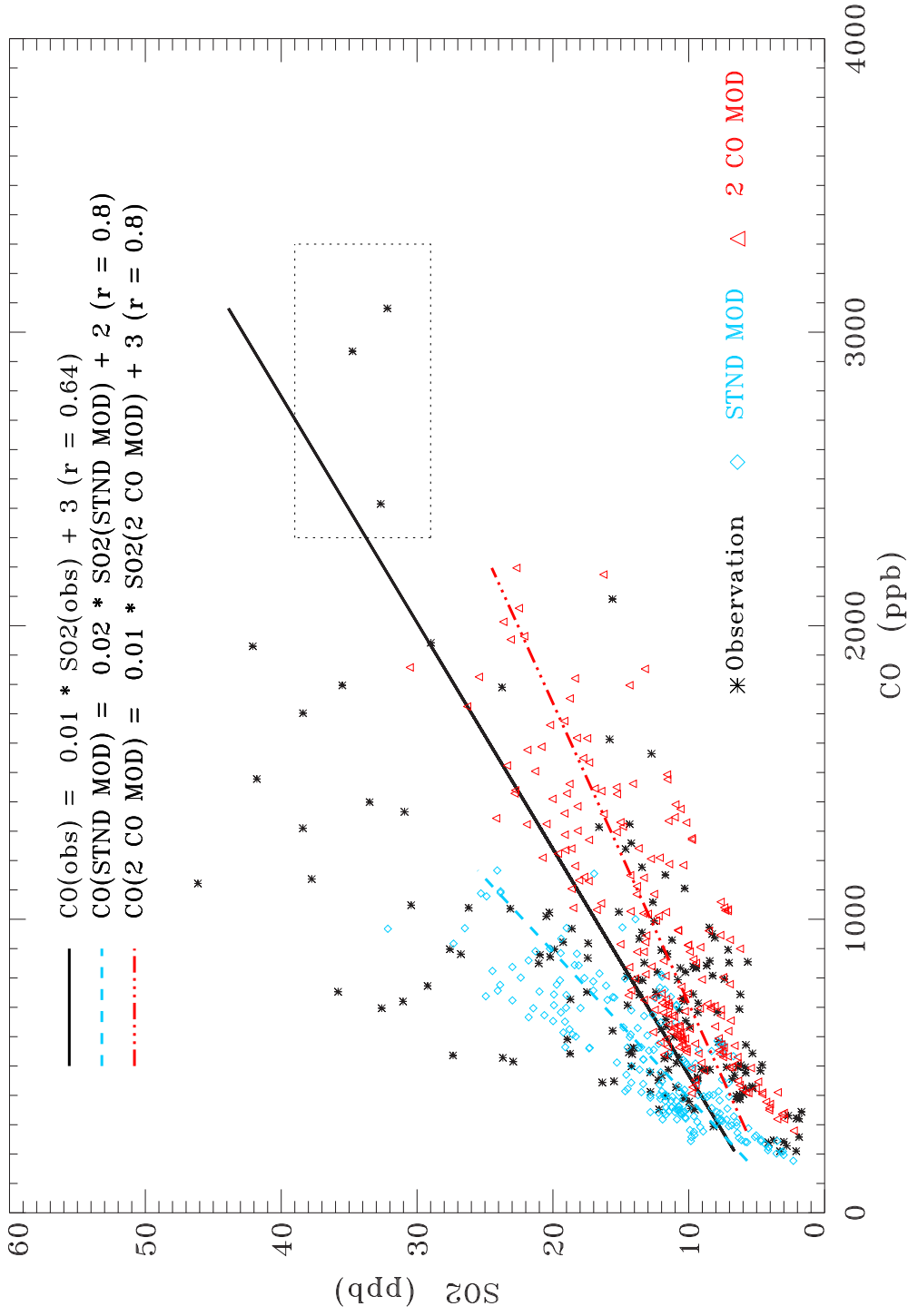


Figure 20: Scatter plot of hourly-averaged observed and model-calculated CO and SO₂ concentrations in photochemically-aged air during the afternoon hours in November, 1999. Model results are illustrated for the Standard Model and the 2 CO test run with CO emissions doubled. Also indicated are linear regressions of CO-SO₂ for each dataset. Three data points with the highest observed CO concentrations and for which back trajectories were calculated are surrounded by dotted square.

These three data points were all recorded during a single day episode in November 23, 1999. There are two interesting aspects to these data points. Firstly, note that if the 2 CO Test run regression line were extended to higher CO and SO₂ concentrations, it would pass close to them. This implies that the three data points occurred during a period when the Linan site was impacted by the hypothesized missing CO source(s). Secondly, note that in addition to the high CO concentrations, these three data points are characterized by relatively high SO₂ concentrations (i.e., > 30 ppbv). This suggests that the Linan site was impacted by significant emissions of SO₂ at the same time it was impacted by the missing CO source(s). Further insight can be gained from the back-trajectories for the three air masses that were at Linan when these high CO concentrations were observed (Figure 21). During the 2 days before arriving at Linan, each trajectory passed over the urban-industrial centers of Hangzhou and near one or more large coal-fired power plant. This along with the fact that the high CO concentrations are accompanied by high SO₂ concentrations suggests that the high CO concentrations from these data points are associated with urban/industrial activities and not biomass burning.

To further investigate the identity of the hypothesized missing CO source, we next plotted the modelled error in CO (i.e., observed CO - calculated CO) as a function of the observed SO₂ concentration (Figure 22). Once again we find that the points tend to fall into two distributions: one in which the modelled CO error is small and essentially independent of SO₂ and the other in which the modelled CO error is positively correlated with observed SO₂. For these points, the largest CO underestimations by the model occur during times when the observed SO₂ is relatively large. This suggests that the hypothesized CO source(s), like the datapoints with high observed CO concentrations, are associated with urban/industrial activities and not biomass burning as suggested by Wang et al. [2002]

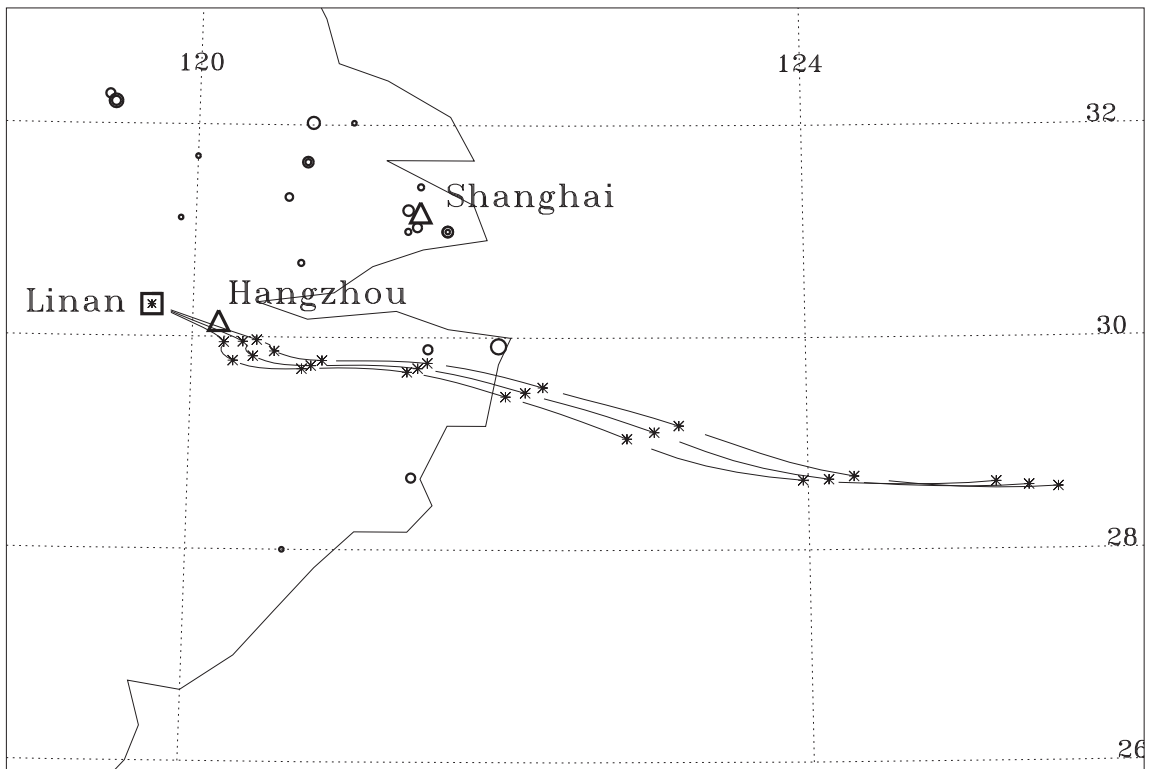


Figure 21: Two-day back-trajectories for three air masses at Linan (square) with the highest recorded hourly-averaged CO concentrations ('*' denotes the location of the air masses every 6 hour). The back trajectories were calculated with the NOAA ARL HYSPLIT model (www.arl.noaa.gov). Also indicated are locations of power plants in China (with the size of the circles being proportional to the capacity of the plant), and the metropolitan areas of Shanghai and Hangzhou (triangles).

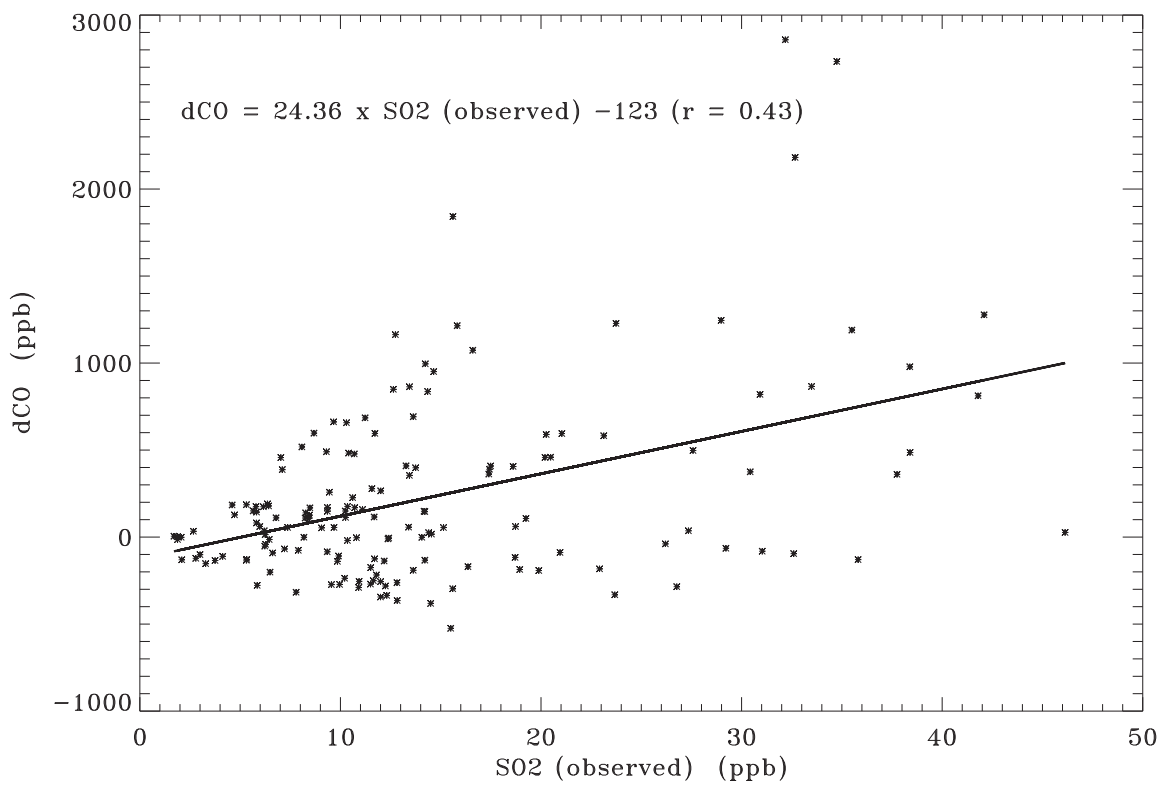


Figure 22: Modeled error ($dCO = \text{Observed (CO)} - \text{Model (CO)}$) (ppb) as a function of observed SO2 concentration (ppb).

Table 14: Factor Loadings for Multivariate Analysis of High-Resolution CO, SO₂, and NO_y Measurements from Linan

	Factor 1 *	Factor 2
CO	0.93	0.29
SO ₂	0.36	0.93
NO _y	0.83	0.49

**Calculated using Equamax Rotation.*

3.5.2 Statistical analysis of high-resolution measurements

The arguments presented above suggest that the missing CO source may be associated with SO₂ emissions. To explore this possibility further we turn to a statistical analysis of the high-resolution (i.e., 1-minute averaged as opposed to hourly-averaged) measurements from Linan. By using the 1-minute averaged data we are able to isolate individual plumes that impact the Linan site and investigate how CO and SO₂ covary within these plumes. Table 14 summarizes the results of a multivariate analysis of the CO, SO₂, and NO_y measurements from November, 1999. About 96% of the variability in these three variables can be explained by two factors: one primarily associated with variations in CO and NO_y, and one primarily associated with variations in SO₂ and NO_y. Nevertheless there is some mixing of CO and SO₂ loadings, with a small but significant loading of CO in the factor associated with SO₂ and vice versa. This is not surprising given the nature of the CO and SO₂ sources (see Figures 12 and 13) and the results illustrated in Figure 20.

While the multivariate analysis confirms that there is a subset of the high-resolution data when CO and SO₂ are correlated, it does not reveal whether there is a consistent distinction between the CO concentrations observed at Linan when CO is correlated with SO₂ and when CO is not correlated with SO₂, and, if so, the nature of that distinction. To examine this possibility, we calculated the running correlation coefficient between CO and SO₂ for subsets of the November dataset. Specifically, we

successively calculated the correlation between the 1-minute CO and SO₂ measurements obtained over the time period from $t-n/2$ to $t+n/2$, where n is the number of minutes of the time interval considered and t is varied to cover the entire month of the dataset. The probability distribution function (PDF) of the correlation coefficients is then plotted together with the average concentration of CO and SO₂ concentrations obtained for that average value of the correlation coefficient (Figure 23). Time intervals range from $n = 5$ minutes to $n = 240$ minutes (i.e., 4 hours).

Ideally, we would use the results obtained using a small value of n , since this would allow us to focus on CO and SO₂ variations in individual plumes that presumably arose from specific source types. However, the correlation coefficients calculated with a very small value of n are not useful because they have no statistical significance. (The statistical significance of a correlation coefficient increases with the square root of $n-2$, degree of freedom). Conversely, choosing a large value of n will yield statistically significant correlation coefficients, but ones that are not very informative with regard to CO and SO₂ emissions since they average together the variabilities for many plumes and begin to be effected by longer-term processes not related to emissions such as expansion and contraction of the boundary layer.

To determine the optimum value of n for our analysis, we calculated the average confidence level for all correlation coefficients obtained from the month-long dataset as a function of n using the student's t -test (Figure 24). We find that the average confidence level is in fact quite low for $n < 10$ minutes and increases rapidly as n is increased. When $n \sim 50$ minutes, the average confidence level reaches 90% and then flattens out with relatively little increase with further increases in n . It would therefore appear that the optimum n is in the range of about 50 - 70 minutes. Examination of the PDF distribution for this range of n -values reveals that there is little or no correlation between CO and SO₂ for the majority of time intervals analyzed. However, for a small percentage of the time intervals analyzed ($\sim 13\%$),

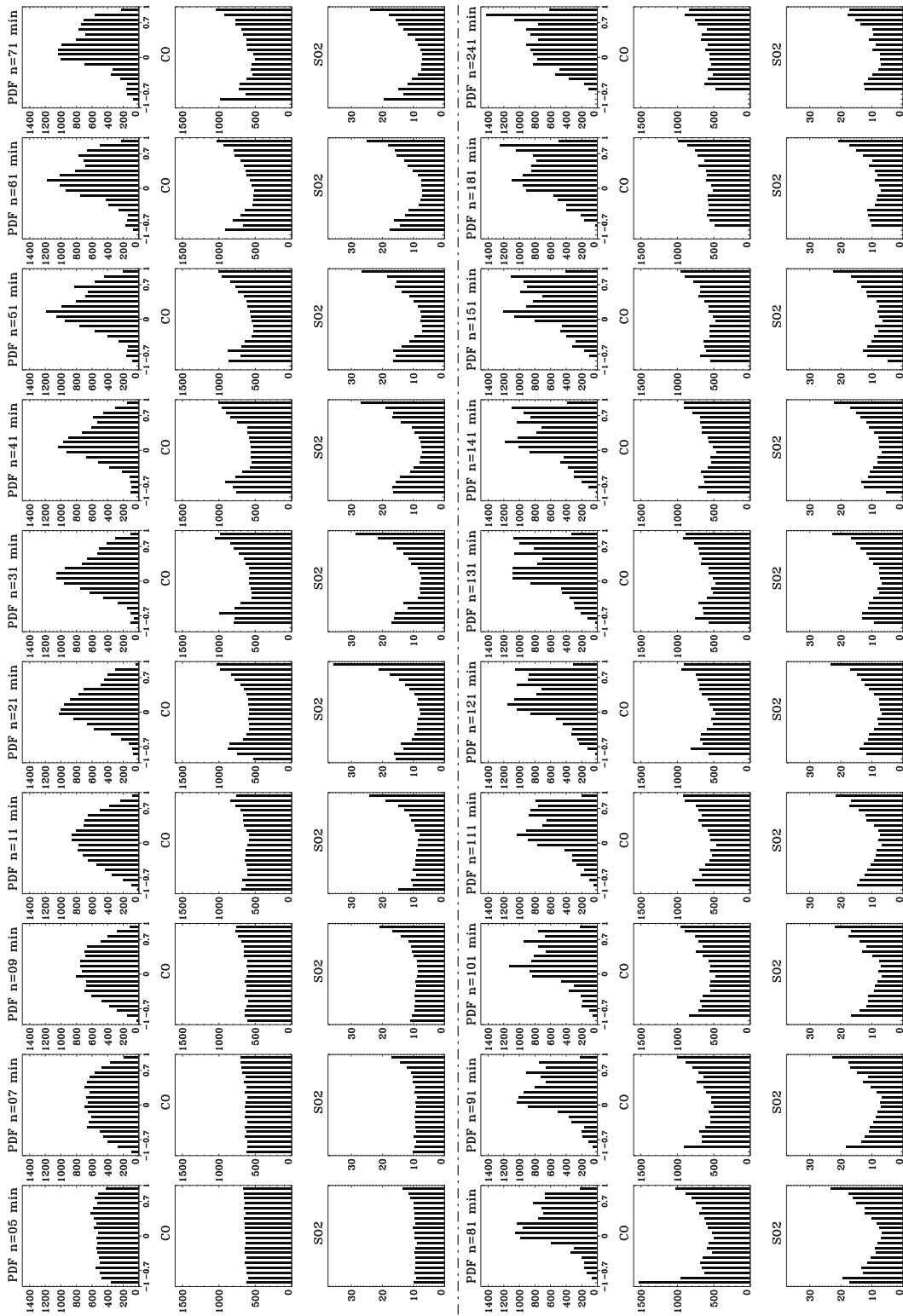


Figure 23: The probability distribution function (PDF) of CO-SO₂ correlation coefficients, and average CO and SO₂ concentrations (in ppbv) for each correlation coefficient bin for values of the time interval, n, varying from 5 to 241 minutes.

there is a significant positive correlation ($r > 0.7$) between CO and SO₂. These results are consistent with what we found with the multivariate analysis. The interesting and unique aspect of the running-correlation analysis is that it yields values for the average CO concentration measured during those time intervals when CO is correlated and not correlated with SO₂. Interestingly we find that the time intervals when CO is highly correlated with SO₂ are generally those time intervals when the CO concentrations are highest (i.e., > 700 ppbv); these are the high concentrations that caused the observed, average CO at Linan to be larger than the model-calculated average CO. When CO is not correlated with SO₂, the CO concentration averages about 500-510 ppbv. This latter CO concentration is in fact quite close to the average CO concentration predicted by our Standard Model simulations using the TRACE-P inventory. One interpretation of these results is that the hypothesized missing CO source(s) that caused the Standard Model to underpredict the CO concentration at Linan is (are) associated with SO₂ sources that are already accounted for in the TRACE-P inventory.

3.5.3 Scenarios that would provide the missing CO emissions

Suppose, as suggested in Section 4, the estimated 50% increase in CO emissions required to bring the Standard Model calculations into agreement with the Linan measurements were uniformly spread throughout China and throughout the year; this would require an additional source of 60 Tg CO yr⁻¹. Moreover suppose as suggested by the analysis presented in Section 5.2, that these additional CO emissions all occurred from sources that also emitted SO₂. What kinds of modification would be required in the emission factors used to develop the TRACE-P emission inventory for CO?

First note that almost all of the SO₂ emitted in China comes from coal-burning: 49% from coal-burning power plants, 36% from industrial coal consumption, and

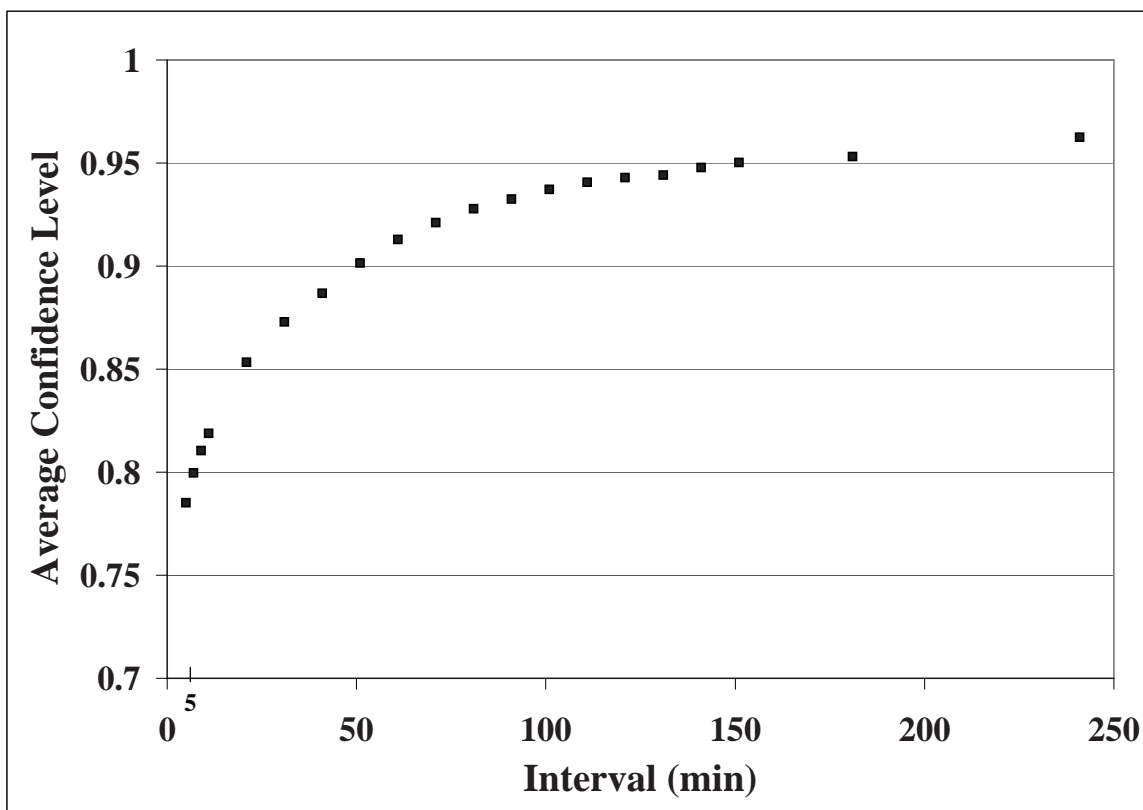


Figure 24: The average confidence level of the CO-SO₂ running correlation as a function of the time interval, n. Confidence levels calculates using the student's t-test.

10% from domestic coal use [Streets et al. 2003]. Thus the requirement that the additional CO emissions come from sources that also emit SO₂ essentially requires that the additional CO emissions also come from coal-burning.

However, while China is the world's largest consumer of coal, coal-burning in China represents a relatively small source of CO in the current TRACE-P inventory (i.e., about 18 Tg yr⁻¹ or 16% of all CO emissions from China); about 9% of the total comes from industry, 7% from domestic sources, and power plants are negligibly small. If the additional emissions are to come from coal-burning, the emission factors used in the TRACE-P inventory for one or more of these sources would need to be adjusted upwards.

In general, CO emission factors from coal combustors are highly variable. If a unit is operated improperly or not well maintained, the resulting CO emissions may increase by several orders of magnitude [US EPA, 1998]. Thus an increase in CO emissions assigned to coal-burning activities in China would require that the coal-burning facilities in China are being operated at significantly lower efficiency than was assumed when the emission inventory was developed.

3.5.3.1 Coal-Fired Power Plants

When estimating CO emission rates, it is generally assumed that power plants operate with high efficiency. For example, the emission factor (EF) for most power plants in United States is 0.25 g/kg, i.e. this corresponds to an operation efficiency in excess of 99.99% [US EPA, 1998]. The CO emission factor (EF) for power plants in China is estimated to be 4g/kg, which corresponds to an efficiency $\sim 99.8\%$. Even though power plants are responsible for more than half of the total coal consumption in China (i.e. ~ 500 Tg yr⁻¹) [Sinton and Fridley, 2000], the resulting CO emissions from power plant is negligibly small (i.e., only 2Tg yr⁻¹). If power plants were responsible for all of the additional 60 Tg yr⁻¹ of CO emissions hypothesized here,

then the CO emission factor from coal-fired power plants in China would have to be increased from 4g/kg to 120 g/kg. While this represents a rather large increase in the CO emission factor, it only requires a decrease in power-plant operating efficiency from the current estimate of 99.8% to 95.6%. Moreover, recent aircraft measurements of coal-fired power plant plumes in United States (US), revealed significantly elevated CO concentrations in some plumes. These observations suggested that the CO emission factors from these power plants is about 30 times higher than that normally assigned to US plants under normal operating conditions [*Nicks, et al., 2003*]. Thus it would appear that there are significant uncertainties in CO emission rates from power-plants. Even larger uncertainties apply to power plants operating in China. Field measurements in China, similar to those of *Nicks et al.* [2003], would help to constrain these uncertainties.

3.5.3.2 Industrial and Domestic

Another possible category of unaccounted for emissions CO is from coal combustors used in small industrial and domestic facilities, such as boilers and cook stoves. Smaller combustors typically emit more CO because they burn at lower temperatures than larger ones [*US EPA, 1998*]. The CO emission factors used in the TRACE-P inventory for the industrial and domestic sectors are 38 and 74 g/kg respectively; these are already 2-3 times higher than comparable sources in the United States [*Streets et al., 2003*]. These emission factors yield 10 and 8 Tg CO yr⁻¹ from industrial and domestic coal burning, respectively. In order to make up the hypothesized 60Tg yr⁻¹ in missing CO emissions, the emission factors from these two sectors would have to be increased by a factor of ~ 3 , i.e., ~ 110 g/kg for industrial boilers and 200 g/kg for cooking stoves. These factors fall near the high-end in emission factors observed for these types of facilities. For example, the US EPA [1998] suggests an emission factor for industrial hand-fed coal combustors (which typically operate at low efficiency) of

138 g/kg. Zhang [1999] observed CO emission factors from cooking stoves in China ranging from 18-170 g/kg.

Of course the above estimated emission factors assumed that the additional CO emissions were coming either entirely from power plants or entirely from industrial and domestic sources. If the emissions were equally divided between these sectors, it would require CO emission factors from power plants, industrial burners, and domestic stoves of ~ 60 , 55, and 100 g/kg. These are large, but perhaps not out of the realm of possible.

3.6 Conclusion

A comparison between model simulations and field measurements of gas and particle species at a rural site in one of the more industrialized regions of China, the Yangtze Delta, during November, 1999 suggests that while the TRACE-P emission inventory for sulfur oxides is accurate, the emissions inventory for CO and Particulate C are underestimated by ~ 50 and 60 - 90%, respectively. Further analysis of the high resolution measurements of CO and SO₂ suggest that the additional source(s) of CO needed to bring the model into agreement with the measurements is most likely associated with SO₂ emissions from coal burning. Significant increases in the CO emission factors typically assigned to power-generating, industrial, and domestic coal-burning processes would be needed to account for the missing CO emissions from these sources. It is not at all clear that such large emission-factor increases are appropriate. A more comprehensive effort to monitor CO and related pollutants in smoke-stacks, pollutant plumes, and ambient air are needed to better constrain the CO emission rate from China and East Asia and identify the contributions from various sources. A similar effort is needed in the case of PC emissions as well.

CHAPTER IV

CONCLUSION

This thesis research carried out to better quantify the magnitude of the pollutant emissions from East Asia and their fate. Major issues that have been investigated include:

1. Spatial distribution of the concentration and deposition patterns of anthropogenic sulfur compounds over East Asia and North Pacific Ocean.
2. Quantification of the budgets of anthropogenic sulfur oxides emitted from East Asia (including individual subregions), their outflows to the North Pacific Ocean, and the morphology of the exported sulfur compounds in spring 1995, the time period when the anthropogenic sulfur emissions from the region peaked in the last decades.
3. Evaluation of the accuracy of current emission inventories for the major air pollutants emanating from East Asia, by using a combination of regional model simulations and simultaneous gas-phase and particulate-phase measurements at a rural site in China.
4. Identification of the nature of inaccuracies of the current emission inventories and suggestions for the future improvement.

The main conclusions of this thesis are summarized in Section 4.1 and plans for future research are given in Section 4.2.

4.1 Major Results

4.1.1 Distribution and budget of sulfur compounds in East Asia

Our regional model simulations of anthropogenic sulfur compounds, which include emissions, transport, chemical conversion, and deposition, suggest that large portions

of East Asia, especially China, have high SO_x concentrations, among them significant areas around major industrial centers has SO_x concentrations higher than the WHO health guideline. Large horizontal and vertical gradients of SO_x exist between industrialized regions and remote ones, surface area and free troposphere, respectively.

Based on the estimated 1995 East Asia sulfur emission inventory, a total of 4 Tg S is emitted into our model domain during spring of 1995 (February to April). Based on our model simulations, $\sim 45\%$ of the total emissions is returned to the model domain by wet deposition and $\sim 35\%$ by dry deposition. More specifically, most subregions within East Asia: China and Mongolia, Southeast Asia, South Korea and North Korea, and Japan, are net exporters of anthropogenic SO_x (i.e. the S emissions from the region are greater than the deposition to the region). Among them, China is responsible for 85% of the total emissions, and $\sim 50\%$ of its total emitted SO_x is exported to locations outside its borders.

During the later winter to early spring when continental outflow conditions predominate, about 20%, i.e. 0.2 Tg S per month of the total emitted SO_x within our model domain have been exported to other regions, mainly North Pacific Ocean. This is comparable to the total natural sources of S to the region from emissions of dimethylsulfide, i.e. 0.1-0.3 Tg S per month. In addition, the anthropogenic SO_x exported from East Asia has been found to be mostly particulate SO_4^{2-} and in the free troposphere, where SO_4^{2-} tends to be longer lived and stronger winds favor more rapid transport. Therefore it appears that the export of anthropogenic SO_x from East Asia during the late winter and early spring is likely large enough to perturb the sulfate aerosol concentration over the North Pacific Ocean.

Comparing with available field and airborne measurements, our coupled regional climate-chemistry model (with online simplified sulfur chemical mechanism and prescribed free radical fields from off-line full chemistry model as inputs) is capable of reproducing the spatial distribution of both concentrations and deposition fluxes of

sulfur compounds on the right magnitude, therefore it is suitable for further climate-sulfate aerosol interaction studies.

4.1.2 Evaluation of East Asia anthropogenic emission inventories

Similarly to the sulfur compounds discussed above, concentrations of most anthropogenic air pollutants, including CO, SO₂, particulate sulfate, and particulate carbonaceous aerosols, simulated by the regional chemical transport model (RADM), peak around the major urban-industrial centers, and demonstrate large spatial inhomogeneities.

After the incommensurability of model simulation and field measurements been taken into consideration, RADM is able to simulate the average magnitude of anthropogenic SO₂ and sulfate when compared with the continuous field measurements of both gaseous and particulate species, which suggests the reliability of current emission inventories for sulfur compounds and our modeling system in general.

Our investigation by integrating numerical simulation with field measurements suggests that CO emissions from East Asia are likely underestimated by $\sim 50\%$. In addition, we suggest a 60-90% underestimation of particulate carbonaceous emission in the current anthropogenic inventories for East Asia.

Through statistical analysis of the high-resolution measurements, as well as multivariate analysis and back-trajectory analysis, we diagnose that the missing CO sources are likely associated with SO₂ sources that are already accounted for in the current inventories. This in turn suggests the emission factors of coal-combustors used in the current inventories are likely underestimated. Further investigations of CO emissions originating from power plants, small industrial and domestic coal-burning facilities are suggested.

4.2 Future Research Plan

This thesis research explores the capacity of on-line and off-line coupled regional climate-chemistry modeling system in studying the anthropogenic air pollutants originated from East Asia from various aspects. The modeling system has been proved to be useful in quantifying the budget and fate of anthropogenic emissions, as well as the reliability of the emission inventories by this study. Some possible future research topic includes:

4.2.1 Fully coupling of regional climate and chemical transport model.

When a complete chemical mechanism runs online with a regional climate model, the fully coupled model is able to simulate the interaction of chemical species with climate conditions, including radiation transfer, cloud processing, general circulation, as well as the hydrological cycles simultaneously, this should provide more realistic assessment of the impacts of anthropogenic air pollutants on the climate, as well as air quality under changed climate conditions.

Based on our model simulations, the spatial distribution of anthropogenic air pollutants, including those with special radiative properties, such as particulate sulfate and particulate carbonaceous compounds, have large spatial inhomogeneities. This suggests the necessity of applying fine resolution regional scale models rather other than coarse global scale models.

4.2.2 Global-regional interaction studies

In order to reduce the uncertainties related to model inputs, we used the observation based reanalysis data as the initial and boundary conditions for current studies. However, for the purpose of impacts assessments, our modeling system also needs to simulate the situations beyond the point when real-time observations are available. Since regional scale climate model is not a self-sustainable system, the lateral boundary conditions from larger scale (global) general circulation models are

required.

One approach that can be used to address the need for high spatial resolution in a given region such as East Asia within a global-modeling framework is to make use of a two-way nesting interface between a coarse-resolution global model and a high-resolution regional scale model for East Asia. In one way, the regional model driven by boundary conditions derived from the global model can predict spatially-specific climate and air quality within East Asia and in the other direction, more realistic subgrid-scale forcing within East Asia can be used to drive the global model.

4.2.3 Interaction of anthropogenic-natural air pollutants.

In the current study, we have been focusing on the anthropogenic air pollutants. In order to assess their impacts in a more comprehensive fashion, it is also necessary to include chemical species with natural origins, of particular interests is the mineral dust in East Asia. During the recent Asian Aerosol Characterization Experiment (ACE-Asia), it has been found that mineral dust, which dominate the coarse mode of aerosols measured in East Asia, perturbs both the radiative and chemical environment of the region(Huebert, 2003).

The mobilization, deposition, and transport of dust can be simulated by adopting existing dust model, Desert Entrainment And Deposition (DEAD) model (Zender et al., 2003), for example, into RegCM. RegCM is capable of hosting such dust module by providing required parameters, including meteorological and surface conditions, to drive the dust module.

Upon coupling with the dust model, the regional climate-chemistry modeling system should be able to study the impacts of Asia dust storms on the atmospheric radiation transfer as well as chemical composition. In addition, it may also be used to study the biogeochemical cycle of important elements, such as iron, of the region.

APPENDIX A

REGIONAL CHEMISTRY MODEL

Atmospheric chemistry transport models (CTMs) consist of mathematical representations of the relevant physical and chemical processes, such as transport, chemical evolution, and removal of selected tracer species. Driven by set of tracer emissions and meteorological conditions, CTMs are able to simulate the tracer's concentrations as a function of space and time [*Eliassen*, 1980; *Fisher*, 1983; *Peters et al.*, 1995; *Seinfeld and Pandis*, 1998; *Jacobson* 1999; *NARSTO Synthesis Team*, 2000; *Russell and Dennis*, 2000; *Seigneur and Moran*, 2003].

Among various CTMs, such as box models (one-dimension, Lagrangian or Eulerian type) as well as the multi-dimension Lagrangian trajectory models and Eulerian (or grid-based) models, the three dimension Eulerian chemical transport models are becoming dominant in air quality studies [*Russell and Dennis*, 2000]. Current Eulerian atmospheric chemistry models originated in the 1970's and have been developed for studies on urban, regional, and global scales [*Reynolds et al.*, 1973, 1974; *Carmichael and Peter*, 1980; *Peters and Jovanis*, 1979]. In the past three decades, the 3D Eulerian CTMs have been significantly improved and applied to address numerous scientific and policy-relevant questions. From scientific perspective, CTMs, especially when they are integrated with the laboratory experiments and field observations can be used to investigate how the different physical and chemical mechanisms affect the fate and distribution of air pollutants. From air quality management and policy making perspective, CTMs can connect the pollutant emissions with the resulting variations in air pollutant concentrations, including the spatial and temporal distributions, therefore provide essential information for assessing the impacts of tracer

species and various emission control strategies [McRae and Seinfeld, 1983; Chang et al., 1987; Venkatram et al., 1988; Carmichael et al., 1991; Morris et al., 1990; Kumar et al., 1994; Odman and Ingram, 1996; Byun and Ching, 1999].

A.1 General Model Description

RADM is designed to calculate the episodic chemical concentrations and dry and wet deposition of acids on subcontinental scales [Chang et al., 1989]. Tracer species are transported and diffused using externally specified meteorological data, in this case from the RegCM. The basic photochemical mechanism is RADM2, which contains about 110 reactions involving 64 species, among which 40 are organic compounds. Aqueous phase chemistry is included in the cloud process module [Walcek et al., 1986]. Wet deposition and dry deposition of species are considered based on the meteorological conditions as well as the physical and chemical properties of tracer species.

RADM used in this study has similar horizontal and vertical structure as RegCM described in the previous section. In order to avoid the uncertainties related to the RegCM simulations near the lateral boundaries, the RADM model domain is slightly smaller than that of RegCM.

The whole RADM system consists of three parts: preprocessing, RADM, and postprocess. In this study we made several modifications to the version of RADM used in Luo [2000].

A.2 Model Inputs

A.2.1 Emissions

Since the focus of this part of our study is the anthropogenic emissions from East Asia in 1999, the TRACE-P emission inventory of SO₂, NO_x, CO, black carbon (BC), organic carbon(OC), and NMVOC for 2000 by Streets et al. [2003] is used as input

Table 15: Summary of Estimated Anthropogenic Emissions within Our Model Domain (Tg) Based on *Streets et al.* [2003].

	Anthropogenic ^b	Large Point	Biomass Burning ^c	Total
SO ₂	17.78	5.77	0.152	23.7
NO _x	13.42	2.62	1.26	17.30
CO	119.7	1.62	28.09	149.51
NMVOG	20.45	0.059	4.92	25.44
BC	1.11	0.0074	0.19	1.31
OC	3.11	0.0059	1.36	4.48

^a Calculation is based on TRACE-P emission inventory by Streets [2003].

^b Major area anthropogenic source includes: industry, domestic, transportation, and power generation.

^c Biomass burning include: forest burning, savanna/grassland burning, and the burning of crop residues in fields after harvest.

to RADM.

The TRACE-P emission inventories are on 1 degree x 1 degree grids in longitude and latitude cover most part of Asia. We first interpolated the data to our 60 km x 60 km Lambert conformal grids through bi-linear interpolations.

Table ?? list the total emissions of all species we used as inputs to RADM. Since China is the major contributor of anthropogenic emissions within our model domain, those summations are very close to the total emissions originated from China [*Streets, et al.*, 2003].

A.2.2 Photolysis rates

Photolysis rates (j-value) in RADM is pre-calculated by a radiative transfer model which includes absorption by O₂ and O₃, scattering and absorption by aerosols and clouds, Rayleigh scattering, and ground reflection. The model solves the radiative transfer equation using the delta-Eddington technique of Joseph et al. [1976]. Before the RADM simulation, the clear sky photolysis rates j_{clear} are calculated for each hour between sunrise and sunset with a spatial increment of 10° latitude over the RADM domain for the Julian days of each simulation. The resulting photolysis rate

constants are then tabulated at three altitude (0, 1, and 10km) for each hour and each 10° latitude. During each time step of RADM simulation, the j-value of each grid is then interpolated from the tabulated data for the appropriate time and location.

A.2.2.1 cloud cover

The cloud cover data required for the j-value calculation are imported from corresponding RegCM outputs. The cloud at each model layer is assumed to be randomly overlaid, therefore the column cloud cover is calculated by:

$$C_{tot} = 1 - \prod_{k=1}^{kmax} (1 - C_k) \quad (19)$$

where C_{tot} is the cloud cover over the whole column, and C_k is that for each model layer.

A.2.3 Meteorological conditions

The meteorological conditions simulated by RegCM are used to drive the RADM. Imported dynamic fields include three dimensional wind, temperature, and water vapor mixing ratios, as well as two dimensional surface temperature, surface pressure and precipitation rates. Those variable are imported to RADM every 6 model hour and linearly interpolated to each time step.

A.3 Regional Acid Deposition Model (RADM)

Driven by the specified emission and meteorology data at each grid point, RADM is able to simulate the time-varying three dimensional distributions of tracer gaseous and particulate species, through appropriately numerical representation of transport, chemical evolution, and removal processes of those chemical species. The model is mathematically described by the following species conservation equation:

$$\frac{\partial C_i}{\partial t} = -\nabla \cdot VC_i + \nabla \cdot (K_e \nabla C_i) + P_{chem} - L_{chem} + E + \left(\frac{\partial C_i}{\partial t}\right)_{clouds} + \left(\frac{\partial C_i}{\partial t}\right)_{dry} \quad (20)$$

$$i = 1, 2, 3, \dots, n.$$

where C_i is the species volume mixing ratio, V is the three dimensional velocity vector at each grid point in the model domain, K_e is the eddy diffusivity used to parameterize the subgrid scale fluxes of trace species due to noncloudy turbulent motions, P_{chem} and L_{chem} are the production and loss rates due to chemical interactions, E is the emission rate, $(\frac{\partial C_i}{\partial t})_{clouds}$ is the rate of change of concentration due to cloud effects (including subgrid scale vertical redistribution, aqueous chemical interactions, and scavenging), and $(\frac{\partial C_i}{\partial t})_{dry}$ is the change in concentration due to dry deposition [Chang *et al.*, 1987].

Current version of RADM [Luo *et al.*, 2000] includes 64 gaseous and particulate species and 110 reactions. Among 64 species, 30 are transported species.

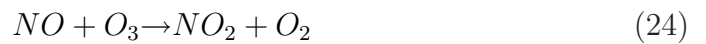
A.3.1 Chemical kinetics and photochemical data

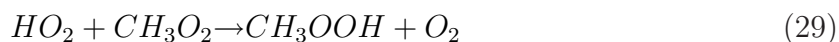
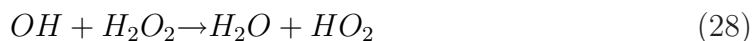
The photochemical reaction rates within RADM have been updated based on Sander *et al.* [2003].

The update involve termolecular reactions:



and second-order reactions:





A.3.2 Transport

Besides large scale horizontal and vertical transport of chemical species simulated based on meteorological condition from RegCM, RADM also calculated the subgrid turbulent transport using first order closure eddy diffusion theory [Louis, 1979]. Luo *et al.* [2000] modified the parameterization of Kz, the eddy diffusion coefficient. In the surface layer, Kz was calculated according to the Monin-Obukov similarity theory [Louis, 1979; Businger *et al.*, 1971]. For the other layers within boundary layer, Kz was calculated using the method of Wyngaard and Brost [1984]. Above boundary layer, Kz was determined using the method of Blackadar [1979].

RADM now uses the same vertical resolution as RegCM, i.e., 15 layers instead of 6 as in Luo *et al.* [2000]. Now there are 5 layers below 2 km. This modification can provide more realistic representation of the planetary boundary layer and also avoid the uncertainties related with vertical interpolations between RegCM results and RADM inputs.

A.3.3 Dry deposition

Dry deposition to the surface is an important sink of tracer species in the troposphere. Based on the tropospheric ozone budget derived by various global CTMs studies (after IPCC [2001]) (Table A.3.3), the surface deposition is in the magnitude at least comparable to the other major tropospheric ozone sources and sinks: surface deposition of ozone ranges from 40% to 230% of the total stratosphere-troposphere exchange and 67% to 793% of the net in situ tropospheric chemical production and loss of ozone.

Besides ozone, dry deposition is also important sink to sulfur compounds. We surveyed the global sulfur budget estimated by different studies since early 1990's

Table 16: Tropospheric Ozone Budgets for Circa 1990 Conditions from a Sample of Global 3-D CTMs since 1996

CTM	STE	P-L	SURF	Burden	Reference
MATCH	1440	-810	620		<i>a</i>
MATCH-MPIC	1103	-478	621		<i>b</i>
ECHAM/TM3	768	-86	681	311	<i>c</i>
ECHAM/TM3*	740	-255	533	266	<i>d</i>
HARVARD	400	+420	820	310	<i>e</i>
GCTM	696	+128	825	298	<i>f</i>
UIO	846	+295	1178	370	<i>g</i>
ECHAM4	459	+75	534	271	<i>h</i>
MOZART	391	+507	898	193	<i>i</i>
STOCHEM	432	+430	862	316	<i>j</i>
KNMI	1429	-855	574		<i>k</i>
UCI	473	+345	812	288	<i>l</i>

After IPCC [2001] Table 4.12.

STE = stratosphere-troposphere exchange (net flux from stratosphere) (Tg/yr).

P-L = net in situ tropospheric chemical production-loss (Tg/yr).

SURF = surface deposition (Tg/yr).

Burden = total content (Tg) (1DU = 10.94 Tg).

* Results using CH₄-only chemistry without NMVOC.

Reference: ^a Crutzen et al. [1999]; ^b Lawrence et al. [1999]; ^c Houweling et al.

[1998]; ^d Houweling et al. [1998]; ^d Wang et al. [1998]; ^e Levy et al. [1997]; ^f

Berntsen et al. [1996]; ^g Roelofs and Lelieveld [1997]; ^h Hauglustaine et al. [1998]; ⁱ

Stevenson et al. [2000]; ^j Wauben et al. [1998]; ^k Wild and Prather [2000].

Table 17: Global Budgets (Tg S/yr) of Major Sulfur Compounds for a Sample of Global Three Dimensional Climate-Chemistry-Aerosol Models since 1991

	Sources [®]	Sinks			Burden	Reference	
		Chem Loss *	Dry Dep.				Wet Dep.
			Tg S /yr	%			
SO ₂	94.5	49.8	30.5	32	14.2	0.30	<i>a</i>
	122.8	62.0	55.0	45	5.8	0.20	<i>b</i>
	95.6	49.1	26.6	28	19.9	0.34	<i>c</i>
	100.5	51.3	40.2	40	9.0	0.43	<i>d</i>
	80.4	44.7	35.5	44	0.2	0.56	<i>e</i>
	90.3	38.5	41.2	46	10.6	0.43	<i>f</i>
	82.5	53.6	24.5	30	1.6	0.40	<i>g</i>
	80.7	44.8	34.8	43	1.0	0.63	<i>h</i>
SO ₄	53.3		8.6	16	44.5	0.77	<i>a</i>
	62.0		17.0	27	45.0	0.80	<i>b</i>
	49.1		5.6	11	43.5	0.53	<i>c</i>
	51.3		6.7	13	44.6	0.61	<i>d</i>
	46.6		9.2	20	37.4	0.73	<i>e</i>
	40.7		5.1	13	34.7	0.63	<i>f</i>
	53.6		3.7	7	51.2	0.40	<i>g</i>
	46.7		5.7	12	41.1	0.72	<i>h</i>

[®] Sources of SO₂ include anthropogenic emissions and oxidations of reduced sulfur compounds, mainly dimethylsulfide (DMS). Sources of sulfate include oxidation of SO₂ and anthropogenic emissions.

* Chem Loss = gas phase oxidation and aqueous phase oxidations.

Reference: ^a Langner and Rodhe, 1991; ^b Pham et al., 1996; ^c Chin et al., 1996;

^d Feichter et al., 1996; ^e Koch et al., 1999; ^f Chin et al., 2000a; ^g Rasch et al., 2000;

^h Koch et al., 2003

(Table A.3.3). Based on different investigations, the dry deposition removes about 25-55 Tg S/yr in the form of SO₂, or 28-46% of total emitted SO₂, and 3.7-17.0 Tg S/yr in the form of sulfate, or 7-27 % of total emitted SO₄.

Acid deposition have been observed to be a large-scale phenomenon since the establishment of network to monitor the surface water chemistry in Europe as early as 1960's. A series of studies by Eville Gorham initiated in 1955 built the foundation of our current understanding of acid deposition that combustion emissions, mainly SO₂ and resulting sulfate are major contributors to the acid deposition [*Seinfeld and*

Pandis, 1998]. The observed decline of the forests during 1970's in regions exposed to acid deposition, for example the extensive dieback of forests in Central Europe over the past decades [*World Bank, 1997*], has shown that the deposition of tracer gaseous and particulate species can have rather destructive impact on the biosphere. The realization of severity of acid deposition then initiated many observational campaigns and modeling exercises to improve the understanding of the mechanisms of the surface gaseous and particulate species exchange [*U.S. NAPAP, 1991; Hicks, 1970; Moller et al., 1970; Bolin and Persson, 1975; Wesely and Hicks, 1977; Wesely et al., 1977*].

The surface exchange of tracer species is a complicated process involved various aspects of related species, ambient atmospheric condition and surface condition. More specifically: (a). Chemical and physical properties of the related tracer species, including the solubility, reactivity, acidity/alkalinity, or likeness to be uptake by vegetation. (b). Near surface meteorological conditions. The intensity of the vertical turbulence will determine the possibility of for the suspended tracer species to collide with the underlaid surface. (c) Physical, chemical, and biological properties of the surface, which include the wetness, smoothness (or roughness), vegetation type, and acidity.

The representation of dry deposition flux within numerical models is usually formulated in terms of deposition velocity and concentration of the tracer species [*Chamberlain and Chadwick, 1953; Wesely and Hicks, 1977*].

$$F_c = V_d C \quad (30)$$

where F_c is the vertical flux of a tracer in the surface boundary layer, C is the concentration of the species at a specific height, usually the lowest level of the model, and V_d is the deposition velocity. V_d is a mathematical convenience that is not always regarded as a comprehensive representation, because its use can result in oversimplification of the complicate surface-atmosphere exchange processes. Nevertheless due

to its simplicity and over all performance, this formula is often used in the regional to global scale atmospheric chemistry models.

In order to derive formulations of the deposition velocity, both empirical and theoretical description of various related processes, including ambient meteorological conditions, planetary boundary layer parameterization, radiation transfer, micro-meteorology of the canopy, and biosphere representation, are combined together and organized in a overlaid resistance-in-series fashion. The flow of tracers cross the interface of atmosphere and underlaid surface is analogous to the flow of electrons cross series of electrical resistance. The dry deposition velocity is represented by:

$$V_d = (R_a + R_b + R_c)^{-1} \quad (31)$$

where R_a is the aerodynamic resistance within the boundary layer. R_b is the resistance in the sub-layer adjacent to the surface, is often called quasi-laminar resistance. R_c is the surface or canopy resistance.

In the previous RADM application by *Luo et al.* [2000], the dry deposition scheme was based on *Walcek et al.* [1986], in which the surface resistance is derived from a lookup table estimated from limited measurements [*Sheih et al.*, 1979]. In this study we applied the resistance-in-series module that takes seasonal variations of land-surface character and difference of physical/chemical properties of tracer species into consideration [*Wesely*, 1989; *Walmsley and Wesely*, 1996]. Some improvements to the original deposition scheme of *Wesely* [1989] include calculating the aerodynamic resistance based on *Jacobson* [1999] and *Byun et al.* [1999], the surface resistance over tundra based on *Jacob et al.* [1992], the surface resistance of NO_2 based on *Ganzeveld* [1995], and the surface resistance of SO_2 over snow based on *Valdez*[1987] and *Ganzeveld* [1998].

A.3.3.1 Aerodynamic resistance

Aerodynamic resistance, R_a represents the resistance of moving species from boundary layer to the surface which is determined by the turbulent mixing above the surface. Within RADM, the r_a for gas and particle is parameterized based on the similarity theory as:

$$R_a = \frac{\int_{z_{0,q}}^{z_r} \Phi_h \frac{dz}{z}}{ku_*} \quad (32)$$

where k is the unitless von Kármán constant, u_* is the friction velocity (m/s), z is the height above the surface (m), z_r is a reference height (10m), $z_{0,q}$ is the surface roughness length of gas and particle q (m), and Φ_h is the dimensionless potential temperature gradient. Because the transport of trace gases is similar to the transport of energy more than it is to the momentum, a dimensionless potential temperature gradient is used instead of a dimensionless wind shear [*Jacobson, 1999*].

In the previous version of RADM [*Luo et al., 2000*] the R_a is calculated based on the formula by *Sheih et al.* [1979] and *Walcek et al.* [1986]:

$$R_a = \frac{\ln(z/z_0) - \psi_h}{ku_*} \quad (33)$$

where ψ_h is an integral diabatic influence function related to the stability, or $\psi_h + \ln(z/z_0)$ is the approximation of the numerator in Equation 32. Under different stability conditions, ψ_h is parameterized based on measurements by *Wesely and Hicks* [1977] and *Wesely et al* [1977], as well as modeling studies by *Sheih et al* [1979].

$$\psi_h = \left\{ \begin{array}{ll} \exp\{0.598 + 0.39\ln(-\frac{z}{L}) - 0.09[\ln(-\frac{z}{L})]^2\} & -1 < \frac{z}{L} < 0 \quad \text{unstable} \\ -5\frac{z}{L} & 0 < \frac{z}{L} < 1 \quad \text{stable} \end{array} \right\} \quad (34)$$

where L is the Monin-Obukhov length. In the *Walcek et al.* [1986] formula, only $|z/L| < 1$ is considered. If $|z/L| > 1$ then $|z/L|$ is set to be 1.

In this study, parameterizations of boundary layer turbulent mixing that covers larger stability range have been used to calculate the aerodynamic resistance. Firstly, the Φ_h is calculated based on parameterizations derived from field measurements by *Bursinger* [1971]:

$$\Phi_h = \left\{ \begin{array}{ll} Pr_t + \beta_h \frac{z}{L} & \frac{z}{L} > 0 \text{ stable} \\ Pr_t(1 - \gamma_h \frac{z}{L})^{-1/2} & \frac{z}{L} < 0 \text{ unstable} \\ Pr_t & \frac{z}{L} = 0 \text{ neutral} \end{array} \right\} \quad (35)$$

where von Kármán constant $k = 0.35$, $\beta_h = 4.7$, $\gamma_h = 9.0$, and $Pr_t = K_{m,zz} / K_{h,zz} \approx 0.74$. Pr_t is the turbulent Prandtl number which approximates the ratio of the eddy diffusion coefficient for momentum to that for energy. *Hogstrom* [1988] suggested another set of parameters: $k = 0.4$, $\beta_h = 7.8$, $\gamma_h = 11.6$, and $Pr_t \approx 0.95$. The later set of parameters are used in this study.

The Equation 35 is then substitute to Equation 32 to calculate the aerodynamic resistance R_a :

$$R_a = \left\{ \begin{array}{ll} \frac{1}{ku_*} [Pr_t \ln \frac{z}{z_0} + \frac{\beta_h}{L} (z_r - z_0)] & \frac{z}{L} > 0 \text{ stable} \\ \frac{Pr_t}{ku_*} [\ln \frac{(1 - \gamma_h \frac{z_r}{L})^{1/2} - 1}{(1 - \gamma_h \frac{z_r}{L})^{1/2} + 1} - \ln \frac{(1 - \gamma_h \frac{z_0}{L})^{1/2} - 1}{(1 - \gamma_h \frac{z_0}{L})^{1/2} + 1}] & \frac{z}{L} < 0 \text{ unstable} \\ \frac{Pr_t}{ku_*} \ln \frac{z}{z_{0,h}} & \frac{z}{L} = 0 \text{ neutral} \end{array} \right\} \quad (36)$$

The above parameterization is derived from observations for the stability range: $|z/L| < 2$, but has been used successfully beyond the range under unstable conditions [*San Jose et al.*, 1985]. Following EPA Models3, we applied a function for the very stable condition ($z/L \geq 1$) to extend the application of surface layer similarity theory [*Holtslag*, 1990; *Byun and Ching*, 1999]:

$$\Phi_h = \left\{ \begin{array}{ll} -\frac{1}{L}(z - z_0) & \frac{z}{L} > 1, \frac{z_0}{L} > 1 \\ 1 - \beta_h - \frac{z}{L} + \beta_h \frac{z_0}{L} & \frac{z}{L} > 1, \frac{z_0}{L} < 1 \\ -1 + \beta_h - \beta_h \frac{z}{L} + \frac{z_0}{L} & \frac{z}{L} < 1, \frac{z_0}{L} > 1 \\ -\beta_h \frac{z}{L} + \beta_h \frac{z_0}{L} & \frac{z}{L} < 1, \frac{z_0}{L} < 1 \end{array} \right\} \quad (37)$$

which indicates that under very stable conditions, the Φ_h will change slower with respect to the $\frac{z}{L}$, i.e. when $\frac{z}{L}$ or $\frac{z_0}{L}$ is larger than 1, the Φ_h will increase by $\frac{z}{L}$ or $\frac{z_0}{L}$ instead of $\beta_h \frac{z}{L}$ or $\beta_h \frac{z_0}{L}$, where $\beta_h = 7.8$ or 8.21 .

Figure 25 illustrates the variation of calculated R_a as a function of stability z/L where z is the height where the R_a is calculated and L is the Monin Obukhov length. When the atmosphere is unstable ($z/L < 0$), three parameterizations give very similar results. When it is stable, the difference by three schemes can be large. The scheme based on *Holtslag* [1990] is used in this study since it covers larger stability range.

Aerodynamic resistance is also a function of surface roughness length and friction velocity, which both varied with land surface properties. Figure 26 plots the calculated aerodynamic resistance as a function of stability (z/L) for different land surface types, including crop field, forest, and ocean that are most common in our model domain, by using typical surface roughness length and friction velocity [*Jacobson, 1999; Seifeld and Pandis, 1998*].

A deficiency of concern in simulating the micro-meteorological conditions on a scale of 60 km (the resolution of our regional scale models), is the description of how wind stress and wind speed in the surface layer vary over surfaces with different roughness lengths. Since adopting sophisticated and extremely fine-mesh numerical modeling to solve the local spatial variation is not applicable, *Walcek et al.*, [1986] and *Byun and Ching* [1999] assumed that the grid averaged wind speed u taken from the output of the mesoscale models, RegCM in this case, conforms to a logarithmic wind profile and the average surface roughness length (Z_0) can be calculated as follows

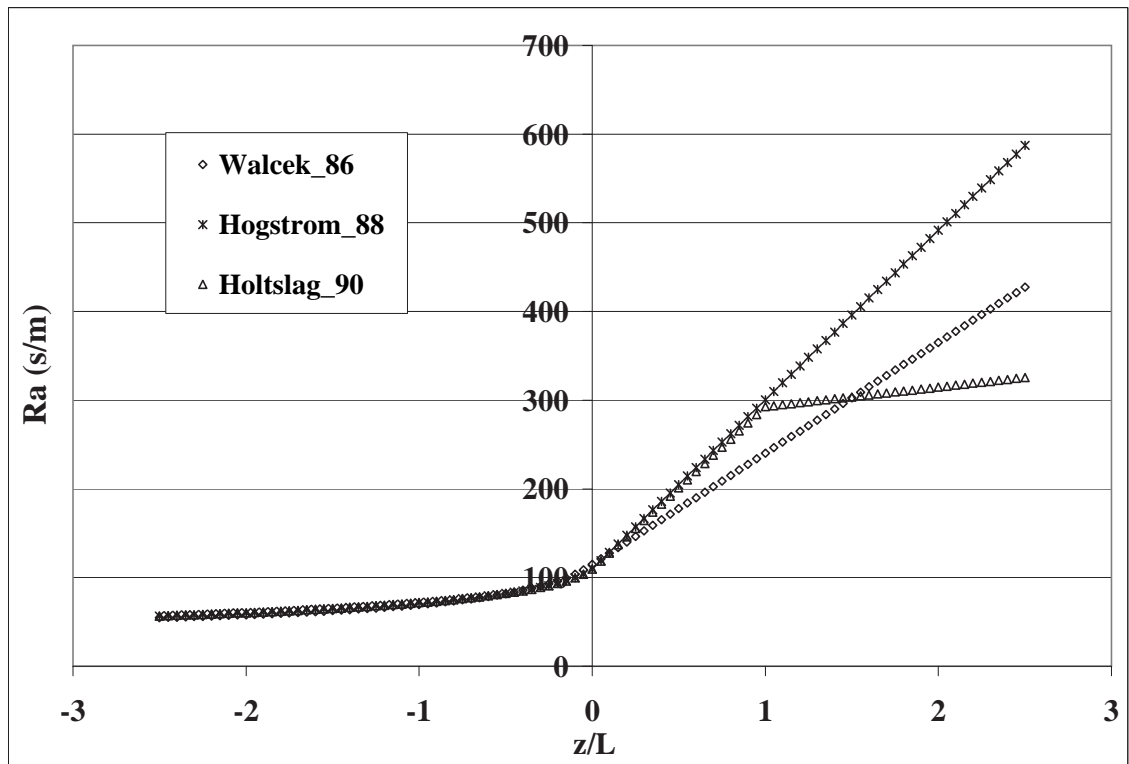


Figure 25: Aerodynamic resistance based on different parameterizations. Where 'Walcek 86' is based on *Walcek et al.*, 1986; 'Hogstrom 88': *Hogstrom*, 1988; 'Holtslag 90': *Holtslag*, 1990.

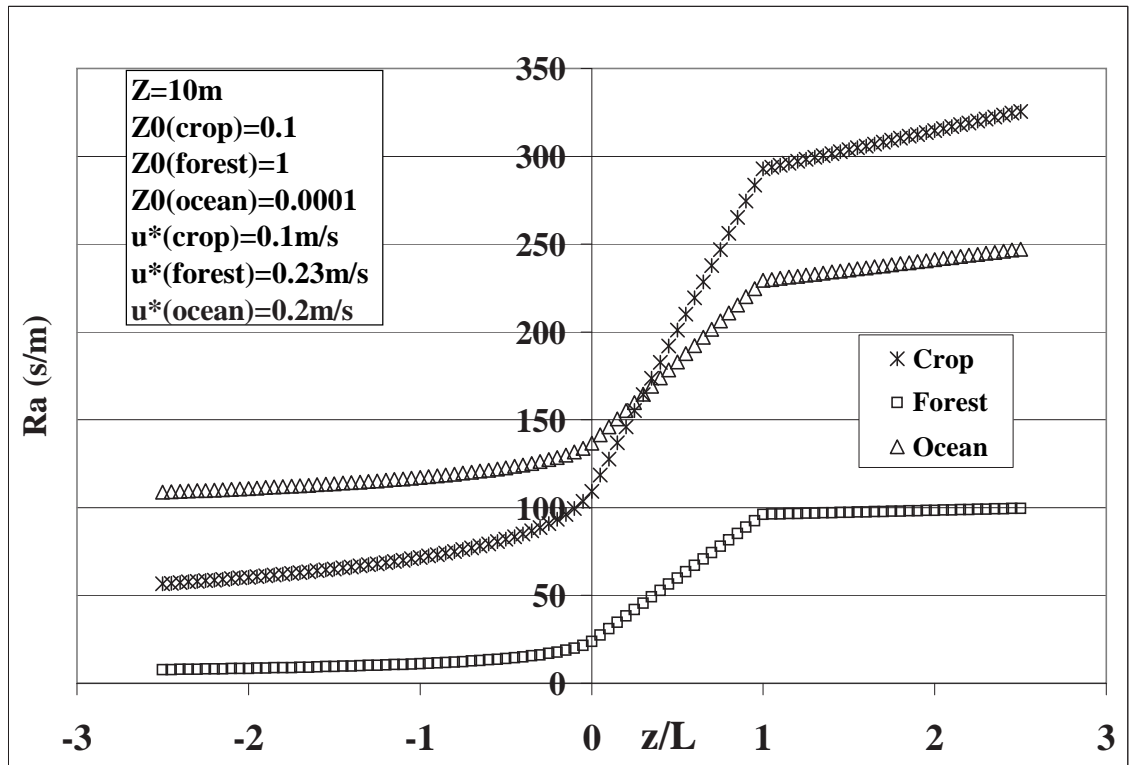


Figure 26: Calculated aerodynamic resistance as a function of stability for different land surface by using typical surface roughness length and friction velocity [Jacobson, 1999]. Where 'Walcek 86' is based on Walcek *et al.*, 1986; 'Hogstrom 88': Hogstrom, 1988; 'Holtslag 90': Holtslag, 1990.

:

$$Z_0 = \exp[\sum f_i \ln Z_{0i}] \quad (38)$$

where f_i is area fraction of landuse apportioned to each land category within the grid cell and Z_{0i} is the surface roughness length for each landuse category. However, it has been found that Equation 38 can be derived from a geometric averaging, and it does not produce a logarithmic wind profile. We adopted a parameterization of the average effective roughness length from EPA CMAQ [*Byun and Ching, 1999*]:

$$Z_0 = Z_r \exp[-(\sum f_i \sqrt{\ln(Z_r/Z_{0i}))}] \quad (39)$$

where Z_r is the reference height, which needs to be within the regime where the log-linear wind profile can be satisfied and it also should be far away from Z_0 . In this study we use $Z_r=10\text{m}$. This parameterization satisfies both the logarithmic wind profile and the linearly-additive wind speed assumptions under the approximation:

$$u_i u_{*i} = u u_* = \text{constant} \quad (40)$$

where u and u_* refer to grid-averaged wind speed and friction velocity, while u_i and u_{*i} refer to the corresponding variables over individual land types within the averaging area.

Z_0 , the surface roughness length, varies from more than 1m over forests to $\sim 10^{-5}$ m over ocean and ice/snow. In the Table 18, we compare the average Z_0 for 6 typical grids in our model domain calculated by different parameterizations: direct weighted average, geometric mean, and logarithmic wind profile. If the grid contains highly variable Z_0 's, the three means can be very different.

Table 18: Average of Surface Roughness Length (Z_0) Derived from the Sub-grid Land Surface Characterization by Different Averaging Techniques.

	Weighted Average	Geometric Mean	Logarithmic Wind Profile
1	0.32	0.035	0.054
2	0.2	0.0006	0.001
3	0.8	0.16	0.28
4	0.36	0.02	0.04
5	0.15	0.0047	0.0082
6	0.24	0.048	0.07

1. Five different landuse types evenly mixed up with Z_{0i} range from 1m to 10^{-5} m.
2. Ocean ($Z_0 = 10^{-5}$ m) dominant (80%).
3. Forest ($Z_0 = 1$ m) dominant (80%).
4. Ocean (33%), forest (33%), and crop ($Z_0 = 0.25$ m) (33%).
5. Ocean (50%), forest (25%), and crop (25%).
6. Ocean (20%), forest (40%), and crop (40%).

A.3.3.2 Surface Resistance

Surface resistance (R_s) refers to the resistance to the uptake of gaseous and particulate species by the surface elements. The surface resistance is the most difficult term to evaluate because many chemical and biological processes occur on surface and in plant canopies [Walcek, 1986; Jacobson, 1999]. Over a given area of land, various plant, soil, water, snow/ice, and other material surfaces are present, each with a characteristic resistance to the uptake of a given pollutant under specified meteorological conditions. In the early studies, the R_s was often quantified by derivation from measured deposition velocity and other resistance, R_a and R_b :

$$R_s = V_d^{-1} - R_a - R_b. \quad (41)$$

Analogous to the series and parallel resistance in the electrical circuits and dry deposition calculation, the total surface resistance can be estimated as a function of individual resistance components based on the parameterization developed by Wesely [1989] and Walmsley and Wesely [1996].

$$R_s = [1/(R_s + R_m) + 1/R_{lu} + 1/(R_{dc} + R_{cl}) + 1/(R_{ac} + R_{gs})]^{-1} \quad (42)$$

where R_s is the bulk leaf stomata resistance, R_m is leaf mesophyll resistance, R_{lu} is leaf cuticles resistance, R_{dc} is the resistance caused by buoyant convection in canopies, R_{cl} is the resistance due to leaves, twigs, bark, or other exposed surfaces in the lower canopy, R_{ac} is the resistance due to canopy height and density, R_{gs} is the resistance due to soil and leaf litter at the ground surface.

The stomata resistance, mesophyll resistance, and cuticles resistance are due to the uptake of chemical species by openings on leaf surfaces, liquid water within leaves, and outer leaf surfaces respectively. Those resistances depend on factors such as type, age, and conditions of the vegetation, as well as water availability, solar radiation level, air temperature, concentration of CO₂ in the air, and soil properties. In the current regional scale modeling studies, it is not yet possible to represent all those characterizations in details. The parameterization of the bulk properties of resistance is therefore required.

In the current dry deposition scheme, the bulk canopy stomatal resistance is calculated by:

$$R_s = R_i \{1 + [200(G + 0.1)^{-1}]^2\} \{400[T_s(40 - T_s)]^{-1}\} \quad (43)$$

where G is the solar irradiation in $W\ m^{-2}$ and T_s is the surface air temperature, and R_i represents the minimum bulk canopy resistance for water vapor to the specified vegetation type. R_s therefore represents the typical stomatal resistance for the uptake of water vapor under giving ambient conditions. This parameterization is derived from several studies by *Baldocchi et al.*, [1987] on specified plant species. The ratio of molecular diffusivity of chemical species (D_x) to that of water vapor (D_{H_2O}) is used to scale the stomatal resistance of species x [*Ball et al.*, 1987]:

$$R_s(x) = R_s(H_2O) * D_{H_2O}/D_x \quad (44)$$

The resistance due to buoyant convection in canopies (R_{dc}) is parameterized based on the intensity of incoming sunlight.

Besides the underlying physical meaning, the value of R_{ac} , R_{gs} and R_{cl} have been adjusted to give good estimates of over all surface resistance, therefore they might not comparable to the specified measurements at given locations and ambient conditions [Wesely *et al.*, 1983; Wesely, 1989].

In the dry deposition scheme, the typical value of different resistance components are given for SO_2 and O_3 based on available observations from [Wesely and Hicks, 1977; Wesely and Hicks, 1979; Wesely *et al.*, 1985]. The surface resistance of other species, including nitrogen dioxide, nitric oxide, nitric acid vapor, hydrogen peroxide, acetaldehyde, formaldehyde, methyl hydroperoxide, peroxyacetic acid, formic acid, ammonia, peroxyacetyl nitrate, nitrous acid, are parameterized based on their solubility and reactivity relative to the SO_2 and O_3 . The effective Henry's Law constant of specified species is used to scale the rate of uptake by the wet surface relative to the uptake of SO_2 . The reactivity of specified species is scaled to that of ozone based on its electron activity and reaction rate with S(IV). The mesophyll resistance is calculated as a function of the solubility and reactivity of each species as well.

The effects of dew and rain on the surface uptake of chemical species are also considered in the dry deposition scheme based on observations for different species and land surface.

It has been observed that the surface resistance for uptake of HNO_3 , SO_2 , and NO_2 by snow increase markedly when the temperature decrease below $-2^\circ C$ [Valdez, 1987]. Therefore it is assumed that the resistance of all surface in the lower canopy and ground will increase with decrease of temperature. Because our model domain covers region as north as $60^\circ N$ and significant region is covered by snow for relatively

long time period each year, we then updated the parameterization of uptake of SO₂ by snow/ice based on the scheme used in ECHAM4 by [Ganzeveld *et al.*, 1998]. Based on field measurements, the uptake of SO₂ by snow/ice surface has strong dependence on temperature, especially in the temperature range of -10° to 0° [Granat and Johansson, 1983; Valdez *et al.*, 1987; Conklin *et al.*, 1993].

When the RegCM simulated snow depth is larger than 1mm H₂O, then the grid is assumed covered by snow. The relationship of surface temperature and surface uptake of SO₂ is derived based on observations mentioned above. The deposition velocity increases exponentially from a minimum value of ~ 0.01 cm s⁻¹ for a temperature of -20°C to a value of ~ 0.25 cm s⁻¹ for 0°C. A detailed physical-chemical model which includes gaseous diffusion into the snow pack, air-water partitioning, and aqueous-phase reactions [Bales *et al.*, 1987] shows a very similar results for calculated deposition velocity of SO₂ to snow/ice, i.e. ~ 0.01 cm s⁻¹ for -20°C to ~ 0.15 cm s⁻¹ for 0°C.

The land surface types represented in RADM are very broad categories. There are 13 different landuse types considered in RADM while RegCM use 20 landuse types based on BATS (Biosphere Atmosphere Transfer Scheme) categorization. Appropriate aggregations have been applied to keep the landuse input consistent in two models. Several landuse categories are not included in the original dry deposition scheme, such as crop-forest mosaic, tundra, etc.. In addition, the mixed forest defined in original dry deposition scheme is mixed forest with wetland, which is different from mixed forest defined in BATS that is a mixture of deciduous and coniferous trees. The surface resistance components of tundra is added based on the observations by [Jacob *et al.*, 1992]. The resistance components for mixed forest and crop-forest mosaic are interpolated from parameters of existing categories. The different resistance

components are assumed to be parallel resistance on each fraction of the land area:

$$R_{mix} = \frac{1}{\sum f_i * \frac{1}{R_i}} \quad (45)$$

where R_{mix} is any of the resistance component described in the Equation 42 for either mixed forest or crop-forest mosaic, f_i is the fraction of the i 'th landuse category in the mixed category, R_i is the corresponding resistance components. In this study we assume mixed forest is a mixture of deciduous (50%) and coniferous (50%) trees, and crop-forest mosaic is mixture of 25% deciduous, 25% coniferous trees, and 50% crop land. $\sim 7\%$ of the land area in our model domain are crop-forest mosaic based on Global Land Cover Characterization (GLCC). It is typical landuse type in the rural area of central to east China, where we are interested in the following studies: the sampling site that will be discussed in the next section is located in such environment.

The seasonal variation of vegetation conditions are only described to a limited degree in RADM. The original *Wesely* [1989] dry deposition scheme uses five pre-determined seasonal categories to describe the changes in vegetative conditions over time. The seasonal transition is described in an abrupt fashion, for example, it will jump from summer on August 31st to autumn on September 1st. As a result some resistance components will change significantly in one model time step, for example, the stomatal resistance of crop land changes from 60s/m in summer to 10^{12} s/m in autumn. In the dry deposition module, if the deposition pathway does not exist, for example the stomatal resistance of deciduous forest in winter, then the resistance component will be set to be a very large value, i.e 10^{12} s/m [*Walmsley and Wesely, 1996*]. In order to take the continuously variation of vegetative condition into consideration, we applied a function to smooth out the abrupt changes from tabulated values.

$$R(t) = \left\{ \begin{array}{ll} R(0) * (e^{\frac{nday}{a}} - 1) / (e^{\frac{(nday-t)}{2}} - 1) & \text{if } R(1) = 10^{12} \\ R(1) * (e^{\frac{nday}{a}} - 1) / (e^{\frac{t}{2}} - 1) & \text{if } R(0) = 10^{12} \\ 10^{12} & \text{if } R(0) = R(1) = 10^{12} \\ R(0) + \frac{R(1)-R(0)}{nday} * t & \text{if } R(0) < 10^{12} \text{ and } R(1) < 10^{12} \end{array} \right\} \quad (46)$$

where R is the any surface resistance component in Equation 42, t is the Julian day between the seasonal transition time. R(0) and R(1) are the resistance components at beginning and end of seasonal transition. Julian day of the beginning and the end of seasonal transition are picked as a function of latitude that is based on the general climatology of East Asia [Arakawa, 1969]. 'nday' is the number of days for seasonal transition, i.e. 15 days in this study. The Equation 46 is used to describe those season variations in a smoother fashion. As illustrated in Figure 27, if one of the resistance components at either beginning or end of the transitional period is very large, then exponential interpolation is applied. If both R(0) and R(1) are smaller than 10^{12} , the linear interpolation will be applied.

The major resistance components used as inputs to the dry deposition scheme are listed in Table 19. In different seasons, the magnitude of surface resistance over different land surface varies largely. For example, before the harvest, the bulk surface resistance for uptake SO₂ and O₃ by forest is smaller than that by crop land, while after harvest, it is opposite.

A.3.3.3 Resistances and overall Dry Deposition Velocity

Our model calculated dry deposition velocities are within the range of observed velocities [Ganzeveld *et al.* 1998 and reference within] and comparable to other regional and global models results: EPA Model-3 [Hu *et al.*, 2003], GO-CART [Chin *et al.*, 2000a], and ECHAM4 [Ganzeveld, *et al.*, 1998] on monthly average basis.

In order to demonstrate the relative contribution of various resistance components to the overall calculated dry deposition velocity, the time series of the reciprocal of

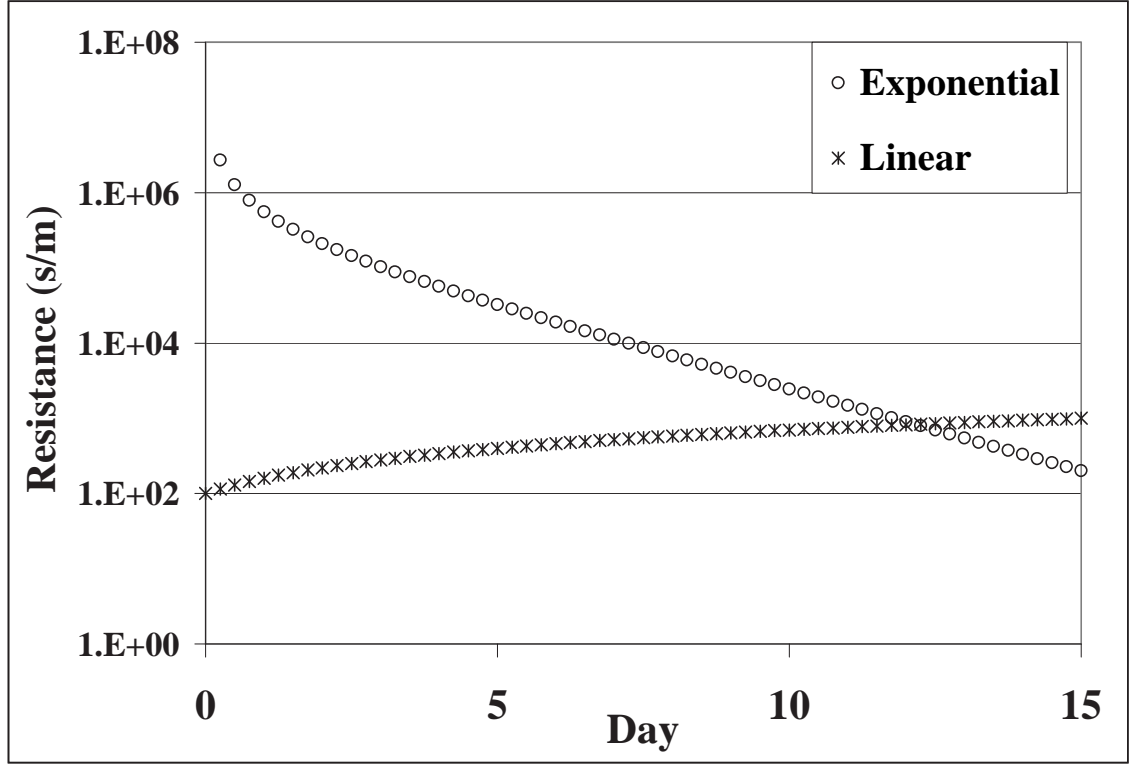


Figure 27: Interpolation of surface resistance components during the seasonal transitions. The start and end point of the seasonal transition is defined for different latitude based on the climatology of East Asia. If the resistance at one end is very large, i.e. 10^{12} s/m, which means the uptake pathway is not existed, then 'Exponential' interpolation is applied. If the resistances at both beginning and end of transition time period are smaller than 10^{12} , then 'Linear' interpolation is applied. See detailed description in Equation 46 and text.

Table 19: Major Components of Surface Resistance for Different Seasons and over Different Land Surface Type.

	Early Fall (Before Harvest)				Late Fall (After Harvest)			
	Crop	Forest	Mosaic	Ocean	Crop	Forest	Mosaic	Ocean
R_i	10^5	250	500	10^5	10^5	250	500	10^5
R_{ac}	150	2000	279	0.1	10	2000	19.9	0.1
$R_g(\text{SO}_2)$	200	500	286	0.1	150	500	230	0.1
$R_g(\text{O}_3)$	150	200	171	2000	150	200	171	2000
$R_s(\text{SO}_2)$	350	227	265	0.1	160	227	167	0.1
$R_s(\text{O}_3)$	300	224	237	2000	160	224	138	2000

R_i is the stomatal resistance.

R_{ac} is the resistance due to canopy density and height.

R_{gs} is the resistance due to soil, leaf litter, etc., at the ground surface.

aerodynamic resistance (R_a^{-1}), surface resistance (R_s^{-1}), and dry deposition velocity (V_d) for SO_2 at Linan, the measurement site that will be discussed in the next section, are plotted in Figure 28. The reciprocal is used to demonstrate the contribution of each resistance to the bulk deposition velocity.

The landuse around the sampling site is complicated: most area around it is categorized as crop-forest mosaic even by the 30" x 30", or $\sim 1 \text{ km} \times 1 \text{ km}$, GLCC dataset. The region is categorized as forest by the Penn Stat/NCAR landuse dataset. Therefore two sets of model runs have been done to test the model sensitivity on the input land surface types. Based on the model calculations illustrated in 28, the R_a over forest is usually smaller than that over the crop/forest mosaic. The surface resistance (R_s) for the forest to uptake SO_2 is larger in the late autumn than that for the crop land, except when there is rain or dew on the surface (due to the solubility of SO_2). At most time of late autumn, R_s determines the magnitude of the bulk V_d . (In the growing season, the R_a and R_s are comparable since the stomatal resistance is much smaller than other resistance component when the photosynthesis is more active.)

A.3.3.4 Dry Deposition Velocity of NO_2 .

The oxides of nitrogen, NO and NO_2 together referred to as NO_x , are key compounds in atmospheric chemistry. Besides anthropogenic emissions, NO_x also originates from natural sources such as microbial production in soil and lightning. Ambient concentrations of NO_x reflect a balance between various emissions, deposition, and conversion of NO_2 to HNO_3 . Since soil and vegetation can be either sources and sinks of NO_x under different conditions there are large variations in measured and estimated NO_x fluxes [Hill, 1971; Hanson *et al.*, 1989; Rondon *et al.*, 1993; Lerday *et al.*, 2000; Gut *et al.*, 2002]. Previous studies have suggested that stomatal conductance is the major pathway for NO_2 deposition, while the uptake of NO has been found to

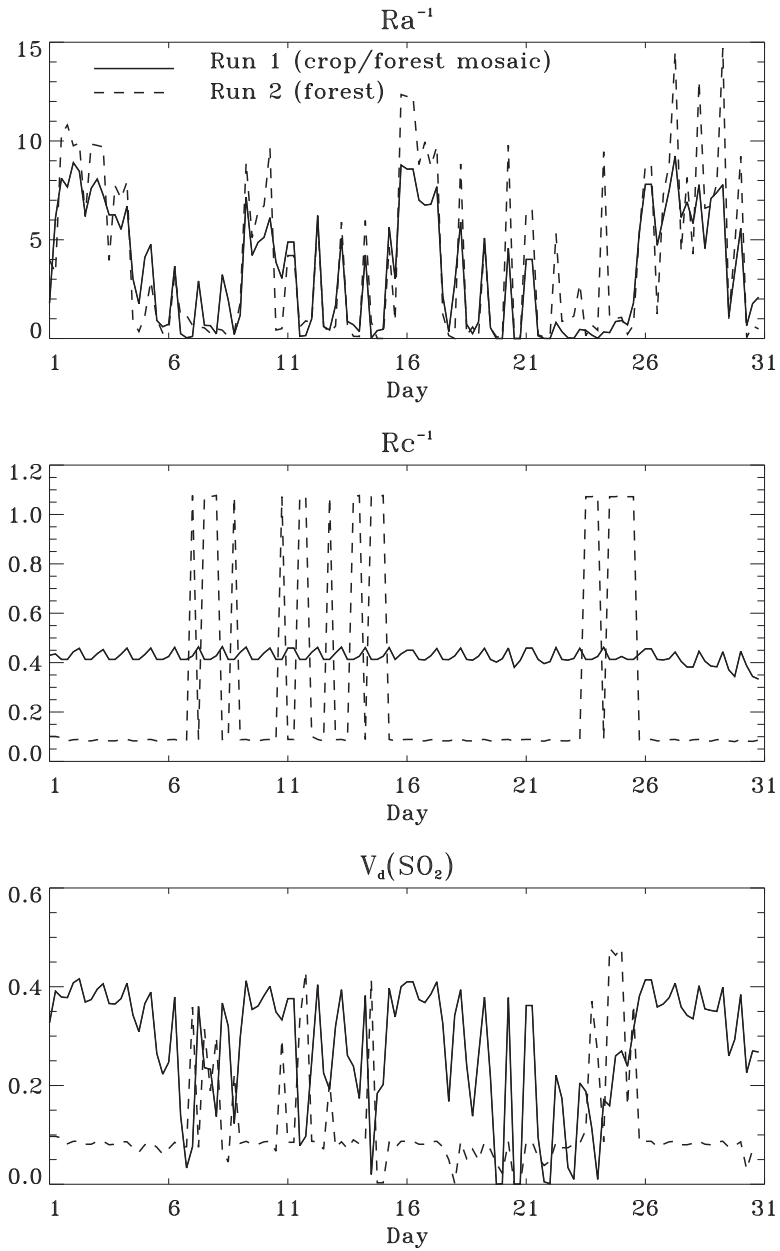


Figure 28: Time series of model calculated aerodynamic resistance (R_a), surface resistance (R_s), and dry deposition velocity (V_d) at a rural site during November 1999, where 'Run 1' and 'Run 2' are model test runs by using landuse data from different sources. In 'Run 1', the rural site is categorized as crop forest mosaic, in 'Run 2', it is categorized as forest. (See text for more detail).

be at least 1 order of magnitude less than that of NO_2 . Therefore the deposition of NO has been ignored in currently dry deposition scheme.

During this study we found that the dry deposition of NO_2 calculated by Wesely's scheme [1989] is very small in late autumn and winter. In the calculation, NO_2 is assumed to be non-soluble and moderate reactive. As the stomatal uptake decrease with season, the calculated dry deposition velocity of NO_2 is only about 10% to 30% to that of O_3 , because all other resistance component of NO_2 are assumed to be much larger than that of O_3 . We did a test run assuming $R_s(\text{NO}_2) = 2/3R_s(\text{O}_3)$ following *Ganzeveld et al.* [1995]. Figure 29 illustrates the model simulated monthly NO_y concentration as compared with measurements. (The details about the measurements will be talked in the following section).

In other model studies, different assumption applied: $R_s(\text{NO}_2) = R_s(\text{O}_3)$ in GEOS-CHEM [*Wang et al.*, 1998], for example. Because of the large uncertainties involved in NO_2/NO surface flux measurements, it is not yet possible to empirically constrain $R_s(\text{NO}_y)$.

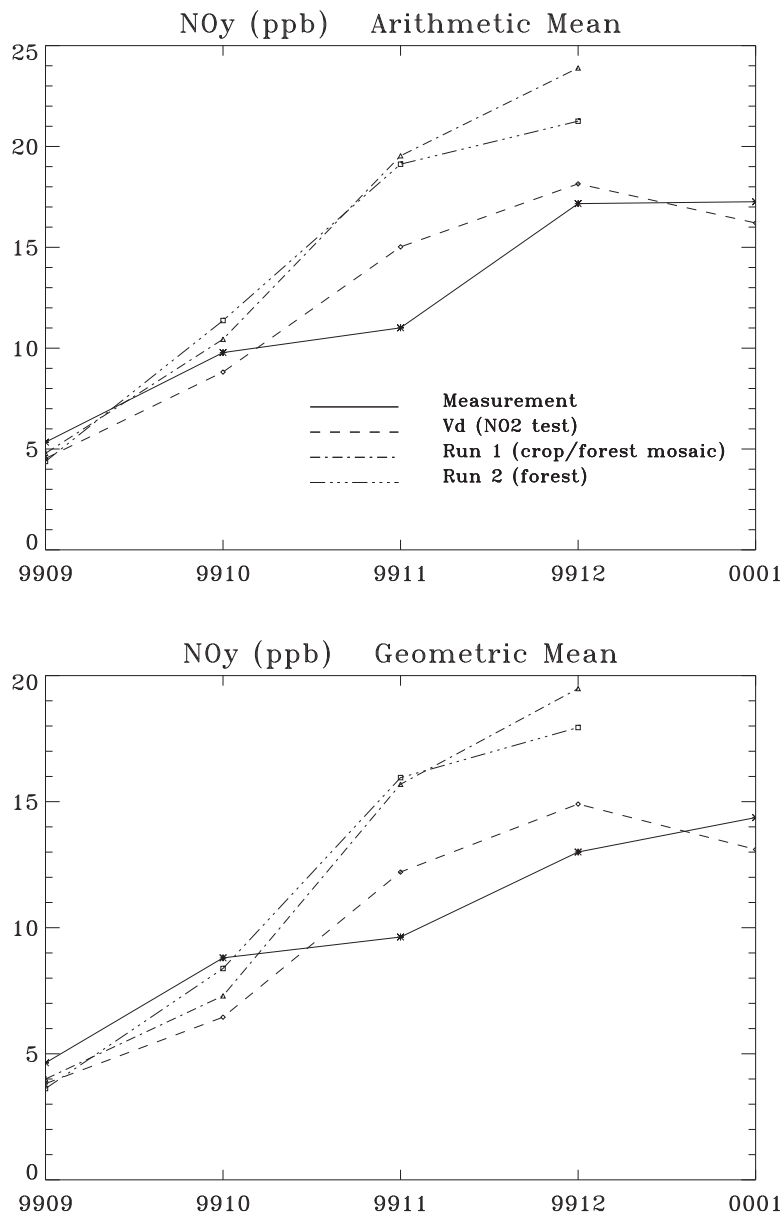


Figure 29: Monthly arithmetic mean and geometric mean of model calculated and measured NO_y (ppb) concentration at a rural site in China. Solid line denotes the measurement, dashed line is the model run with NO₂ dry deposition velocity calculated followed that by *Ganzeveld et al., 1995*, dot-dashed lines are model results by 'Run 1' and 'Run 2' in which the NO₂ deposition velocity are calculated by using *Wesely's [1989]* scheme.

REFERENCES

- [1] Adams, P., J. Seinfeld and D. Koch, Global concentrations of tropospheric sulfate, nitrate, and ammonium aerosol simulated in a general circulation model, *J. Geophys. Res.*, *104*, D11, 13,791-13,823, 1999
- [2] Akimoto, H., and H. Narita, Distribution of SO₂, NO_x, and CO₂ emissions from fuel combustion and industrial activities in Asia with 1° × 1° resolution, *Atmos. Environ.*, *28*, 213-225, 1994.
- [3] Andreae, M. O., et al., Vertical distribution of dimethylsulfide, sulfur dioxide, aerosol ions, and radon over the northeast Pacific Ocean, *J. Atmos. Chem.*, *6*, 149-173, 1988
- [4] Anthes, R. A., The development of asymmetries in a three-dimensional numerical model of the tropical cyclone, *Mon. Wea. Rev.*, *100*, 461-476, 1972
- [5] Anthes, R. A., A cumulus parameterization scheme utilizing a one-dimensional cloud model, *Mon. Wea. Rev.*, *117*, 1423-1438, 1977
- [6] Anthes, R. A., and T. T. Warner, Development of hydrodynamic models suitable for air pollution and other mesometeorological studies, *Mon. Wea. Rev.*, *106*, 1045-1078, 1978
- [7] Anthes, R. A., E. Y. Hsie, and Y. H. Kuo, Description of the Penn State/NCAR Mesoscale Model Version 4 (MM4), NCAR Tech. Note, NCAR/TN-282+STR, 66pp, 1987
- [8] Arakawa, H., Climates of Northern and Eastern Asia, World Survey of Climatology, Volume 8, Elsevier Publishing Company, Amsterdam, 1969
- [9] Arakawa, A., Closure Assumptions in the Cumulus Parameterization Problem, *The Representation of Cumulus Convection in Numerical Models*, American Meteor. Society, Boston, 1993
- [10] Arimoto, R., R. A. Duce, et al., Comparisons of trace constituents from ground stations and the DC-8 aircraft during PEM-West B, *J. Geophys. Res.*, *102*, 28539-28550, 1997
- [11] Arndt, R.L., G.R. Carmichael, D.G. Streets, and N. Bhatti, Sulfur dioxide emissions and sectoral contributions to sulfur deposition in Asia, *Atmos. Environ.*, *31*, 1553-1572, 1997
- [12] Atkinson, R., J. N. Pitts, Jr., and S. M. Aschman, Tropospheric reactions of dimethyl sulfide with NO₃ and OH radicals, *J. Phys. Chem.*, *88*, 1584-1587, 1984

- [13] Baldocchi, D. D., B. B. Hicks, and P. Camara, A canopy stomatal resistance model for gaseous deposition to vegetated surfaces, *Atmos. Environ.*, *21*, 91-101, 1987
- [14] Bales, R. C., M. P. Valdez, and G. A. Dawson, Gaseous deposition to snow, 2, Physical-chemical model for SO₂ deposition, *J. Geophys. Res.*, *92*, 9789-9799, 1987
- [15] Balkanski, Y., D. Jacob, and G. Gardner, Transport and residence time of tropospheric aerosols inferred from a global three-dimensional simulation of 210Pb, *J. Geophys. Res.*, *98*, D11, 20,573-20,586, 1993
- [16] Ball, J. T., Calculations related to gas exchange, *Stomatal Function*, Ed. E. Zeiger, G. D. Farquhar, I. R. Cowan, 445-476, Stanford University Press, Stanford, CA, 1987
- [17] Barsseur, G. P., D. A. Hauglustaine, et al., MOZART, a global chemical transport model for ozone and related chemical tracers, 1. Model description, *J. Geophys. Res.*, *103*, 28,263-28,289, 1998
- [18] Bates, T. S., J. D. Cline, R. H. Gammon, and S. R. Kelly-Hansen, Regional and Seasonal Variations in the Flux of Oceanic Dimethylsulfide to the Atmosphere, *J. Geophys. Res.*, *92*, 2930-2938, 1987
- [19] Benkovitz, C. M., C. M. Berkowitz, R.C. Easter, S. Nemesure, R. Wagener, and S.E. Schwartz, Sulfate over the North Atlantic and adjacent continental regions: Evaluation for October and November 1986 using a three dimensional model driven by observation-derived meteorology, *J. Geophys. Res.*, *99*, 20,725-20,756, 1994.
- [20] Benkovitz, C.M., et al., Global gridded inventories of anthropogenic emissions of sulfur and nitrogen, *J. Geophys. Res.*, *101*, 29239-29252, 1996
- [21] Bergin, M., et al., Aerosol radiative, physical, and chemical properties in Beijing during June, 1999, *J. Geophys. Res.*, *106*, D16, 17,969-17,980, 2001
- [22] Berntsen, T., I. S. A. Isaksen, W. C. Wang, and X. Z. Liang, Impacts of increased anthropogenic emissions in Asia on tropospheric ozone and climate - a global 3-D model study, *Tellus*, *48*, 13-32, 1996
- [23] Berntsen, T. K., S. Karlsdottir, and D. A. Jaffe, Influence of Asian emissions on the composition of air reaching the North Western United States, *Geophys. Res. Lett.*, *26(14)*, 2171-2174, 1999
- [24] Berresheim, H., D. D. Davis, and P. H. Wine, Sulfur in the Atmosphere, in *Composition, Chemistry, and Climate of the Atmosphere*, H. B. Singh (ed.), Van Nostrand Reinhold Publishers, 251-307, 1996
- [25] Bey, I., R. M. Yantosca, and D. J. Jacob, Export of pollutants from eastern Asia: a simulation of the PEM-West(B) aircraft mission using a 3-D model driven by assimilated meteorological fields, presented at AGU spring meeting, 1999

- [26] Blackadar, A. K., High resolution models of the planetary layer, *Advances in Environmental Science and Engineering*, Ed. J. R. Pfafflin and E. N. Ziegler, 50-85, Gordon and Breach, Newark, N. J., 1979
- [27] Bolin, B., and C. Persson, Regional dispersion and deposition of atmospheric pollutants with particular application to sulfur pollution over Western Europe, *Tellus*, *27*, 281, 1975
- [28] Boucher, O. and T.L. Anderson, GCM assessment of the sensitivity of direct climate forcing by anthropogenic sulfate aerosols to aerosol size and chemistry, *J. Geophys. Res.*, *100*, 26117-26134, 1995
- [29] Businger, J. A., J. C. Wyngaard, Y. Izumi, and E. F. Bradley, Flux-profile relationship in the atmospheric surface layer, *J. Atmos. Sci.*, *28*, 181-189, 1971
- [30] Byun, D. W., and J.K.S. Ching, *Science algorithm of the EPA Models-3 Community Multiscale Air Quality (CMAQ) modeling system*, EPA/600/R-99/030, 1999
- [31] Byun, D.W., J. Pleim, R. Tang, and A. Bourgeois, Meteorology-Chemistry interface processor (MCIP) for Models-3 Community Multiscale Air Quality (CMAQ) Modelling System, in *Science Algorithms of the EPA Model-3 Community Multiscale Air Quality (CMAQ) Modelling System*, Washinton, DC, 1999
- [32] Calvert, J. G., and W. R. Stockwell, Acid generation in the troposphere by gas-phase chemistry, *Environ. Sci. Technol.*, *17*, 428A-443A, 1983
- [33] Carmichael, G. R. and L. K. Peters, The transport, chemical transformation and removal of SO₂ and sulfate in the Eastern United States, *Atmospheric Pollution*, Ed. M. Benarie, Elsevier, Amsterdam, 31-36, 1980
- [34] Carmichael, G. R., Peter L. K., and R. D. Saylor, The STEM-II regional scale acid deposition and photochemical oxidant model - 1. An overview of model development and applications, *Atmospheric Environment 25A*, 2077-2090, 1991
- [35] Carmichael, G. R., Uno I, M. J. Phadnis, Y. Zhang, Y. Sunwoo, Tropospheric ozone production and transport in the springtime in east Asia, *J. Geophys. Res.*, *103*, 10649-10671, 1998
- [36] Carmichael, G., et al., Evaluating regional emission estimates using the TRACE-P observations, *J. Geophys. Res.*, *108*, D21, 8810, 2003
- [37] Chamberlain, A. C., and Chadwick, R. C., Deposition of airborne radioiodine vapor, *Nucleonics*, *2*, 22-25
- [38] Chameides, W. L., The Photochemistry of a Remote Marine Stratiform Cloud, *J. Geophys. Res.*, *89*, 4739-4755, 1984
- [39] Chameides, W. L., et al., Ozone precursor relationships in the ambient atmosphere, *J. Geophys. Res.*, *97*, D5, 1992

- [40] Chameides, W. L., et al., Growth of continental-scale metro-agroplexes, regional ozone pollution and world food production, *Science*, *264*, 74-77, 1994
- [41] Chameides, W. L., et al., The Yantze Delta of China as an evolving Metro-Plex, 55 pp., proposal to NASA, Georgia Inst. of Technol., Atlanta, Georgia, 1995
- [42] Chameides, W. L., X. S. Li, X. Y. Tang, et al., Is ozone pollution affecting crop yields in China, *Geophys. Res. Lett.*, *26*, 867-870, 1999a
- [43] Chameides, W. L., H. Yu, S. C. Liu, et al., Case study of the effects of atmospheric aerosols and regional haze on agriculture: An opportunity to enhance crop yields in China through emission control, *P. Natl. Acad. Sci. USA*, *96*, 13626-13633, 1999b
- [44] Chameides, W. L., et al., Correlation between model-calculated anthropogenic aerosols and satellite-derived cloud optical depth: Indication of indirect effects?, *J. Geophys. Res.*, *107*, D10, 2002a
- [45] Chameides, W. L. and M. Bergin, Enhanced: Soot Takes Center Stage, *Science* *297*, 2214-2215, [DOI: 10.1126/science.1076866], 2002b
- [46] Chang, J.S., et al., A three-dimensional Eulerian acid deposition model: Physical concepts and formulation, *J. Geophys. Res.*, *92*, D12, 14,681-14,700, 1987
- [47] Charlson, R. J., J. Langner, and H. Rodhe, Sulfate aerosols and climate, *Nature*, *348*, 22, 1990
- [48] Charlson, R. J., J. Langner, H. Rodhe, C. B. Levey, and S. G. Warren, Perturbation of the northern hemisphere radiative balance by backscattering from anthropogenic sulfate aerosols, *Tellus*, *43AB*, 152-163, 1991
- [49] Charlson, R. J., S. E. Schwartz, J. M. Hales, R. D. Cess, J. A. Coakley Jr., J. E. Hense, and D. J. Hoffman, Climate forcing by anthropogenic aerosols, *Science*, *255*, 423-430, 1992
- [50] Charney, J.G., R. Fjortoft, and J. V. Neumann, Numerical integration of the barotropic vorticity equation, *Tellus* *2*, 237-254, 1950
- [51] Chatfield, R. B., and P. J. Crutzen, Sulfur dioxide in remote ocean air: cloud transport of reactive precursors, *J. Geophys. Res.*, *89*, 7111-7132, 1984
- [52] Chen, G., D. Davis, P. Kasibhatla, A. Bandy, D. Thornton, and D. Blake, A mass-balance/photochemical assessment of DMS sea-to-air flux as inferred from NASA GTE PEM-West A and B, *J. Geophys. Res.*, *104*, 5471-5482, 1999
- [53] Chin, M., and D. Jacob, Anthropogenic and natural contributions to tropospheric sulfate: A global model analysis, *J. Geophys. Res.*, *101*, 18691-18699, 1996

- [54] Chin, M., R. Rood, et al. Atmospheric sulfur cycle simulated in the global model GOCART: Model description and global properties, *J. Geophys. Res.*, *105*, 24,671-24,687, 2000a
- [55] Chin, M., D. L. Savoie, et al., Atmospheric sulfur cycle simulated in the global model GOCART: Comparison with field observations and regional budgets, *J. Geophys. Res.*, *105*, 24689-24712, 2000b
- [56] China, State Environmental Protection Administration, Report on the state of the environment in China 2002, Beijing, China, 2003
- [57] China State Statistical Bureau, *China Statistical Yearbook 2002*, Beijing, China, 2002
- [58] Cohan, D.S., J. Xu, R. Greenwald, M. H. Bergin, and W. L. Chameides, W.L.D., The impact of aerosol light attenuation on C-uptake by green plants, *Biogeochemical Cycles*, *16*, 10.1029/2001GB001441 2002
- [59] Collins, W. D., et al., Description of the NCAR Community Atmosphere Model (CAM2), National Center of Atmospheric Research, Boulder, 2003
- [60] Conklin, M. H., R. A. Sommerfeld, S. K. Laird, and J. E. Villinsi, Sulfur dioxide reactions on ice surfaces: Implications for dry deposition to snow, *Atmos. Environ. Part A*, *27*, 159-166, 1993
- [61] Cox, R. A., and D. Sheppard, Reaction of OH radicals with gaseous sulphur compounds, *Nature*, *284*, 330-331, 1980
- [62] Crutzen, P. J., M. G. Lawrence and U. Poschl, On the background photochemistry of tropospheric ozone, *Tellus*, *51 A-B*, 123-146, 1999
- [63] Dana, T., and J. Hales, Statistical aspects of the washout of polydisperse aerosols, *Atmos. Environ.*, *10*, 45-50, 1976
- [64] Davis, D., G. Chen, M. Chin, Atmospheric sulfur, *Handbook of weather, climate and water*, T. Potter and B. Colman, Ed., McGraw-Hill, 2002
- [65] DeMore, W. G., S. P., Sander, D. M. Golden, R. F. Hampson, M. J. Kurylo, C. J. Howard, A. R. Ravishankara, C. E. Kolb, M. J. Monila, *Chemical Kinetics and Photochemical Data for Use in Stratospheric Modelling*, Evaluation No. 11, JPL Publication 94-26. Jet Propulsion Laboratory, Pasadena, CA, 1994
- [66] Dentener, F., P. Crutzen, Reaction of N_2O_5 on tropospheric aerosols: Impact on the global distributions of NO_x , O_3 and OH, *J. Geophys. Res.*, *98*, D4, 7149-7163, 1993
- [67] Dickinson, R. E., R. M. Errico, F. Giorgi, and G. T. Bates, A regional climate model for the western U.S., *Climatic Change*, *15*, 383-422, 1989

- [68] Dignon, J., NO_x and SO_x emissions from fossil fuels: A global distribution, *Atmos. Environ.*, *26A*, 1157-1163, 1992
- [69] Dignon, J. and S. Hameed, Global emissions of nitrogen and sulfur oxides from 1860 to 1980, *J. Air Pollut. Control. Assoc.*, *39*, 180-186, 1989
- [70] Ding, G., et al., About acid deposition in China, *The report of National Key Project of Acid Rain*, China National Council of Science, Beijing, China, 1995 [in Chinese]
- [71] Dockery, D.W., and C.A. Pope, III, Acute respiratory effects of particulate air pollution, *Annual Rev., Public Health*, *15*, 107 - 132, 1994
- [72] Duce, R. A., et al., Long-range atmospheric transport of soil dust from Asia to the tropical North Pacific: Temporal variability, *Science*, *209*, 1522-1524, 1980
- [73] Ehhalt, D.H., Gas phase chemistry of the troposphere. Chapter 2 in *Global Aspects of Atmospheric Chemistry*, Ed. Deutsche Bunsen-Gesellschaft fur Physikalische Chemie, New York, Springer, pp 21-109, 1999
- [74] Eliason A., A review of long-range transport of air pollutants: long-range transport modelling, *J. Appl. Meteorol.*, *19*, 231-240, 1980
- [75] Elliott, S., D. R. Blake, et al., Motorization of China implies changes in Pacific air chemistry and primary chemistry, *Geophys. Res. Lett.*, *24*, 2671-2674, 1997
- [76] Feichter, J., E. Kjellstrom, H. Rodhe, F. Dentener, J. Lelieveld, and G. J. Roelofs, Simulation of the tropospheric sulfur cycle in a global climate model, *Atmos. Env.* *30*, 1693-1707, 1996
- [77] Feichter, J, U. Lohmann, and I. Schult, The atmospheric sulfur cycle in ECHAM-4 and its impact on the shortwave radiation, *Climate Dynamic*, *13*, 235-246, 1997
- [78] Fisher, B.E.A., A review of the process and models of long range transport of air pollutants, *Atmos. Environ.*, *17*, 1865-1880, 1983
- [79] Friedman, Robert Marc. *Appropriating the Weather: Vilhelm Bjerknes and Construction of a Modern Meteorology*, Cornell University Press, 1989
- [80] Fujita, S., Y. Ichikawa, R. Kawaratani, and Y. Tonooka, Preliminary inventory of sulfur dioxide emission in East Asia, *Atmos. Environ.*, *25A*, 1409-1411, 1991.
- [81] Galloway, J., D. Zhao, J. Xiong, G. E. Likens, Acid rain: China, United States, and a Remote area, *Science Vol. 236*, 1559-1562, 1987.
- [82] Galloway, J. N., Atmospheric acidification: Projections for the future, *Ambio*, *18*, 161-166, 1989

- [83] Galloway, J. N., H. Levy, P. S. Kasibhatla, Year 2020: Consequences of population growth and development on deposition of oxidized nitrogen, *Ambio* 23, 120-123, 1994
- [84] Ganzeveld, L. and J. Lelieveld, Dry deposition parameterization in a chemistry general circulation model and its influence on the distribution of reactive trace gases, *J. Geophys. Res.*, 100, D10, 20,999-21,012, 1995
- [85] Ganzeveld, L., J. Lelieveld, and G.J. Roelofs, A dry deposition parameterization for sulfur oxides in a chemistry and general circulation mode, *J. Geophys. Res.*, 103, D5, 5679-5694, 1998
- [86] Giorgi, F., and W. L. Chameides, Rainout Lifetimes of Highly Soluble Aerosols and Gases as Inferred From Simulations With a General Circulation Model, *J. Geophys. Res.* 91, 14,367-14,376, 1986
- [87] Giorgi, F., and G. T. Bates, The climatological skill of a regional model over complex terrain, *Mon. Wea. Rev.*, 117, 2325-2347, 1989
- [88] Giorgi, F., M. R. Marinucci, and G. T. Bates, Development of a second generation regional climate model (RegCM2), Boundary-layer and radiative transfer process, *Mon. Weather Rev.*, 121, 2794-2813, 1993a
- [89] Giorgi, F., M. R. Marinucci, G. T. Bates, and G. De Canio, Development of a second generation regional climate model (RegCM2), Convective processes and assimilation of lateral boundary conditions, *Mon. Weather Rev.*, 121, 2814-2832, 1993b
- [90] Giorgi, F., Y. Huang, K. Nishizawa, and C. Fu, A seasonal cycle simulation over eastern Asia and its sensitivity to radiative transfer and surface processes, *J. Geophys. Res.*, 104, D6, 6403-6423, 1999a
- [91] Giorgi, F., and L. O. Mearns, Regional climate modeling revisited, An introduction to the special issue, *J. Geophys. Res.*, 104, 6335-6352, 1999b
- [92] Giorgi, F., X. Bi, and Y. Qian, Direct radiative forcing and regional climate effects of anthropogenic aerosols over East Asia: a regional coupled climate-chemistry/aerosol model study, *J. Geophys. Res.*, 107, AAC7, 2002
- [93] Granat, L., H. Rodhe, and R.O. Hallberg, The global sulfur cycle, in *Nitrogen, Phosphorus, and Sulfur - Global Cycles (SCOPE Report 7)*, edited by B.H. Svensson, and R. Soderlund, pp. 89-134, Ecol. Bull., Stockholm, 1976
- [94] Granat, L., and C. Johansson, Dry deposition of SO₂ and NO_x in winter, *Atmos. Environ.*, 17, 191-192, 1983
- [95] Grell, G., J. Dudhia, and D. Stauffer, A description of the fifth-generation Penn State/NCAR Mesoscale Model (MM5), NCAR/TN-398+STR, NCAR, Boulder, 1996

- [96] Gut, A, M. Scheibe, S. Rottenberger, U. Rummel, M. Welling, C. Ammann, G.A. Kirkman, U. Kuhn, F.X. Meixner, J. Kesselmeier, B.E. Lehmann, W. Schmidt, E. Muller, M.T.F. Piedade, Exchange fluxes of NO₂ and O₃ at soil and leaf surfaces in an Amazonian rain forest, *J. Geophys. Res.*, *107*, D20, 8060, 2002
- [97] Hanson, P. J., S. E. Lindberg, Dry deposition of reactive nitrogen compounds: A review of leaf, canopy and non-foliar measurements, *Atmos. Environ. Ser. A*, *25*, 1615-1634, 1991
- [98] Hao, J. M., and B. J. Liu, Acid rain in China: Patterns, trends, and impacts, National Environmental Protection Agency, Beijing, 1997
- [99] Hauglustaine, D.A., G.P. Brasseur, S. Walters, P.J. Rasch, J.-F. Miller, L.K. Emmons and M.A. Carroll, MOZART, a global chemical transport model for ozone and related chemical tracers: 2. Model results and evaluation, *J. Geophys. Res.*, *103*, 28291-28335, 1998
- [100] Haywood, J. M., and K. P. Shine, The effect of anthropogenic sulfate and soot aerosol on the clear sky planetary radiation budget, *Geophys. Res. Lett.*, *603-606*, 1995
- [101] Haywood, J.M., D.L. Roberts, A. Slingo, J.M. Edwards, and K.P. Shine, General circulation model calculations of the direct radiative forcing by anthropogenic sulphate and fossil-fuel soot aerosol, *J. Clim.*, *10*, 1562-1577, 1997
- [102] Hegg, D. A., and Hobbs, P. V., Comparisons of sulfate production due to ozone oxidation in cloud with a kinetic rate equation, *Geophys. Res. Lett.*, *14*, 719-721, 1987
- [103] Hicks, B. B., The measurement of atmospheric fluxes: A generalised approach, *J. Appl. Met.*, *6*, 386-388, 1970
- [104] Hill, A. C., Vegetation: a sink for atmospheric pollutants, *J. Air Pollu. Control. Ass.*, *21*, 341-346, 1971
- [105] Hogstrom, U., Non-dimensional wind and temperature profiles in the atmospheric surface layer: A reevaluation. *Boundary-Layer Meteor.*, *42*, 55-78, 1987
- [106] Horowitz, L., et al., A global simulation of tropospheric ozone and related tracers: Description and evaluation of MOZART, version 2, *J. Geophys. Lett.*, *108*, D24, 4784, doi:10.1029/2002JD002853, 2003
- [107] Houweling, S., F. Dentener and J. Lelieveld, The impact of non-methane hydrocarbon compounds on tropospheric photochemistry, *J. Geophys. Res.*, *103*, 10673-10696, 1998
- [108] Hu, Y., D. Cohan, M. T. Odman, and A. Russell, *Air Quality Modeling of the August 11-20, 2000 Episode for the Fall Line Air Quality Study*, Prepared for Georgia Department of Natural Resources, Environmental Protection Division, Prepared by Georgia Institute of Technology, 2004

- [109] Huebert, B. J., T. Bates, et al., An overview of ACE-Asia: Strategies for quantifying the relationships between Asian aerosols and their climatic impacts, *J. Geophys. Res.*, 108 (D23), 8633, doi: 10.1029/2003JD003550, 2003
- [110] Husar R. B., J. D. Husar, L. Martin, Distribution of continental surface aerosol extinction based on visual range data, *Atmos. Environ.*, 34, 5067-5078, 2000
- [111] IPCC, *Climate Change, the IPCC Scientific Assessment*. J.T. Houghton, G.J Jenkins and J. J. Ephraums (eds.), Cambridge University Press, Cambridge, UK, 1990
- [112] IPCC, *Climate Change 1992: The supplementary report to the IPCC scientific assessment*. J.T. Houghton, G.J Jenkins and J. J. Ephraums (eds.), Cambridge University Press, Cambridge, UK, 1992
- [113] IPCC, *Climate Change 1995, The Science of Climate Change*, Contribution of Working Group I to the Second Assessment Report of the Intergovernmental Panel on Climate Change, Cambridge Univ. Press, New York, 1995
- [114] IPCC, *Climate Change 2001*, IPCC Third Assessment Report, <http://www.grida.no>, 2001
- [115] IPCC, *Emissions Scenarios*, IPCC Special Report, Cambridge Univ. Press, New York, 2000
- [116] Jacob, D. J., S.-M., Fan, S.C. Wofsy, et al., Deposition of ozone to tundra, *J. Geophys. Res.*, 97, 16,473-16479, 1992
- [117] Jacob, D., et al., Effects of rising Asian emissions on surface ozone in the United States, *Geophys. Res. Lett.*, 26, 2175-2178, 1999
- [118] Jacob, D., et al., Transport and chemical evolution over the Pacific mission: Design, execution, and first results, *J. Geophys. Res.*, 108 (D20), 8781, 2003
- [119] Jacobson, M. Z., *Fundamentals of Atmospheric Modeling*, Cambridge University Press, 1999
- [120] Jacobson, M. Z., Global direct radiative forcing due to multicomponent anthropogenic and natural aerosols, *J. Geophys. Res.*, 106, 1551-1568, 2001
- [121] Jaegle, L. et al., Sources and budgets for CO and O₃ in the northeastern Pacific during the spring of 2001: Results from the PHOBEA-II Experiment, *J. Geophys. Res.*, 108(D20), 8802, doi:10.1029/2002JD003121, 2003
- [122] Jaffe, D. A., et al., Impact of Asia emissions on the remote North Pacific atmosphere: Interpretation of CO data from Shemya, Guam, Midway and Mauna Loa, *J. Geophys. Res.*, 102, 28,627-28,635, 1997
- [123] Jaffe, D., et al., Transport of Asian air pollution to North America, *Geophys. Res. Lett.*, 26, 711-714, 1999

- [124] Jaffe D., McKendry I., Anderson T., and Price H. Six 'new' episodes of trans-Pacific transport of air pollutants. *Atmos. Environ.* *37*, 391-404, 2003
- [125] Joseph, J. H., W. J. Wiscombe, and J. A. Weinman, The delta-Eddington approximation for radiative flux transfer, *J. Atmos. Sci.*, *33*, 2452-2459, 1976
- [126] Kasibhatla, P., W. L. Chameides, and J. St. John, A three-dimensional global model investigation of seasonal variations in the atmospheric burden of anthropogenic sulfate aerosols, *J. Geophys. Res.*, *102*, 3737-3759, 1997
- [127] Kasibhatla, P., et al., Top-down estimate of a large source of atmospheric carbon monoxide associated with fuel combustion in Asia, *Geophys. Res. Lett.*, *29*, 19, 1900, 2002
- [128] Kato, N., and H. Akimoto, Anthropogenic emissions of SO₂ and NO_x in Asia: emission inventory, *Atmos. Environ.*, *26A*, 2997-3017, 1992
- [129] Kaiser, D., Y. Qian, Decreasing trends in sunshine duration over China for 1954-1998: Indication of increased haze pollution? *Geophys. Res. Lett.*, *29*(21), 2042, doi:10.1029/2002GL016057, 2002
- [130] Kellogg, W.W., et al., The sulfur cycle, *Science*, *175*, 587-596, 1972
- [131] Kiehl, J. T., and B. P. Briegleb, The relative roles of sulfate aerosols and greenhouse gases in climate forcing, *Science*, *260*, 311-314, 1993
- [132] Kiehl, J. T., and H. Rodhe, Modeling geographical and seasonal forcing due to aerosols, *Aerosol Forcing of Climate*, Ed. R. J. Charlson and J. Heintzenberg, 281-296, John Wiley, New York, 1995
- [133] Kiehl, J. T., et al., Description of the NCAR Community Climate Model (CCM3), Technical Report NCAR/TN-420+STR, National Center for Atmospheric Research, Boulder, Colorado, 1996
- [134] Kiehl, J. T., T. L. Schneider, P. J. Rasch, M. C. Barth and J. Wong, Radiative forcing due to sulfate aerosols from simulations with the NCAR community model (CCM3), *J. Geophys. Res.*, *105*, 1441-1458, 2000
- [135] Kiley, C., et al., An intercomparison and evaluation of aircraft-derived and simulated CO from seven chemical transport models during the TRACE-P experiment, *J. Geophys. Res.*, *108*, D21, 2003
- [136] Kim, B. G., J. S. Han, S. U. Park, Transport of SO₂ and aerosol over the Yellow sea, *Atmos. Environ.*, *35*, 727-737, 2001
- [137] Klimont, Z., J. Cofala, W. Schopp, M. Amann, D.G. Streets, Y. Ichika, and S. Fujita, Projections of SO₂, NO_x, NH₃ and VOC emissions in East Asia upto 2030, *Water, Air, and Soil Pollut.*, *130*, 193-198, 2001

- [138] Klonecki, A., et al., Seasonal changes in the transport of pollutants into the Arctic troposphere-model study, *J. Geophys. Res.*, *108*, D4, 8367, doi:10.1029/2002JD002199, 2003
- [139] Koch, D., D. Jacob, I. Tegen, D. Rind, and M. Chin, Tropospheric sulfur simulation and sulfate direct radiative forcing in the Goddard Institute for Space Studies general circulation model, *J. Geophys. Res.*, *104*, 23,799-23,822, 1999
- [140] Koch, D., Transport and direct radiative forcing of carbonaceous and sulfate aerosols in the GISS GCM, *J. Geophys. Res.*, *106*, D17, 20,311-20,332, 2001
- [141] Koch, D., J. Park, A. D. Genio, Clouds and sulfate are anticorrelated: A new diagnostic for global sulfur models, *J. Geophys. Res.*, *108*, D24, 4781, doi:10.1029/2003JD003621, 2003
- [142] Kritiz, M. A., J. C. LeRouilly, and E. F. Danielson, The China Clipper: Fast advective transport of radon-rich air from the Asia boundary layer to the upper troposphere near California, *Tellus*, *4213* 46-61, 1990
- [143] Kumar, N., M. T. Odman, A. G. Russell, Multiscale air quality modeling: application to Southern California, *J. Geophys. Res.*, *99*, 5385-5397, 1994
- [144] Kuo, H. L., Further Studies of the Parameterization of the Influence of Cumulus Convection on Large-Scale Flow, *J. Atmos. Sci.*, *31*, 1232-1240, 1974
- [145] Langner, J. and H. Rodhe, A global three-dimensional model of the tropospheric sulphur cycle, *J. Atmos. Chem.*, *13*, 225-263, 1991
- [146] Lawrence M., P. Crutzen, P. J. Rasch, B. E. Eaton, and N. Mahowald, A model for studies of tropospheric photochemistry: Description, global distributions, and evaluation, *J. Geophys. Res.*, *104*, D21, 26,245-26,277, 1999
- [147] Lerdau, M. T., J. W. Munger, and D. J. Jacob, The NO₂ flux conundrum, *Science*, *289*, 2291-2293, 2000
- [148] Levine, S. Z., and S. E. Schwartz, In-cloud and below-cloud scavenging of nitric acid vapor, *Atmos. Environ.*, *16*, 1725-1734, 1982
- [149] Levy, H., H. and W. J. Moxim, Influence of long-range transport of combustion emissions on the chemical variability of the background atmosphere, *Nature*, *338*, 326-328, 1989
- [150] Leung, R., L. Mearns, F. Giorgi, and R. Wilby, Regional Climate Research, *BAMS*, 89-95, 2003
- [151] Levy, H., P. S. Kasibhatala, W. J. Moxim, A. A. Klonecki, A. I. Hirsch, S. J. Oltmans and W. L. Chameides, The global impact of human activity on tropospheric ozone, *Geophys. Res. Lett.*, *24*, 791-794, 1997

- [152] Liu, H., et al., Transport pathways for Asia pollution outflow over the Pacific: Inter-annual and seasonal variation, *J. Geophys. Res.*, *108*, D21, 8786, 2003
- [153] Logan, J. A., M. J. Prather, S. C. Wofsy, M. B. McElroy, Tropospheric chemistry: A global perspective, *J. Geophys. Res.*, *86*, 7210-7254, 1981
- [154] Louis, J. F., A parametric model of vertical eddy fluxes in the atmosphere, *Boundary Layer Meteorol.*, *17*, 187-207, 1979
- [155] Loveland, T.R., Reed, B.C., Brown, J.F., Ohlen, D.O., Zhu, J, Yang, L., and Merchant, J.W., Development of a Global Land Cover Characteristics Database and IGBP DISCover from 1-km AVHRR Data, *International Journal of Remote Sensing* , *V. 21*, no. 6/7, p. 1,303-1,330, 2000
- [156] Luo, C., J. C. St. John, X. Zhou, K. S. Lam, T. Wang, and W. L. Chameides, A non-urban ozone air pollution episode over eastern China: Observations and model simulations, *J. Geophys. Res.*, *105*, 1889-1908, 2000
- [157] Manabe, S., Climate and the ocean circulation: 1. The atmospheric circulation and the hydrology of the earth's surface, *Mon. Wea. Rev.*, *97*, 739-774, 1969
- [158] Manabe, S., K. Bryan, and M.J. Spelman, A global ocean-atmosphere climate model: part 1. The atmospheric circulation, *J. Phys. Oceanography* *5*, 3-29, 1975
- [159] Mauzerall, D. L., G. Brasseur, and D. Hauglustaine, Production and export of tropospheric ozone from Asia: Global modelling and analysis of PEM-West B data, International Symposium on Atmospheric Chemistry and Future Global Environment, Nagoya, Japan, Science Council of Japan and National Space Development Agency, 1997
- [160] Mauzerall D., X. Wang, Protecting agricultural crops from the effects of troposphere ozone exposure: Reconciling Science and Standard setting in the United States, Europe, and Asia, *Annu. Rev. Energy Environ.*, *26*:237-68, 2001
- [161] McRae, G. J., J. H. Seinfeld, Development of a second generation mathematical model for urban air pollution, - II Evaluation of model performance, *Atmos. Environ.*, *17*, 501-522
- [162] Mearns, L., Issues in the impacts of climate variability and change on agriculture, *Clim. Change*, *60*, 1-6, 2003
- [163] Menon, S., et al., Climate effects of black carbon aerosol in China and India, *Science*, *297*, 2250-2253, 2003
- [164] Merrill, J. T., Atmospheric long range transport to the Pacific Ocean, in *Chemical Oceanography*, *10*, ed. by J. P. Riley and R. Duce, pp 15-50, London, Academic Press, 1989

- [165] Meskhidze, N.; Chameides, W. L.; Nenes, A.; Chen, G, Iron mobilization in mineral dust: Can anthropogenic SO₂ emissions affect ocean productivity? *Geophys. Res. Lett.*, *30*, No. 21, 2085 10.1029/2003GL018035, 2003
- [166] Michalakes, J., et al., Development of a next-generation Regional Weather Research and Forecast Model (WRF), in *Developments in Teracomputing: Proceedings of the Ninth ECMWF Workshop on the Use of High Performance Computing in Meteorology*. Eds. Walter Zwiefelhofer and Norbert Kreitz. World Scientific, Singapore. 2001
- [167] Moller, U., and G. Schumann, Mechanisms of transport from the atmosphere to the Earth's surface, *J. Geophys. Res.*, *75*, 3013-3019, 1970
- [168] Moller, D., Estimation of the global man-made sulfur emission, *Atmos. Environ.*, *23*, 671-687, 1989
- [169] Morris, R. E. and T. C. Myers, User's guide for the Urban Airshed Model, Vol. 1, User's manual for UAM (CB-IV), US EPA Report EPA/450/4-90/007A, 1990
- [170] Myhre, G., F. Stordal, K. Restad, and I. Isaksen, Estimates of the direct radiative forcing due to sulfate and soot aerosols. *Tellus*, *50B*, 463-477, 1998
- [171] NARSTO, North American Research Strategy for Tropospheric Ozone, *An Assessment of Tropospheric Ozone Pollution: A North American Perspective*, W. L. Chameides and K. L. Demerjian, 2000
- [172] National Research Council, *Rethinking the Ozone Problem in Urban and Regional Air Pollution*, 50pp, Natl. Acad. Press, Washington, D. C., 1991
- [173] National Research Council, *The Atmospheric Sciences Entering the Twenty-First Century*, National Academy Press, Washington, D.C., 364 pp, 1998.
- [174] Nicks, D. K., et al., Fossil-fueled power plants as a sources of atmospheric carbon monoxide, *J. Environ. Monit.*, *5*, 35-39, 2003
- [175] Odman, M. T., and C. T. Ingram, Multiscale air quality simulation platform (MAQSIP), *Source Code Documentation and Validation*, MCNC Research Triangle Park, NC, 1996
- [176] Oliver, J.G., et al., Description of EDGAR Version 2.0: A set of global emission inventories of greenhouse gases and ozone-depleting substances for all anthropogenic and most natural sources on a per country basis and on 1° × 1° grid, REPORT 771060002, National Institute of Public Health and the Environment (RIMV), The Netherlands, 1996
- [177] Palmer, P., et al., Inverting for emissions of carbon monoxide from Asia using aircraft observations over the western Pacific, *J. Geophys. Res.*, *108*, D21, 8828, 2003

- [178] Parrish, D. D. M. Trainer, M. P. Buhr, B. A. Watkins, F. C. Fehsenfeld, Carbon monoxide concentrations and their relation to concentrations of total reactive oxidized nitrogen at 2 rural United-States sites, *J. Geophys. Res.*, *96*, 9309-9320, 1991
- [179] Parrish, D. D., et al., Indications of photochemical histories of Pacific air masses from measurements of atmospheric trace species at Pt. Arena, California, *J. Geophys. Res.*, *97*, 15,883-15,901, 1992
- [180] Parrish, D. D., M.P. Buhr, M. Trainer, R.B. Norton, J.P. Shimshock, F.C. Fehsenfeld, K.G. Anlauf, J. W. Bottenheim, Y. Z. Tang, H.A. Wiebe, J.M. Roberts, R.L. Tanner, L. Newman, V.C. Bowersox, K.J. Olszyna, E.M. Bailey, M.O. Rodgers, T. Wang, Herresheim, U.K. Roychowdhury and K.L. Demerjian, The total reactive oxidized nitrogen levels and the partitioning between the individual species at six rural sites in eastern North America, *J. Geophys. Res.* *98*, 2927-2939, 1993
- [181] Penner, J. E., C. S. Atherton, and T. A. Graedel, Global emissions and models of photochemically active compounds, in *Global Atmospheric-Biospheric Chemistry*, edited by R. G. Prinn, pp. 223-247, Plenum, New York, 1994.
- [182] Penner, J.E., et al., Aviation and the Global Atmosphere, A special Report of IPCC Working Groups I and III, Cambridge University Press, Cambridge, UK, 373pp, 1999
- [183] Peters, L. K. and A. A. Jouvanis, Numerical simulation of the transport and chemistry of CH₄ and CO in the troposphere, *Atmospheric Environment*, *13*, 1443-1462, 1979
- [184] Peters, L., et al., The current state and future direction of Eulerian models in simulating the tropospheric chemistry and transport of trace species: A review, *Atmos. Environ.*, *29*, 1995
- [185] Phadnis, M. J., and G. R. Carmichael, Transport and distribution of primary and secondary non-methane volatile organic compounds in east Asia under continental outflow conditions, *J. Geophys. Res.*, *105*, 22311-22336, 2000
- [186] Pham, M., J.-F. Mller, G. P. Brasseur, C. Granier, and G. Mgie, A 3D model study of the global sulphur cycle: Contributions of anthropogenic and biogenic sources. *Atmos. Env.*, *30*, 1815-1822, 1996
- [187] Phillips, N.A., The general circulation of the atmosphere: a numerical experiment, *Quarterly J. Royal Meteo. Soc.* *82*, 352, 123-164, 1956
- [188] Prospero, J.M., and D.L. Savoie, Effect of continental sources of nitrate concentrations over the Pacific Ocean, *Nature*, *339*, 687-689, 1989
- [189] Qian, Y, F. Giorgi, Interactive coupling of regional climate and sulfate aerosol models over eastern Asia, *J. Geophys. Res.*, *104*, 6477-6499, 1999

- [190] Qian, Y, F. Giorgi, Y. Huang, W. Chameides, and C. Luo, Regional simulation of anthropogenic sulfur over East Asia and its sensitivity to model parameters, *Tellus B 53B*, 171-191, 2001
- [191] Rasch, P., M. Barth, J. Kiehl, S. Schwartz, and C. Benkovitz, A description of the global sulfur cycle and its controlling processes in the National Center for Atmospheric Research Community Climate Model, Version 3, *J. Geophys. Res.*, *105*, D1, 1367-1385, 2000
- [192] Reynolds, S. D., P. M. Roth, J. H. Seinfeld, Modeling of photochemical air pollution - I. Formation of the model, *Atmospheric Environment*, *7*, 1033-1061, 1973
- [193] Reynolds, S. D., M. Liu, T. A. Hecht, P. M. Roth, and J. H. Seinfeld, Modeling of photochemical air pollution - III. Evaluation of the model, *Atmospheric Environment*, *8*, 563-596.
- [194] Richardson, L. F., *Weather Prediction by Numerical Process*, Cambridge University Press, Cambridge, 1922
- [195] Rind, D., and J. Lerner, Use of on-line tracers as a diagnostic tool in general circulation model development, 1., Horizontal and vertical transport in the troposphere, *J. Geophys. Res.*, *101*, 12,667-12,683, 1996
- [196] Rind, D., J. Lerner, K. Shah, and R. Suozzo, Use of on-line tracers as a diagnostic tool in general circulation model development, 2, Transport between the troposphere and the stratosphere, *J. Geophys. Res.*, *104*, 9123-9139, 1999
- [197] Rodhe, H., Human impact on the atmospheric sulfur balance, *Tellus*, *51*, 110-122, 1999
- [198] Robinson, E., and R.C. Robbins, Gaseous nitrogen compound pollutants from urban and natural sources, *J. Air Pollut. Control Assoc.*, *20 (5)*, 303-306, 1970a
- [199] Robinson, E., and R.C. Robbins, Gaseous sulfur pollutants from urban and natural sources, *J. Air Pollut. Control Assoc.*, *20 (4)*, 233-235, 1970b
- [200] Roelofs, G. J. and J. S. Lelieveld, Model study of cross-tropopause O₃ transport on tropospheric O₃ level, *Tellus*, *49B*, 38-55, 1997
- [201] Rogers, R. R., and M. K. Yau, *A Short Course in Cloud Physics*, Third Edition, Pergamon Press, Oxford, UK., 1989
- [202] Rondon, A., C. Johansson, and L. Granat, Dry deposition of nitrogen dioxide and ozone to coniferous forest, *J. Geophys. Res.*, *98*, 5159-5172, 1993
- [203] Russell, A., Regional photochemical air quality modeling: Model formulations, history, and state of the science, *Annu. Rev. Energy Environ.* *22*, 537-588, 1997

- [204] Russell, A., and R. Dennis, NARSTO critical review of photochemical models and modeling, *Atmos. Environ.*, *34*, 2283-2324, 2000
- [205] Sander, S. P., et al., Chemical kinetics and photochemical data for use in atmospheric studies, *JPL Publication 02-25*, 2003.
- [206] San Jose, R., J. L. Casanova, R. E. Vilorio, and J. Casanova, Evaluation of the turbulent parameters of the unstable surface boundary layer outside Businger's range, *Atmos. Environ.*, *19*, 1555-1561, 1985
- [207] Schwartz, S. E., The Whitehouse effect- Shortwave radiative forcing of climate by anthropogenic aerosols: An overview, *J. Aerosol Sci.*, *27*, 359-382, 1996
- [208] Schwartz, S. E., M. O. Andreae, Uncertainty in climate change caused by aerosols, *Science*, *272*, 1121-1122, 1996
- [209] Seigneur, C., and M. Moran, Chemical transport models, *Particulate Matter Science for Policy Makers, A NARSTO PM Assessment*, Elect. Power Res. Inst., Palo Alto, Calif, 2003
- [210] Seinfeld, J. H. and S. N. Pandis, Chemistry of the atmospheric aqueous phase, in *Atmospheric Chemistry and Physics*, 337-407, John Wiley, New York, 1998
- [211] Sheih, C. M., M. L. Wesely, and B. B. Hicks, Estimated dry deposition velocity of sulfur over the eastern United States and surrounding regions, *Atmos. Environ.*, *13*, 1361-1368, 1979
- [212] Sinton, J., and D. Fridley, "What goes up" recent trends in China's energy consumption, *Energy Policy*, *28*, 671-687, 2000
- [213] Smagorinsky, J., S. Manabe, and J. L. Holloway, Numerical results from a nine-level general circulation model of the atmosphere, *Mon. Wea. Rev.*, *93*, 727-768, 1965
- [214] Spiro, P.A., D.J. Jacob, and J.A. Logan, Global inventory of sulfur emissions with a 1° x 1° resolution, *J. Geophys. Res.*, *97*, 6023-6036, 1992
- [215] Stevenson, D.S., C.E. Johnson, W.J. Collins, R.G. Derwent and J.M. Edwards, Future tropospheric ozone radiative forcing and methane turnover - the impact of climate change. *Geophys. Res. Lett.*, *27*, 2073-2076, 2000
- [216] Streets, D., G. R. Carmichael, M. Amann, and R. L. Arndt, Energy Consumption and acid deposition in Northeast Asia, *Ambio* *28*, 135-143 1999
- [217] Streets, D.G., and S.T. Waldhoff, Present and future emissions of air pollutants in China: SO₂, NO_x and CO, *Atmos. Environ.*, *34*, 363-374, 2000a
- [218] Streets, D.G., N.Y. Tsai, H. Akimoto, and K. Oka, Sulfur dioxide emissions in Asia in the period 1985-1997, *Atmos. Environ.*, *34*, 4413-4424, 2000b

- [219] Streets, D.G., K. Jiang, X. Hu, et al., Recent Reductions in China's greenhouse gas emissions, *Science*, *294*, 1835-1837, 2001a
- [220] Streets, D.G., N. Tsai, H. Akimoto, and K. Oka, Trends in emissions of acidifying species in Asia, *Water, Air, and Soil Pollut*, *130*, 187-192, 2001b
- [221] Streets, D.G., S. Gupta, S.T. Waldhoff, M.Q. Wang, T.C. Bond, and B. Yiyun, Black carbon emissions in China, *Atmos. Environ.*, *35*, 4281-4296, 2001c
- [222] Streets, D.G., T.C. Bond, et al., An inventory of gaseous and primary aerosol emissions in Asia in the year 2000, *J. Geophys. Res.*, *108*, D21, 8809, 2003
- [223] Talbot, R. W., et al., Chemical characteristics of continental outflow from Asia to the troposphere over the western Pacific Ocean during Feb.-March 1994: Results from PEM-West B., *J. Geophys. Res.*, *102*, 28,255-28,274, 1997
- [224] Tan, Q., Y. Huang, W. L. Chameides, The Budget and Export of Anthropogenic SO_x From East Asia During Continental Outflow Conditions, *J. Geophys. Res.*, *107*, D13, 10.1029/2001JD000769, 2002
- [225] Tanre, D., J. F. Geleyn, and J. Slingo, First results of the introduction of an advanced aerosol-radiation interaction in the ECMWF low resolution global model, *Aerosols and their Climate Effects*, Ed. H. F. Gerber and A. Deepak, Deepak Publishing, 133-177, 1984
- [226] Taylor, K. E., and J. E. Penner, Response of the climate system to atmospheric aerosols and greenhouse gases, *Nature*, *369*, 734-737, 1994
- [227] Thornton, D., A. Bandy, B. Blomquist, A. Driedger, and T. Wade, Sulfur dioxide distribution over the Pacific Ocean 1991-1996, *J. Geophys. Res.*, *104*, D5, 5845-5854, 1999
- [228] Tonooka, Y., A. Kannari, H. Higashino, and K. Murano, NMVOCs and CO emission inventory in East Asia, *Water, Air, and Soil Pollut*, *130*, 199-204, 2001
- [229] Trainer, M., D.D. Parrish, M.P. Buhr, R.B. Norton, J.P. Shimshock, F.C. Fehsenfeld, K.G. Anlauf, J. W. Bottenheim, Y. Z. Tang, H.A. Wiebe, J.M. Roberts, R.L. Tanner, L. Newman, V.C. Bowersox, K.J. Olszyna, E.M. Bailey, M.O. Rodgers, T. Wang, Herresheim, and K.L. Demerjian, Correlation of ozone with NO_y in photochemically aged air, *J. Geophys. Res.* *98*, 2917-2915, 1993
- [230] United Nations, *United Nations Statistical Yearbook*, 41st issue, 886 pp, New York, 1996
- [231] U.S. Central Intelligence Agency, *World Factbook*, Washinton, DC, 2003.
- [232] U.S. Department of Energy, *International Energy Outlook*, Office of Integrated Analysis and Forecasting, Washington, DC, 2003.

- [233] U.S. Environmental Protection Agency, Compilation of Air Pollutant Emission Factors, AP-42, Fifth Edition, (<http://www.epa.gov/ttn/chief/ap42/>) 1998
- [234] U.S. The National Acid Precipitation Assessment Program's 1990 Integrated Assessment Report, chapter 2; National Acid Precipitation Assessment Program, Washington, DC, 1991
- [235] U.S. NOAA, 1998 <http://lwf.ncdc.noaa.gov/oa/reports/chinaflooding/chinaflooding.html>
- [236] U.S. State Department, *Background Note: China*, Bureau of East Asian and Pacific Affairs March 2004
- [237] Valdez, M., et al., Gaseous deposition to snow, 1. Experimental study of SO₂ and NO₂ deposition, *J. Geophys. Res.*, *92*, D8, 9779-9787, 1987
- [238] van Aardenne, J. A., G. R. Carmichael, H. Levy II, D. Streets, and L. Hordijk, Anthropogenic NO_x emissions in Asia in the period of 1990-2020, *Atmos. Environ.*, *33*, 633-646, 1999
- [239] Varhelyi, G., Continental and global sulfur budgets, I. Anthropogenic SO₂ emissions, *Atmos. Environ.*, *19*, 1029-1040, 1985
- [240] Venkatram, A., P. K. Karamchandani, P. K. Misra, Testing a comprehensive acid deposition model, *Atmos. Environ.*, *22*, 737-747, 1988
- [241] Walmsley, C.J., and M. L. Wesely, Modification of coded parameterization of surface resistances to gaseous dry deposition. *Atmospheric Environment*, *30*, 1181-1188.
- [242] Walcek, C.J., et al., SO₂, sulfate and HNO₃ deposition velocities computed using regional landuse and meteorological data, *Atmospheric Environment*, *20*, 949-964 1986
- [243] Walcek, C. J., W. R. Stockwell, and J. S. Chang, Theoretical estimates of the dynamic radiative and chemical effects of clouds on tropospheric gases, *Atmos. Res.*, *25*, 53-69, 1990
- [244] Wang, S., and Z. Zhao, Drought/flood variation for the last 2000 years in China and comparison with global climate change. In: *The climate of China and global climatic change*, D. Ye et al. (Eds.), China Ocean Press, Beijing, China, 1987
- [245] Wang, S., and D. Gong, Enhancement of the warming trend in China, *Geophys. Res. Lett.*, *27*, 2581-2584, 2000
- [246] Wang, W., and T. Wang, On the origin and the trend of acid deposition in China, *Water Air Soil Pollut.*, *85(4)*, 2295-2300, 1995
- [247] Wang, T., et al., Emission characteristics of CO, NO_x, SO₂ and indications of biomass burning observed at a rural site in eastern China, *J. Geophys. Res.*, *107*, D12, 2002

- [248] Wang, Y., D. J. Jacob, and J. A. Logan, Global simulation of tropospheric O₃-NO_x-hydrocarbon chemistry, 1. Model formulation, *J. Geophys. Res.*, *103*, 10,713-10,726, 1998
- [249] Wauben, W.M.F., J.P.F. Fortuin, P.F.J. van Velthoven and H. Kelder, Comparison of modelled ozone distributions with sonde and satellite observations. *J. Geophys. Res.*, *103*, 3511-3530, 1998
- [250] Wesely, M. and B. Hicks, Some factors that affect the deposition rate of sulfur dioxide and similar gases on vegetation, *J. Air. Pollut.*, *27*, 1110-1116, 1977
- [251] Wesely, M. L., B. B. Hicks, W. P. Dannevik, S. Frisella, and R. B. Husar, An eddy-correlation measurement of particulate deposition from the atmosphere, *Atmos. Environ.*, *11*, 561-563, 1977
- [252] Wesely, M.L., Cook, D.R., Hart, R.L., and Speer, R.E., Measurements and Parameterization of Particulate Sulfur Dry Deposition Over Grass, *J. Geophys. Res.* *90*, 2131-2143, 1985.
- [253] Wesely, M.L., Parameterization of surface resistance to gaseous dry deposition in regional-scale numerical models, *Atmospheric Environment*, *23*, 1293-1304, 1989
- [254] Wesely, M. L. and B. B. Hicks, A review of the current status of knowledge on dry deposition. *Atmos. Environ.*, *34*, 2261-2282, 2000.
- [255] Wild, O. and M. J. Prather, Excitation of the primary tropospheric chemical mode in a global CTM, *J. Geophys. Res.* *105*, 24647-24660, 2000
- [256] Wilkening, K. E., L. A. Barrie, M. Engle, Atmospheric science - Trans-Pacific air pollution, *Science*, *290*, 65-67, 2000
- [257] Wolf, M. E., and G. M. Hidy, Aerosols and climate: Anthropogenic emissions and trends for 50 years, *J. Geophys. Res.*, *102*, 11113-11121, 1997
- [258] World Bank, *Clear water, blue skies*, China's Environment in the new century, China 2020 series, Washington, DC, 1997
- [259] World Resources 1998-99, Environmental Change and Human Health, Oxford University Press, 1998.
- [260] Wyngaard, J. C., and R. A. Brost, Top-down and bottom-up diffusion of a Scalar in the convective boundary layer, *J. Atmos. Chem.*, *41*, 102-112, 1984
- [261] Xu, J., et al., Measurement of aerosol chemical, physical and radiative properties in the Yangtze delta region of China, *Atmos. Environ.*, *36*, 161-173, 2002
- [262] Xu, Q., Abrupt change of the mid-summer climate in central east China by the influence of atmospheric pollution, *Atmos. Environ.*, *35*, 5029-5040, 2001

- [263] Xu, Y., and G. Carmichael, An assessment of sulfur deposition pathways in Asia, *Atmos. Environ.*, *33*, 3473-3486, 1999.
- [264] Yan, P., C. Luo, X. Xu, R. Xiang, G. Ding, J. Tang, M. Wang, and X. Yu, The study of distribution character of O₃, NO_x and SO₂ at rural areas in China, *Q. J. Appl. Meteorol.*, *8*, 53-60, 1997
- [265] Yu, S. et al., A comparison of signals of regional aerosol-induced forcing in eastern China and the southeastern United States, *Geophys. Res. Lett.*, *28*, 713-716, 2001
- [266] Yu, X., J. Tang, X. Li, and B. Liang, Application of FP-IC method in sampling and analysis of sulfur dioxide and nitrogen dioxide in clean air, in *Ozone Changes and their Influence on Climatic Environment in China*, 82-91, edit by X. Zhou, China Meteorology Press, Beijing, China, 1996
- [267] Zhang, J., et al., Carbon monoxide from cookstoves in developing countries: 1 Emission factors, *Chemosphere: Global Change Science*, *1*, 353-366, 1999
- [268] Zhai, P and F. Ren, On changes of China's maximum and minimum temperature in 1951-1990, *ACTA Meteorology Sinica*, *13*,, 3 278-290, 1999

VITA

Qian Tan was born in Lanzhou, China, February, 1974. In 1992, she entered Nanjing University, China, and received her Bachelor of Science Degree in Atmospheric Dynamics in 1996. Then she enrolled in the Graduate School of Nanjing University for two years. In 1998, she began to pursue her Ph.D. in Atmospheric Chemistry under the guidance of Dr. William L. Chameides at School of Earth and Atmospheric Science, Georgia Institute of Technology. After six years as a research and teaching assistant, she completed her Ph.D. work in April, 2004.